



HAL
open science

Phenomenology of the scalar sector beyond the standard model

Jean-Baptiste Flament

► **To cite this version:**

Jean-Baptiste Flament. Phenomenology of the scalar sector beyond the standard model. Physics [physics]. Université Claude Bernard - Lyon I, 2015. English. NNT : 2015LYO10178 . tel-01367530

HAL Id: tel-01367530

<https://theses.hal.science/tel-01367530>

Submitted on 16 Sep 2016

HAL is a multi-disciplinary open access archive for the deposit and dissemination of scientific research documents, whether they are published or not. The documents may come from teaching and research institutions in France or abroad, or from public or private research centers.

L'archive ouverte pluridisciplinaire **HAL**, est destinée au dépôt et à la diffusion de documents scientifiques de niveau recherche, publiés ou non, émanant des établissements d'enseignement et de recherche français ou étrangers, des laboratoires publics ou privés.

Thèse de doctorat
présentée devant
l'Université Claude Bernard Lyon 1
École Doctorale de Physique et d'Astrophysique

Spécialité

PHYSIQUE THÉORIQUE / PHYSIQUE DES PARTICULES

présentée par

M. Jean-Baptiste Flament

en vue de l'obtention du grade de

DOCTEUR de L'UNIVERSITÉ CLAUDE BERNARD LYON 1

PHENOMENOLOGY OF THE SCALAR SECTOR
BEYOND THE STANDARD MODEL

Soutenue publiquement le 22 Octobre 2015 devant la commission d'examen
formée de:

Mme. S. GASCON	<i>Présidente du jury</i>	- IPN Lyon
Mme. G. BÉLANGER	<i>Rapporteuse</i>	- LAPTH Annecy
M. C. GROJEAN	<i>Rapporteur</i>	- DESY Hamburg
M. C. SMITH	<i>Examinateur</i>	- LPSC Grenoble
M. G. CACCIALAGLIA	<i>Examinateur</i>	- IPN Lyon
M. A. DEANDREA	<i>Directeur de thèse</i>	- IPN Lyon

Résumé

Suite à l'annonce le 4 juillet 2012 par les collaborations travaillant sur les expériences du LHC, CMS et ATLAS, de la découverte d'une nouvelle particule aux propriétés semblables à celles du boson prédit près de 50 ans plus tôt par plusieurs théoriciens, la dynamique de recherche de nouvelle physique a été complètement modifiée. En effet, cette particule manquait jusqu'ici à l'appel dans les expériences pour confirmer le modèle de brisure de symétrie inclus dans le Modèle Standard de la physique des particules (SM), le mécanisme de Higgs. Cette découverte a donc rejeté ou limité la possibilité de nombreuses théories, tout en renforçant la crédibilité de ce dernier.

Cependant, il existe toujours des faits ou mesures expérimentales qu'il ne peut expliquer, comme par exemple l'existence de matière noire ou le caractère massif des neutrinos. On sait ainsi depuis longtemps que ce modèle ne peut pas être le mot final de la physique des particules. De ce fait, l'étude de la phénoménologie du secteur scalaire (fondamental), nouvellement découvert expérimentalement, est devenu une priorité, car il constitue une porte potentielle vers d'autres secteurs de la physique. Le premier chapitre de cette thèse sera consacré à la présentation du cadre physique utilisé qu'est le SM, et particulièrement le secteur du boson de Higgs et sa phénoménologie, avant de nous pencher dans la deuxième partie sur l'ensemble des outils statistiques qui sont utilisés dans ces analyses et que nous serons amenés à manipuler. Les trois chapitres suivants seront plus particulièrement consacrés à divers aspects de la phénoménologie.

Dans un premier temps, nous étudierons une manière de paramétrer les couplages du boson de Higgs afin de pouvoir réinterpréter les grandeurs mesurées dans les expériences au CERN, et de voir dans quelle mesure l'étude de ces couplages peut être utilisée pour contraindre des modèles décrivant de la physique au-delà du modèle standard (Beyond the Standard Model, BSM). Ce paramétrage, traite différemment les couplages existant à l'arbre et les couplages existant seulement grâce à des boucles dans le modèle standard. Par ce biais, il permettrait, en étant utilisé directement par les expérimentateurs, de lever une corrélation entre certains paramètres influençant conjointement les prédictions pour différentes observables. La procédure de contrainte des modèles BSM qui en découle consiste à comparer les valeurs de ces paramètres calculés pour des modèles particuliers aux distributions de probabilités fournies par les collaborations expérimentales. Cependant, les contraintes fournies par les expérimentateurs ne couvrant pas ce paramétrage, la procédure présentée ici passe par une extraction des mesures liées aux couplages du boson de Higgs publiées par les collaborations expérimentales, et leur extrapolation vers un modèle de fonction de vraisemblance gaussien, avant de les combiner en une unique fonction de vraisemblance portant sur le bon jeu de paramètres, que l'on pourra utiliser pour contraindre certains modèles BSM particuliers. Nous nous pencherons notamment sur les cas de modèles de Higgs fermiophobiques, de modèles présentant un dilaton. Il sera également possible d'en chercher le maximum, afin de déterminer les valeurs de ces paramètres les plus favorisées

par les données utilisées.

Dans un deuxième temps, nous verrons en quoi cette combinaison de paramétrage et de contraintes peut également être utilisée dans le cadre de recherches d'un scalaire élémentaire supplémentaire, plus léger que celui effectivement observé, et ayant échappé aux recherches passées, qui se concentraient sur la recherche d'un boson semblable à celui prédit dans le SM. Nous verrons également, à titre d'exemple, l'application à deux exemples de modèles pouvant contenir un tel scalaire. Le Modèle à deux doublets de higgs (Two-Higgs-Doublet Model, 2HDM), dans un premier temps, est une théorie très similaire au SM, auquel s'ajoute simplement un second doublet semblable à celui permettant le mécanisme de Higgs, modifiant la phénoménologie de ce dernier. Puis nous nous pencherons dans un second temps sur le cas du Modèle Suivant le Modèle Standard Supersymétrique Minimal (Next-to-Minimal Supersymmetric Standard Model, NMSSM), qui s'appuie quant à lui sur la supersymétrie. Cette extension des symétries spatiales du SM (le groupe de Lorentz), crée un lien entre des degrés de liberté bosoniques et fermioniques. Le spectre du SM s'en retrouve alors doublé par l'apparition de partenaires supersymétriques des particules déjà définies (sfermions et bosinos). Parmi les conséquences de cette symétrie, un second doublet électrofaible scalaire apparaît notamment, avec des conséquences similaires à celles déjà évoquées pour le 2HDM. Dans l'étude de chacun de ces deux modèles dépendant de plusieurs paramètres, des points ont été tirés au hasard. Chacun des points sondés dans l'espace de définition de ces modèles a ensuite été soumis à différentes contraintes expérimentales ou théoriques s'y appliquant, telles que des contraintes sur les observables de saveur ou des contraintes directes venant de recherches passées, afin de voir dans quelle mesure ces points décrivent des modèles réalistes en prenant en compte leurs influences sur d'autres observables. Nous verrons notamment que certains points non exclus par les contraintes à la date de l'analyse pourraient induire un signal observable au LHC.

Enfin, nous verrons dans quelle mesure des paramètres ainsi définis peuvent une application supplémentaire : en effet, le boson de Higgs du modèle standard peut avoir des influences sur les observations dans d'autres analyses expérimentales, notamment hors de sa couche de masse, dans la production d'une paire de bosons de jauge. Cet effet et ses conséquences expérimentales ont déjà été étudiés, et des analyses expérimentales ont été menées, montrant l'intérêt de cette mesure. Nous verrons donc que la définition particulière et fondamentale des paramètres utilisés permet leur réutilisation dans l'interprétation de ces données supplémentaires, dans certains cas, permettant notamment de lever la quasi-dégénérescence expérimentale existant entre deux paramètres. Nous verrons finalement deux limitations de cette approche, à savoir la modélisation des distributions de fonctions de vraisemblance, ou la restriction de la validité de notre approche aux modèles de nouvelle physique ne changeant pas les formes des distributions cinématiques, ainsi que des propositions manières pour les contourner. Nous nous pencherons pour cela brièvement sur les tentatives de publication de distributions de fonctions de vraisemblances par les collaborations expérimentales, puis sur les efforts menant à des publications communes, avant de nous intéresser au concept de pseudo-observables et à leur usage pour décrire une plus grande variété de modèles.

Mots-Clés :

Phénoménologie, boson de Higgs, paramétrage, LHC, scalaire léger, off-shell

Summary

Following the announcement on the 4th of July, 2012 by the collaborations working on the LHC experiments CMS and ATLAS, of the discovery of a new particle with properties resembling those of the boson predicted around 50 years earlier by several theorists, the dynamics of the research for traces of New Physics has been completely overhauled. This missing piece indeed proved wrong or constrained a whole set of theories, while giving more credit to the Standard Model of particle physics.

However, because of some features of reality it fails to describe, we know this model is not the final word of the story. From there on, the study of the phenomenology of this experimentally newly discovered scalar sector becomes a priority, as it is a new potential gate towards other sectors of physics.

In a first step, we will present a way to parametrise the couplings measured in the experiments held at CERN, in order to try and use the constraints on those couplings to constrain more fundamental models describing physics beyond the standard model. This parametrisation, describing differently the couplings existing in the Standard Model at tree-level from those only existing thanks to the intervention of loops, would allow, when used by experimentalists, to remove correlations existing between parameters having a joint influence on different observables.

We will then advocate for the use of this same method to look for an additional fundamental scalar, lighter than the one already observed, which would have escaped the previous experiments dedicated to looking for a scalar similar to the Higgs boson. We will also describe two models, the 2HDM and NMSSM for which some values of the parameters yet unconstrained give rise to such a scalar.

Finally, we will see how these definitions can have an additional application: indeed, the existence of the Standard Model Higgs boson has an influence on other experimental analyses than direct searches, especially outside of its mass shell, in the joint production of two weak gauge bosons. In this case, we will show that this analysis can be used in a coherent manner with on-shell Higgs measurements to constrain its couplings. We will also have a brief look at some limitations of this approach, before suggesting ways to overcome them.

Keywords:

Phenomenology, Higgs boson, parametrisation, LHC, light scalar, off-shell.

Acknowledgements - Remerciements

Bien que le titre soit à moitié en anglais, il s'agit du seul chapitre de cette thèse qui sera en français. Je fais confiance à mes quelques lecteurs anglophones (Daniël, I'm writing about you) pour avoir fait suffisamment de progrès en français pour la lire - ou au moins y retrouver leur nom !

Pour commencer, et en tout premier lieu, je voudrais bien entendu remercier mon directeur de thèse, Aldo Deandrea et le reste de l'équipe avec qui j'ai travaillé pendant ces trois ans, à savoir Giacomo Cacciapaglia et Guillaume Drieu La Rochelle. J'ai beaucoup appris à leur contact, au travers de toutes les opportunités de conférences, d'écoles et de collaborations que j'ai eues, ou tout simplement au cours de la recherche au quotidien. Je pourrais élaborer un long paragraphe sur ce que chacun m'a apporté, mais je peux également faire court en disant que grâce à chacun d'eux trois, j'ai appris une foule considérable de choses, qui me seront également utiles en dehors de la physique des particules.

L'obtention du doctorat ne serait pas possible sans la journée fatidique de la soutenance, et sans la présence du jury. À ce titre, j'aimerais remercier Christophe Grojean, Geneviève Bélanger et Christopher Smith, qui ont accepté de faire partie de mon jury de thèse, d'avoir fait le déplacement, et d'avoir lu et commenté mon manuscrit.

Je cite à part la dernière membre du Jury, Suzanne Gascon-Shotkin, parce qu'elle a eu un rôle particulier dans mon aventure en physique des particules. En effet, c'est avec elle et le reste du groupe CMS (Nicolas Chanon, Olivier Bondu, Hugues Brun, Moran Lethuillier entre autres) que j'ai découvert ce domaine en stage de M1. Les collaborations et discussions avec l'équipe CMS qui ont été ainsi commencées, également avec l'équipe top (avec Viola Sordini, Stéphane Perries, Anne-Laure Pequegnot, Sébastien Brochet) n'en ont été que facilitées.

Restent maintenant les gens qui n'ont pas de rapport direct avec le travail de thèse, mais qui ont joué un rôle tout aussi important durant cette période.

Évidemment, je voudrais remercier l'école doctorale (et son directeur Christophe Dujardin) le laboratoire, l'IPNL (et son directeur Guy Chanfray), et particulièrement le groupe théorie (avec son chef Dany Davesne) de m'avoir permis de conduire mes recherches dans un cadre idéal, et de m'avoir permis de voir la vie du laboratoire au travers du rôle de représentant des doctorants au conseil du laboratoire que j'ai assumé pendant 2 ans.

Sur un plan plus festif, je voudrais aussi mentionner l'APPN, association importante pour la vie du laboratoire, avec qui j'ai eu l'occasion de participer à l'organisation de tournois, de repas,

et d'événements, expérience enrichissante, au sein d'une équipe toujours de bonne humeur et efficace.

Mais un doctorat ne serait jamais le même (et je n'aurais jamais tenu 3 ans) sans l'entourage des autres jeunes chercheurs du laboratoire, qu'ils soient doctorants ou stagiaires. Pour les soirées, les cafés, les midis à rallonge, les billards, les volleys, les barbecues, la pétanque, et tout le reste, j'aimerais remercier dans un ordre un peu aléatoire Julien Chasserat, Maxime Guilbaud, Cécile Kefelian, Louis Sgandurra, Sébastien Brochet, Martin Elmer, Maël Le Guillou, Gwenaëlle Silberman, Nicolas Galy, Guillaume Victor, Jean-Luc Ley, Robin Jodon, Pierre-Alexandre Pantel, Alexandre Biguet, Pierre Becker, Arnaud Steen, Rémi Été, Anne-Laure Pequegnot, Lola Sarrazin, Boris Teyssier et les autres que ma mémoire trahit. Merci à tous, car encore une fois sans vous, ces trois années m'auraient paru bien plus longues.

Quelques doctorants sont absents de la liste précédente, parce qu'ils ont eu un rôle encore plus particulier dans mon quotidien : ceux avec qui j'ai partagé mon bureau pendant cette période. Pour les discussions sur la géométrie différentielle, et pour les démonstrations de mathématiques absurdes, et toutes les échanges sur nos domaines différents, un grand merci à Daniël Prins. Pour son expérience à mon arrivée en doctorat, ses histoires du Liban, le thé et les pâtisseries, merci à Ahmad Tarhini. Pour sa culture de l'internet WTF, son humour douteux et pour les discussions sur les dimensions supplémentaires, merci à Nicolas Deutschmann. Enfin, pour sa bonne humeur, son esprit détendu et ses goûts musicaux, merci à Mika Marini. J'espère que mes plantes survivront encore quelque temps grce vous.

Toujours dans le côté détente, je mentionnerai aussi les amis en dehors du laboratoire, qui ont maintes fois servi à prendre un bol d'air non chargé de particules : Les Bobs (Bob Lavau, Bob de Fromont, Bob Berger et Bob Guichardaz) et les soires cin, Catherine Sempere, Julien Bernaud, Étienne Pertreux, Guillaume Lheureux, Emeric Bergmann. En s'éloignant un peu mais en restant à Lyon, merci également à Hélène Lopez, pour beaucoup de choses (entre autres m'avoir permis de casser sa voiture), à Maxime Champion, Jean-Yonnel Chastaing et bien d'autres pour l'accueil quand je revenais à l'ENS, à Clymond Goobert, Michel Lavau, Clémence, Vincent Llorens, Robin Guichardaz et Barbara Fol pour nos intermèdes musicaux hebdomadaires, et à Aurélie de Freslon et Caroline pour la même chose (mais moins hebdomadaire).

En s'éloignant encore, merci à Samy, Brice, Johann, Sofia, Julie, Romaric, pour leur amitié depuis de nombreuses années, et qui permettait les week-end où l'on se voyait de parler de tout et n'importe quoi, et de jouer à tout et n'importe quoi.

Je garde bien sûr les quelques meilleurs pour la fin. Cécile, qui est arrivée dans ma vie au cours de mon doctorat, et qui l'a embellie. Un énorme merci à elle pour tout, et particulièrement pour sa patience dans les moments où je n'étais pas des plus agréables, notamment pendant la rédaction du manuscrit, où son soutien moral a été décisif.

Enfin, un dernier paragraphe et un grand merci pour les trois personnes qui m'ont fait grandir et apprécier les sciences jusqu'au point où j'ai pu écrire ce manuscrit : mon frère Thomas et mes parents.

Encore merci à tous.

Outline

Acknowledgements - Remerciements	vii
Outline	2
Introduction	3
1 Global overview of Particle Physics	5
1.1 Building up the standard model	5
1.2 Higgs Physics and phenomenology	8
1.2.1 The Higgs mechanism	9
1.2.2 Production mechanisms at a hadron collider	11
1.2.3 Decay channels	14
1.3 Shortcomings of the Standard Model	16
2 Statistics in particle physics	19
2.1 Mathematical tools	19
2.1.1 Basic definitions	19
2.1.2 Likelihood	21
2.1.3 Best fit, maximum likelihood	22
2.1.4 CLs	22
2.1.5 p-value	23
2.1.6 Confidence intervals (C.I.) and exclusion regions	24
2.2 Use in experiments	24
2.2.1 Selection channels	25
2.2.2 Signal strengths	27
2.2.3 Tests in experiments	27
2.2.4 Correlations	29
3 Higgs couplings beyond the standard model	31
3.1 Parametrisations of the Higgs couplings	31
3.1.1 Rescaled couplings	32
3.1.2 Loop-inspired parametrisation	33
3.1.3 Comparison of the two frameworks	35

3.2	Link with experimental constraints	36
3.2.1	Selection channels	36
3.2.2	Exclusion contours	38
3.3	Constraints	41
3.3.1	Models studied	42
3.3.2	Generic model	45
3.3.3	Fermiophobic Higgs	50
3.3.4	Dilaton model	51
4	Search for possible light additional scalars	53
4.1	Description of the parametrisation	53
4.2	Two-Higgs Doublet Model	55
4.2.1	Description	55
4.2.2	Model specific constraints	58
4.3	NMSSM	59
4.3.1	Description	60
4.3.2	Model specific constraints	61
4.4	Results	61
4.4.1	Generic model	61
4.4.2	2HDM and NMSSM	62
5	Further developments	67
5.1	Off-shell implications	67
5.2	Likelihood functions	72
5.3	Pseudo-observables	73
	Conclusion	75

Introduction

Two months before the beginning of this Ph.D., on the 4th of July of 2012, the CMS and ATLAS experimental collaborations publicly announced the discovery of a new particle, resembling the long-searched Higgs boson, missing piece of the standard model of particle physics and its still mysterious electroweak symmetry breaking. With this discovery, rewarding more than 20 years of efforts building the Large Hadron Collider, the approach of the phenomenology of this sector was modified, as one of the free parameters of the standard model (SM), the mass of the scalar, became measurable. It was also a consecration for theorists who predicted, about 50 years before that, the existence of this particle, when building up a framework for the symmetry breaking to take place, necessary for the weak interaction to behave the way it does, almost unobservable on macroscopic scales.

However, what is considered fundamental at a time rarely stays so for long, as scientific knowledge moves on. Just a bit more than a century ago, atoms were still considered as elementary particles as the scientific community was still oblivious to the nucleus and its proton/neutron structure, let alone its quark structure, or unstable particles such as the muon or heavier quarks. Theorists therefore keep building models beyond the SM, trying to find smaller structures to the universe surrounding us, and to fill in for the few flaws we could already observe in the SM predictions. The development of experiments at colliders therefore go alongside other experiments, such as neutrino or dark matter detectors, trying to sort out the most accurate description of our universe from this swarm of models.

In this context, the couplings of the Higgs boson made their entrance as a new way to constrain the SM and models beyond, as they might take values different from the ones we expect. However, making sense of their measurements is an intricate process and with their increasing accuracy, it is necessary to find a way to make the best use of them. In this prospect, the development of parametrisations of the couplings of the Higgs boson, at the interface between theory and experiments is very important, and we focused along this thesis on the use of a specific parametrisation, tailored to constrain models in which the couplings of the Higgs appearing with loops (and not at tree-level) play an important role. Since the discovery, this kind of framework became increasingly important, which was one of the aims of the work done along this thesis.

This kind of parametrisation is also interesting in extensions of the SM where new scalars are added. In this case, one expects the properties of the various scalars to be related, thus allowing a correlation between the determination of their couplings. Enlarging the scalar sector of the SM is a common practice in many theories (as, *e.g.*, in supersymmetry or 2 Higgs doublet models) and have been the subject of many studies, both at the phenomenological and the experimental level.

LEP, for instance, provides through its searches for a light SM Higgs constraints on theories with an additional light scalar, while the LHC provides at present analyses for heavy scalars. However, interpreting those measurements together has not yet become a standard, and parametrisations of the whole sector in a consistent way would improve such studies.

The first two chapters of this thesis will be dedicated to the description of the framework surrounding the phenomenology of the Higgs boson, by first describing the standard model and more specific aspects of the scalar sector, before describing the statistical apparatus needed to make sense of the experimental measurements and published results.

The third chapter will focus on the presentation of parametrisations of the Higgs couplings, and more specifically of one tailored to decorrelate modifications of the loop-induced couplings coming from new particles in loops and from modification of the tree-level couplings. We will then recast the experimental constraints from the CMS and ATLAS collaborations in this parametrisation, and use them to constrain a set of models.

The fourth chapter will focus on another aspect of the scalar sector: the possible presence of additional scalars, and more precisely in our case, of one lighter than 125 GeV . After extending the previous parametrisation to this second scalar, we will see to what extent it can be used to constrain models in which it exists, first in a model independent way, and then by taking the example of to sample models: the 2HDM and the NMSSM.

Finally, the fifth and last chapter will focus on possible improvements for this constraining method. We will first see that in a reasonable case, it can be used to consistently include recent measurements of the contribution of the Higgs boson to processes while it is off-shell, focusing on the case of its participation to $gg \rightarrow 4\ell$. We will also present two possible ways of improving the procedure by reducing the number of approximations, with the use of likelihood functions provided by experiments on the one hand, and the introduction of pseudo-observables for a more general framework.

Chapter 1

Global overview of Particle Physics

The aim of Physics as a science is to understand and to be able to predict how or why phenomena we observe occur the way we observe them in the world around us. To reach this purpose, physicists set up as rigorous and repeatable experiments as possible, and then develop models and techniques, based on assumptions, approximations and mathematical rules, deducing behaviour rules for the system they try to represent, to match with their observations. This vast project has led with time to the construction of a wide variety of models, describing phenomena in all domains of physics.

However, according to most physicists, for identical predictions, the less assumptions a model has to rely upon, the better. In order to match with this criterion – known as Occam's razor – and as we understood more and more about our world, models describing different phenomena were gathered in unified descriptions, as for instance in the case of the description of electric and magnetic fields, described respectively by the laws of electrostatics and magnetostatics, which were united through Maxwell's equations modelling electromagnetism. On this path, particle physics is one of the most successful models in physics, describing matter and three of the four fundamental interactions with computed predictions matching experiments with outstanding precision.

These predictions are based on the so-called Standard Model of particle physics (SM), the (ever-growing) most complex structure and basis in terms of models, relying on an astonishingly small number of assumptions and parameters. The construction of this model, nowadays based on the notion of fields and symmetries, is alongside General Relativity the furthest outreach of the search for a theory explaining every aspect of our environment at the fundamental level.

1.1 Building up the standard model

In the Standard Model [1–3], in a simplified description, matter is built out of a limited number of elementary kinds of fermions, and three of the four known fundamental interactions between them (electric, weak and strong) are represented by the exchange of gauge bosons. The fermions are divided into two categories, leptons and quarks, according to whether or not they are affected by the strong interaction. The gauge bosons on the other hand, are named gluons when transmitting

the strong interaction, the 3 weak ones are called W^+ , W^- and Z^0 , and the photon, A or γ is associated to the electromagnetic interaction.

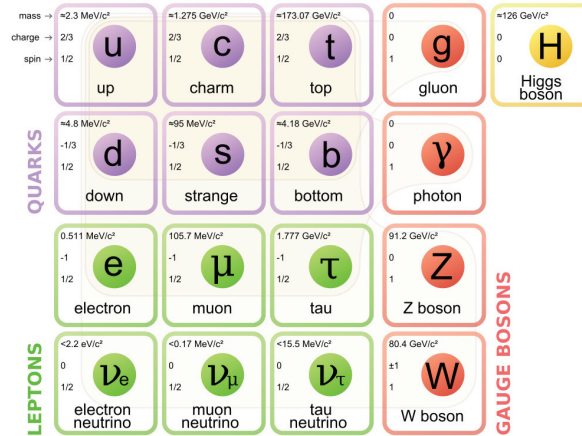


Figure 1.1: Particles building up the standard model and their interactions. Image courtesy of Wikimedia

The fermions can be gathered into three generations, each composed of two leptons and two quarks. The first generation is made of the up and down quarks, and of the electron and its associated neutrino, and makes up most of the matter in the universe. The second and third generations consist of particles possessing the same quantum numbers, but with higher masses. The quarks are called charm, strange, bottom and top, and the leptons muon and tau, again with their associated neutrinos. This is summed up in figure 1.1.

This description relies on many different developments, among which Lagrangian mechanics. In this framework, the assumption of a given expression for the Lagrangian makes it possible to determine the equations of motion, using the principle of stationary action (sometimes minimal or extremal action). This theory, first developed for point-like particles, transformed into quantum field theory, which is the basis for all calculations in the SM.

Symmetries in physics

One particularly interesting notion in physics in general, and in particular in the study of the properties implied by the choice of a Lagrangian is the idea of symmetries, *i.e.* transformations under which the system (or in our case, the Lagrangian describing the system) is invariant. Some simple examples include for instance translations or rotations of space. When considering more complex transformations, such as the exchange of particles, very interesting conclusions might be drawn, such as the links between the couplings of different particles.

Gauge symmetries are a particular type of symmetries, as they are local *i.e.* a type of symmetry where the transformation applied to the fields is different in every point of space-time. As these transformations are then affected by space transformation, in order to keep the theory coherent, it is necessary to modify the way the dynamics of particles are described, with the introduction

Type	Notation	$SU(3)_C$	$SU(2)_W$	$U(1)_Y$	$U(1)_{em}$
Quarks (fermion, $s=1/2$)	$Q_L = \begin{pmatrix} u_L \\ d_L \end{pmatrix}, \begin{pmatrix} c_L \\ s_L \end{pmatrix}, \begin{pmatrix} t_L \\ b_L \end{pmatrix}$	3	2	1/6	$\begin{pmatrix} 2/3 \\ -1/3 \end{pmatrix}$
	u_R, c_R, t_R	3	1	2/3	2/3
	d_R, s_R, b_R	3	1	-1/3	-1/3
Leptons (fermion, $s=1/2$)	$l_L = \begin{pmatrix} \nu_e \\ e_L \end{pmatrix}, \begin{pmatrix} \nu_\mu \\ \mu_L \end{pmatrix}, \begin{pmatrix} \nu_\tau \\ \tau_L \end{pmatrix}$	1	2	-1/2	$\begin{pmatrix} 0 \\ -1 \end{pmatrix}$
	e_R, μ_R, τ_R	1	1	-1	-1
Gauge bosons	W_i^μ	1	3	0	0, ± 1
	g_a^μ, G_a^μ	8	1	0	0
	B^μ	1	1	0	0

Table 1.1: Particle content of the SM. One can notice the chiral character of the weak interaction, through the distinct quantum numbers of right-handed and left-handed fermions.

of gauge fields and covariant derivative, which takes parallel transport into account. The gauge fields therefore carry some information about how the gauge transformations vary in space-time.

Since the set of symmetries of a problem is mathematically described by the notion of a group, meaning mainly that the combination of two symmetries must remain a symmetry, one has to resort to **group theory** to describe properly these symmetries. Furthermore, as all fields describing particles are objects on which those transformations act, it is useful to also use **representation theory**. They will then be described as representations of the symmetry group, specifying how each field behaves under the action of each transformation. As we want the transformations to be symmetries of the Lagrangian, the latter must be formed of operators which do not transform, or singlets.

In the SM, the gauge group is the semi-simple Lie group $SU(3)_C \times SU(2)_W \times U(1)_Y$, describing the strong, weak, and electromagnetic interactions, and providing us with the 12 previously described gauge bosons: 8 gluons, the weak gauge bosons W^\pm and Z^0 , and the photon A .

However, the property of confinement of QCD making the colour structure of objects invisible in non-hadronic physics studies, the 8 gluons have a very similar phenomenology, and are often referenced under only one name. This confinement and screening property also makes the strong interaction effectively short-ranged, in a different manner from the weak interaction as we will see further on.

When trying to build a Lagrangian giving the proper description of the dynamics of those

particles, QFT tells us it must take the following form:

$$\begin{aligned}\mathcal{L} &= \mathcal{L}_{gauge} + \mathcal{L}_{fermions} \\ \mathcal{L}_{Gauge} &= -\frac{1}{4} \left(\sum_X X_a^{\mu\nu} X_{\mu\nu}^a + 2m_X^2 X^\mu X_\mu \right) \\ \mathcal{L}_{Fermions} &= \sum_\psi \bar{\psi} (\not{D} - m_\psi) \psi\end{aligned}$$

where ψ spans each kind of fermion, and X each kind of gauge boson, $D\psi$ is the covariant derivative of ψ , m_X is the mass of the X gauge boson. $B^{\mu\nu}$, $W_i^{\mu\nu}$ and $G_a^{\mu\nu}$ are the field strengths of the gauge bosons, with expressions:

$$\begin{aligned}D^\mu \psi &= (\partial - ig_s G_a^\mu T^a - ig_W W_i^\mu t^i - ig_1 Y B^\mu) \psi \\ B^{\mu\nu} &= \partial^\mu B^\nu - \partial^\nu B^\mu \\ W_i^{\mu\nu} &= \partial^\mu W_i^\nu - \partial^\nu W_i^\mu + g_W \varepsilon_{ijk} B_j^\mu G_k^\nu \\ G_a^{\mu\nu} &= \partial^\mu G_a^\nu - \partial^\nu G_a^\mu + g_s f_{abc}^{SU(3)} G_b^\mu G_c^\nu\end{aligned}$$

t^i and T^a represent the generators of the $SU(2)$ and $SU(3)$ gauge groups, and Y is the hypercharge. They are defined by their commutation relations and the structure constants ε_{ijk} and f^{abc} , and their action on the spinor ψ depends on the representation of the group the fermion is in (in the SM, T^a are either 0 or the Gell-Mann matrices, and t^i are either 0 or the Pauli matrices). We can see when expanding this Lagrangian that gauge interactions come straight from the kinetic terms, with the need for covariant derivatives for the consistence of the theory.

However, although seemingly giving the proper equations of motion, this Lagrangian does not respect the required symmetries, especially in the mass terms: they either combine left-handed with right handed spinors or mix non-compatible gauge eigenstates for fermions, and are not gauge invariant for gauge bosons if $m_X \neq 0$.

1.2 Higgs Physics and phenomenology

The masslessness of the gluons and the photon makes this problem disappear, however the description of weak gauge bosons can't slip through that escape hole. The first clue that weak gauge bosons are massive and that there was a need for such an $m_X^2 X^\mu X_\mu$ goes back to before there even was a gauge theory, to the fact that the weak interaction is short-ranged.

As it was identified as the source of β -radioactivity, therefore an interaction between baryons and leptons, it was first modelled as a contact interactions between four fermions, using so-called Fermi interactions. However, when working in 4 dimensions in which case spinors describing fermions are considered as dimension 3/2, this description included six-dimensional operators in the Lagrangian, which implied the non-renormalisability of the theory, *i.e.* problems with phase-space integration for large values of impulsions, if the theory is true at those scales.

This means that this description was only a low-energy effective description of a theory where this point-like interaction is actually induced by the exchange of a boson between two pairs of fermions. For a massive vector boson, quantum field theory predicts that for a centre-of-mass energy much lower than the boson mass, the propagator can be considered at leading order as constant and proportional to the inverse of the squared mass of the exchanged boson, effectively being described by the 6-dimensional operator used previously.

However, the gauge theory, which was developed to describe electrodynamics, only describes massless gauge bosons, since as we stated previously, a mass term $m^2 X^\mu X_\mu$ is not invariant under gauge transformations. This led to the introduction of the Higgs mechanism in the formulation of the electroweak part of the SM. [1–3]

1.2.1 The Higgs mechanism

The Higgs mechanism is a process, inspired from the spontaneous symmetry breaking (SSB) in a condensed matter context [4], which provides the Standard Model with a renormalisable, gauge invariant Lagrangian accounting for the mass of gauge bosons.

In the SM, the framework for this spontaneous symmetry breaking to happen requires the inclusion of an additional elementary scalar field, doublet under $SU(2)_W$:

Type	Notation	$SU(3)_C$	$SU(2)_W$	$U(1)_Y$	$U(1)_{em}$
Scalar (boson, s=0)	$\Phi = \begin{pmatrix} \phi^+ \\ \frac{1}{\sqrt{2}}(\phi^0 + i\tilde{\phi}^0) \end{pmatrix}$	1	2	1/2	$\begin{pmatrix} 1 \\ 0 \end{pmatrix}$

Among the various terms included in the Lagrangian with the inclusion of this new field Φ , the ones essential for it to play its symmetry-breaking role are its self interactions, which can be modified by radiative correction through the intervention of other particles. They are modelled by the most general renormalisable and gauge-invariant potential:

$$V = -\mu^2 \Phi^\dagger \Phi + \lambda (\Phi^\dagger \Phi)^2 \quad (1.1)$$

However for $\mu^2, \lambda > 0$, the only gauge-invariant equilibrium state in this potential, $\Phi = 0$, is unstable and the Higgs doublet therefore experiences a SSB: the set of stable equilibrium positions is still invariant under the electroweak gauge transformations, but the individual states no longer are. Therefore, establishing one specific state makes the physical state asymmetric under the symmetries of the equations, breaking them 'spontaneously'.

Since the vacuum is uncharged and not \mathcal{CP} -violating, only ϕ^0 acquires a vacuum expectation value (vev) corresponding to the minimum of the potential $v = \frac{\mu u}{\sqrt{2}\lambda}$ and we can write the value of the equilibrium position in this potential as

$$\langle \Phi \rangle = \frac{1}{\sqrt{2}} \begin{pmatrix} 0 \\ v \end{pmatrix}$$

In order to make the effective Lagrangian more readable, the Φ field can be expanded around its vev, so that one can write $\phi^0 = v + h$ and the Higgs boson h finally makes its appearance as the leftover field after the SSB, for which the potential induces a mass term $m_H = 2\mu$. After the breaking occurs, three of the four degrees of freedom of the doublet behave as Goldstone bosons, and appear in the Lagrangian as longitudinal components of the massive gauge bosons.

The Lagrangian of the SM is therefore completed by

$$\mathcal{L}_H = (D^\mu \phi)^\dagger (D_\mu \phi) - \mu^2 \Phi^\dagger \Phi + \lambda (\Phi^\dagger \Phi)^2$$

with again

$$D\Phi = \partial\Phi - ig_W W_i^\mu t^i \Phi$$

When using the $\phi = v + h$ expansion, and developing explicitly the $SU(2)$ matrix products of the kinetic term in \mathcal{L}_H , 4 new states formed by a mixing of the $SU(2)_W \times U(1)_Y$ gauge bosons appear as bosons with effective mass terms

$$\begin{aligned} A^\mu &= \sin \theta_W W_3^\mu + \cos \theta_W B_\mu \\ Z^\mu &= \cos \theta_W W_3^\mu - \sin \theta_W B_\mu \\ W_\pm^\mu &= \frac{W_1^\mu \mp iW_2^\mu}{\sqrt{2}} \end{aligned}$$

with the Weinberg angle θ_W defined by $\cos \theta_W = \frac{g_W}{\sqrt{g_W^2 + g_1^2}}$ and $\sin \theta_W = \frac{g_1}{\sqrt{g_W^2 + g_1^2}}$

and with $m_A = 0$, $m_W = \frac{v g_W}{2}$, $m_Z = \frac{m_W}{\cos \theta_W}$ and $e = \frac{g_W g_1}{\sqrt{g_W^2 + g_1^2}}$

We can here notice that the presence of the doublet vev v in the expression of the masses of the bosons, shows explicitly the role of the doublet and of the SSB in the existence of these terms. As a side note, the two parameters of the Higgs potential μ and λ can be translated directly into v and m_H , and with the measurement of the gauge boson masses, the vev can be measured, leaving only m_H as a parameter of the symmetry breaking.

Yukawa couplings

Another nice feature of the Higgs mechanism is that in addition to providing a simple, gauge invariant framework explaining the existence of masses of the gauge bosons, it also provides without too many further assumptions mass terms for the fermions that do not break the electroweak symmetry. As a weak doublet, and taking into account the quantum numbers of the standard model gauge fields, the Φ field can be used to couple left-handed and right-handed fermions as needed to form a mass term without breaking the SM symmetries. The terms included in the Lagrangian in that prospect can be written in their most general form

$$\mathcal{L}_Y = - \sum_{i,j=1}^3 Y_{ij}^u Q_{L,i}^\dagger (i\sigma_2 \Phi^*) u_{R,j} - \sum_{i,j=1}^3 Y_{ij}^d Q_{L,i}^\dagger \Phi d_{R,j} - \sum_{i,j=1}^3 Y_{ij}^l L_{L,i}^\dagger \Phi l_{R,j} + h.c.$$

where Y_{ij}^u , Y_{ij}^d , and Y_{ij}^l are 3×3 complex matrices called the Yukawa couplings, mixing the different generations of each kind of fermions. After symmetry breaking, these terms can be decomposed into charged currents, neutral currents, couplings of the fermions to the Higgs boson, and finally where the vev appears, mass terms. To diagonalise them to real diagonal matrices and get mass terms involving only one fermion, we introduce 6 hermitian matrices $V_{L,R}^{u,d,l}$ rotating each kind of fermion, so that

$$Y_{diag}^u = V_L^u Y^u V_R^{u\dagger}, \quad Y_{diag}^d = V_L^d Y^d V_R^{d\dagger}, \quad \text{and} \quad Y_{diag}^l = V_L^l Y^l V_R^{l\dagger}$$

However, V_L^u and V_L^d are both matrices rotating the doublet Q_L in generation space, but are not identical in general, since Y^u and Y^d are random matrices in the SM. Therefore the redefinition of fields needed to define mass eigenstates will have an influence on the kinetic term of Q_L , and more particularly on the weak part of the covariant derivative, which will not couple mass eigenstates but rather a mixing through a term proportional to $u_{L,i}^\dagger d_{L,j} \mathcal{V}_{ij} W^+$ where $\mathcal{V} = V_L^u V_L^{d\dagger}$ is the so-called Cabibbo-Kobayashi-Maskawa (CKM) matrix, describing the mixing of generations through the weak interaction.

As we have seen, the Higgs boson therefore interacts with most particles in the standard model, through loops of other particles if not at tree-level. Two more non-obvious couplings that will be useful are the coupling to a pair of gluons and the one with a pair of photons, which will be slightly detailed further on.

Moreover, in the case a light Higgs boson, i.e. with a mass around or under the value of the vev v , which is the case of the observed boson, its width is quite small, meaning that it has a long lifetime (for a 125 GeV Higgs boson in the SM, $\Gamma_H \approx 4 \text{ MeV}$). In that situation, its propagator can be considered as “peaked” enough to impose that the transferred centre-of-mass energy \sqrt{s} in its production is equal to its mass, and production and decay can be studied independently with a good approximation. We will therefore see the characteristics of the main production and decay modes of the Higgs boson in the case of a hadron collider such as the LHC. [5]

1.2.2 Production mechanisms at a hadron collider

As most elementary particles in the SM, the Higgs boson is unstable, with a very short lifetime. Because of this, it cannot be observed directly, and must therefore be looked for indirectly, by studying processes its existence affects. To observe these, the experiments must be held in conditions as precise as possible. Particle colliders are the only known way to produce in a controlled way particles with such short lifetimes and heavy masses. Moreover, the easiest way to observe a particle is often to observe its decay products after it has been produced, which is

the case for the Higgs boson. The phenomenology studies must therefore include both how it is produced and to what final states it decays.

The relevant ways in which the Higgs boson is produced experimentally depend on the type of experiment being conducted. The interesting production mechanisms involved at lepton colliders such as the LEP are different from the ones involved at hadron colliders such as the LHC or TeVatron. The production modes of the Higgs boson can be at leading-order (LO) divided in the same way as its couplings were, through gauge bosons or through Yukawa couplings.

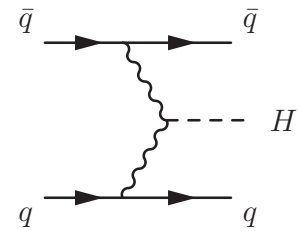
We will here focus on the case of a 125 GeV boson and give values for $\sqrt{s} = 8 \text{ TeV}$, in which case there are mainly four modes representing more than 99% of the total cross section.

Electroweak related production modes

As stated several times before, the Higgs boson has a privileged link to the electroweak gauge bosons, since it was introduced in the standard model specifically to give them mathematically-coherent mass terms. Therefore it seems quite clear that one way to produce it will come through the intermediate of its coupling to the gauge bosons. However although important, and even dominant in lepton colliders, these are not the dominant production modes at hadron colliders.

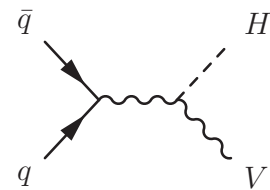
Vector Boson Fusion (VBF)

At the LHC, the most prominent electroweak-related production mode is through the fusion of two W^\pm or two Z bosons radiated by incoming quarks. The production cross section through this mode is $\sigma_{VBF} \approx 1.75 \text{ pb}$ [6], which means it represents about 7% of the total cross section. It has the particular signature of having two additional jets from the outgoing quarks, often highly energetic and close to the beam axis, and can therefore be distinguished from other production modes through an adequate veto on the observed events.



Associated production (VH)

The other main way to produce the Higgs boson through its coupling to weak gauge bosons is by producing of an off-shell gauge boson which then radiates a Higgs boson to come to its mass shell. With the contribution of both gauge bosons, $\sigma_{WH} + \sigma_{ZH} \approx 0.695 + 0.41 \text{ pb}$ [6]. It also has a distinctive signature, as the decay products of the Higgs boson have to be looked for alongside those of a weak gauge boson, which is experimentally separated into two searches, as W and Z have very different decay modes.



Yukawa-related production modes

At hadron colliders such as the LHC, where QCD and therefore quarks play an important role, this sector leads to two main ways of producing the Higgs boson. In particular, the top quark plays a notable role among the other quarks, as it has the largest Yukawa coupling.

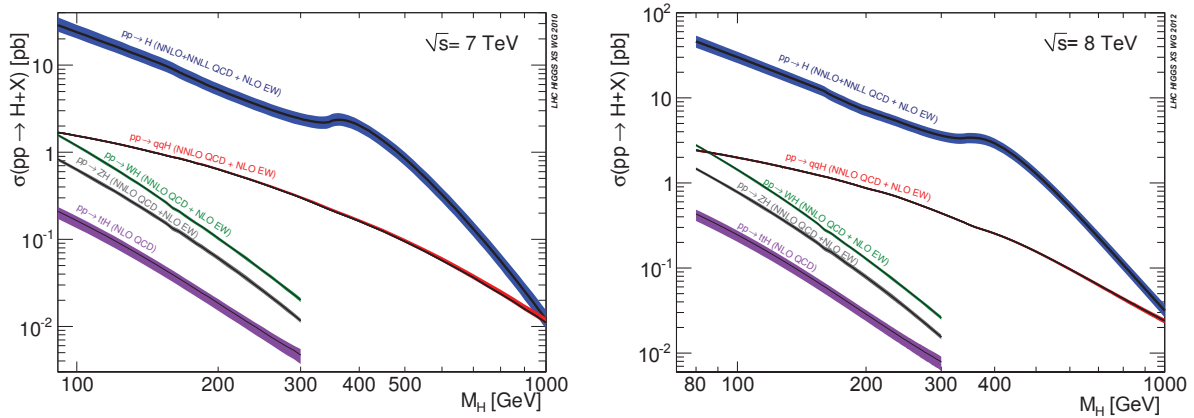
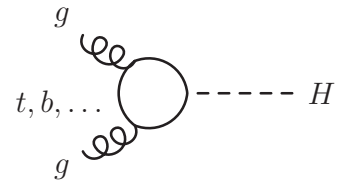


Figure 1.2: Contribution of the different Higgs production modes as a function of the Higgs mass, for a proton-proton collider and for $\sqrt{s} = 7$ and 8 TeV [6]

Gluon fusion (ggh)

In this production mode, quarks and Yukawa couplings only appear as messengers between gluons and the Higgs boson. Even though gluons are not coupled directly to the Higgs boson (as it does not carry any colour charge), this production mode is the most prominent one at the LHC, to be accounted for about 87% of produced Higgs bosons with $\sigma_{ggh} \approx 19 \text{ pb}$. This effect comes from Parton Distribution Functions (PDF), describing the probability of finding a given parton of given momentum inside a hadron. In the case of highly energetic protons, the high probability of finding highly energetic gluons is very high, making up for the loop-reduced coupling. At LO and without taking PDFs into account, the cross section is given by: $\sigma_{LO}(gg \rightarrow H) = \pi^2 \Gamma_{LO}(H \rightarrow gg) \delta(\sqrt{\hat{s}} - m_H) / 8m_H^2$, where $\sqrt{\hat{s}}$ is the gluon pair invariant energy squared, and $\Gamma_{LO}(H \rightarrow gg)$ will be expressed more explicitly later on.



Top-quark-pair-associated production ($t\bar{t}h$)

The large top Yukawa coupling plays a more direct role in this production mode, in which the Higgs boson is produced in association with a top-antitop quark pair. With $\sigma_{t\bar{t}h} \approx 0.12 \text{ pb}$, this production mode represents less than 1% of the total cross section and therefore yields a very low number of events. However, the distinct experimental signature of a $t\bar{t}$ pair still makes this production mode experimentally interesting, since it can be used as a direct probe for the $t\bar{t}h$ coupling

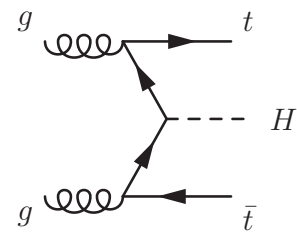
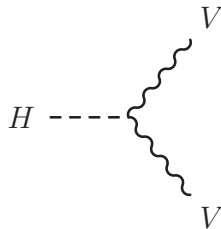


Figure 1.2 represents the contribution of the various mechanisms to the production of Higgs bosons, as a function of the mass of the would-be Higgs boson, for $\sqrt{s} = 7TeV$ on the left and $8TeV$ on the right. As one could expect, the heavier the boson is, the harder it is to produce, and all cross section curves decrease as m_H goes up. One slight bump occurs in the ggh production cross section at the threshold above which the top quarks in the loop can be on-shell. On the other hand, for a higher value of \sqrt{s} , cross sections increase, giving colliders at higher energies another reason to be interesting.

In order for the predictions of these cross sections to be as precise as possible, the calculations include more than the tree-level diagrams shown here, and take into account inclusive production, meaning including the production of Higgs bosons jointly with other particles building up the underlying event which can hardly be constrained because of pile-up, as well as diagrams including more loops. However, these corrections, coming mostly from QCD, can approximately be included by multiplying by a K-factor, rescaling a given computed cross sections by a constant number. Another important factor in the relative importance of the different modes are the PDFs, making for instance the ggh stand out a lot more than could be expected, because of the large proportion of low-momentum gluons in a proton. One can notice that for higher masses the VBF mode, based on an initial state with quarks, catches up with the ggh mode.

1.2.3 Decay channels

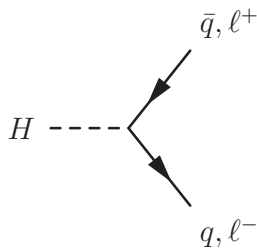
In a similar fashion, in the SM the main final states into which the standard Higgs boson decays can be split into three categories : gauge-related, Yukawa-related, or through loops, which might mix those two sources. Concerning the phenomenology, the partial widths Γ_i are of little importance, but what matter are the branching ratios (BR) $BR_i = \Gamma_i/\Gamma_H$ with $\Gamma_H = \sum_i \Gamma_i$, since they determine the fraction of produced Higgs boson decaying through the channel i .



Decays to gauge bosons

The Higgs can decay to a final state with two gauge bosons, however depending on its mass, the two bosons might not be on their mass shell. On fig.1.3, we can see that around the thresholds of $m_H = 160 GeV$ the WW final state takes a lot of importance with all other BR rapidly decreasing, then around $m_H = 180 GeV$ the ZZ final state rises. At high masses, they are the dominant

final states, but under the thresholds they take the form of WW^* or ZZ^* with the off-shell boson immediately decaying, and become less important at low m_H .



Decays to fermions

The direct decays to quarks suffer from the low Yukawa couplings giving small partial widths, as most of them are $\lesssim 1/100$, and therefore only profit of the absence of the gauge boson ones at low m_H . On the other hand, the only quark with a $\mathcal{O}(1)$ coupling, the top quark, cannot form $t\bar{t}$ pairs as there is not enough phase-space available at these masses, and only appear above the threshold

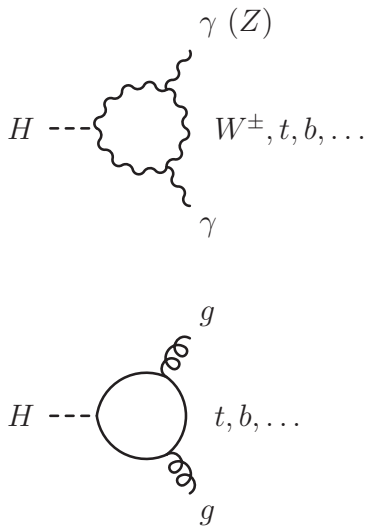
of $m_H = 2m_t \approx 350 GeV$. For light fermions, in the Born approximation the partial decay width

is given by:

$$\Gamma_{Born}(H \rightarrow f\bar{f}) = \frac{G_F N_c}{4\sqrt{2}\pi} m_H m_f^2 \left(1 - \frac{m_f^2}{m_H^2}\right)^{3/2}$$

where N_c is the number of colours of the fermion and G_F is the Fermi constant, and we can see that the partial widths grow with fermion masses, and below $m_H = 2m_t$ they are in order of importance $b\bar{b}$, $\tau^+\tau^-$, $c\bar{c}$, $\mu^+\mu^-$, $s\bar{s}$, $d\bar{d}$, $u\bar{u}$ and e^+e^- . However at hadron colliders, QCD noise makes final states with quarks hard to identify, and $b\bar{b}$ is the only one identifiable through efficient b-tagging (method aimed at detecting displaced vertices of the decay of “long-lived” B mesons), with a BR up to more than 80%. On the lepton side, only the $\tau^+\tau^-$ final state is interesting, $\mu^+\mu^-$ and e^+e^- representing too few events.

Decays through loops



These Higgs boson decays only appear at loop-level: even though the Higgs boson doesn't carry either electrical or colour charges, it can decay to a pair of photons or a pair of gluons through loops of weak gauge bosons or quarks, which should therefore represent small partial widths because of the loop suppression. Once again at hadron colliders, the QCD noise drowns out the gluon decay signal whose signature is simply two jets. On the other hand, as the photon is stable and cleanly measurable, the $\gamma\gamma$ signal is clean, even though it suffers from a very low BR. The decay mode γZ also exists through the same loops as the $\gamma\gamma$ one, but is less sensitive experimentally because of the Z decaying, and we won't focus on it in this thesis. At one loop, the partial widths to gg and $\gamma\gamma$ are given by:

$$\Gamma(H \rightarrow gg) = \frac{G_F \alpha_s^2 m_H^3}{36\sqrt{2}\pi^3} \left| \frac{3}{4} \sum_q \mathcal{A}_{1/2}(\tau_q) \right|^2 \quad (1.2)$$

$$\Gamma(H \rightarrow \gamma\gamma) = \frac{G_F \alpha^2 m_H^3}{128\sqrt{2}\pi^3} \left| \sum_f N_c Q_f^2 \mathcal{A}_{1/2}(\tau_f) + \mathcal{A}_1(\tau_W) \right|^2 \quad (1.3)$$

where $\mathcal{A}_{1/2}$ and \mathcal{A}_1 are the form factors of these loops for spin- $\frac{1}{2}$ and spin-1 particles:

$$\begin{aligned} \mathcal{A}_{1/2}(\tau) &= \frac{2}{\tau^2} (\tau + (\tau - 1)f(\tau)) , \\ \mathcal{A}_1(\tau) &= -\frac{1}{\tau^2} (2\tau^2 + 3\tau + 3(2\tau - 1)f(\tau)) , \end{aligned}$$

with the parameters $\tau_i = \frac{m_H^2}{4m_i^2}$ and

$$f(\tau) = \begin{cases} \arcsin^2 \sqrt{\tau} & \tau \leq 1 \\ -\frac{1}{4} \left[\log \frac{1+\sqrt{1-\tau^{-1}}}{1-\sqrt{1-\tau^{-1}}} - i\pi \right]^2 & \tau > 1 \end{cases} .$$

These expressions will come in handy when discussing the search for new physics through the Higgs boson couplings.

At this point, it is worth noticing that even though the various couplings of the Higgs boson don't change when its mass changes (it is a free parameter in the SM), its phenomenology does change a lot, since the phase space available to different decay modes change drastically. From this point of view, $m_H = 125 \text{ GeV}$ stands in the peculiar zone between two windows, one at lower mass where most of the produced Higgs bosons would decay to a pair of b quarks without little to no sign of gauge bosons and another one at high mass, where on the contrary it would almost exclusively decay to weak gauge bosons, without trace of the Yukawa couplings. This particularity, even though slightly diminishing each branching ratio, makes at the same time more final states available, and therefore more couplings testable.

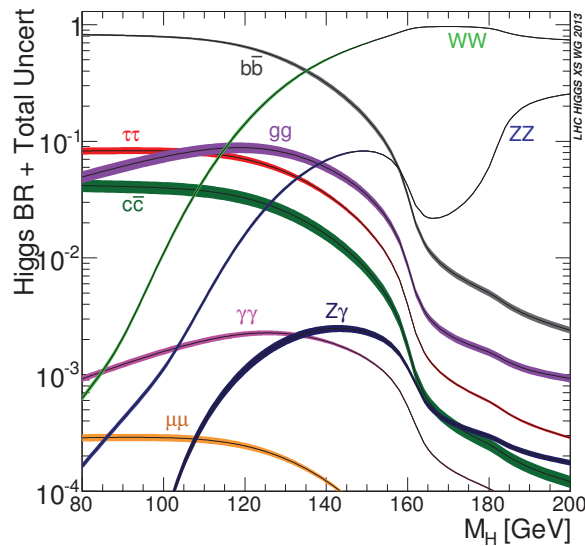


Figure 1.3: Branching ratios of the most prominent decay modes of SM Higgs boson with their uncertainties, as a function of the Higgs boson mass

1.3 Shortcomings of the Standard Model

As we said at the beginning of this chapter, along its development, the SM has reached a precision in the description of the behaviour of (what we consider to be) the most elementary components of the universe that is far from being equalled in other domains of physics. Notwithstanding those marvellous accomplishments, a few shortcomings still blot the picture, making it obvious that this description should still be extended. The short list presented here is of course not extensive.

\mathcal{CP} -strong

The \mathcal{CP} symmetry was thought for a long time to be a symmetry of elementary processes, meaning that simultaneously exchanging particles with their anti-particles and reversing all directions of space would keep the rate of a process unchanged. When it was discovered that it was not a symmetry of the electroweak interaction, broken by a complex phase in mixing parameters of the CKM matrix, there was no reason to still think that it would be a symmetry of the strong interaction either. But when including the \mathcal{CP} -breaking term built on the gluon field strength $\theta \varepsilon^{\mu\nu\rho\sigma} G_{\mu\nu} G_{\rho\sigma}$, constraints from the absence of a measurable electric dipole in the neutron imply that $|\theta| < 10^{-11}$. The smallness of this parameter is therefore subject to question, as it has no reason to be so small when compared to other parameters of the Lagrangian. One of the attempts explaining this matter is the Peccei-Quinn mechanism [7].

Hierarchies

Two different hierarchy debates are present in the SM. The first one concerns the fermion masses, given by the Yukawa matrices which are parameters that seem to grow with generation for no apparent reason. Moreover, these masses span over almost 5 orders of magnitude even when not taking into account the neutrino masses which now appear to exist. Without any mechanism to explain this wide spread, this set of Yukawa couplings brings for a single sector numerous parameters seemingly unrelated and only dictated by experimental values of the masses.

The other hierarchy present in the SM is even wider and concerns the characteristic scales of the different interactions: Λ_{QCD} , $v(EW)$, M_{Pl} . There is no problem concerning the QCD scale, as it is a dynamical quantity. However the difference between the electroweak vev v and M_{Pl} , characteristic scale of gravitation, around $10^{19} GeV$, is unexplained. This becomes even more of a problem when looking at radiative corrections to the mass of the Higgs, which gets quadratically divergent contributions from the W^\pm and Z bosons, its self-coupling and the top quark:

$$\delta m_h^2 \sim \frac{1}{32\pi^2} \left[\left(\frac{1}{4}(3g_W^2 + g_1^2) + 6\lambda - 6y_t^2 \right) \Lambda^2 + \mathcal{O}(\log \Lambda) \right]$$

where Λ is the cut-off scale, meaning that the bare mass present in the Lagrangian would have to be very finely tuned to be as low as $125 GeV$ with such large corrections if the SM were true up to M_{Pl} .

Gravitation

One of the most problematic issues of the SM comes from the absence in the description of gravitation. This lack comes from the fact that this interaction is very weak compared to the others, only having a noticeable influence on macroscopic scales, where on average matter is not charged under the SM gauge group. However, as it is one of the 4 fundamental interactions, it seems necessary to find a way to reconcile general relativity and quantum mechanics, which were developed independently. There are many efforts in this path, such as quantum gravity and spinfoams, string theory or supergravity, but none of them is yet completely satisfactory.

Neutrino masses [8]

Neutrinos have recently been proved to have a mass, because of oscillations occurring between the different flavours of neutrinos, giving a clue of a mixing matrix of the kind of the CKM, called the PMNS matrix in extensions including it. However, the simple solution of adding to the SM spectrum a right-handed species of neutrino and using it to build mass terms as it was done for other fermions is not a satisfying answer, and more complicated solutions have been proposed, such as seesaw mechanisms or Majorana masses, to cope with other problems at the same time.

Dark matter, dark energy

Along the XXth century, more and more evidence has come from cosmology to support the idea that most of the matter in our universe is not made of baryonic matter such as the one surrounding us (mainly protons), and no particle in the SM matches the requirements for abundance, electric neutrality, stability. This claim also gains in credibility from the fact that those pieces of evidence come from different scales and types of experiments: galaxies with rotation curves, galaxy clusters with gravitational lensing, global scale with the cosmological microwave background, or red shift in galaxies and Hubble's law. In addition to this dark matter, the SM also seems to lack the description of an even more mysterious dark energy, or cosmological constant, with another fine tuning problem. Even though some theories try to avoid having to include those, such as MODified Newtonian Dynamics (MOND) or replacing dark matter with MASSive Compact Halo Objects (MACHOs), no final answer has been given to this question.

Chapter 2

Statistics in particle physics

2.1 Mathematical tools

Like all models of physics, the SM (and its extensions) is only a model, and the description it makes of reality is expected to only match with observations within some range. This limitation might come from a lot of different possible sources, whether it is from uncertainties on the validity of approximations used, on the measurements, from statistical fluctuation,... But although in many other domains of physics this uncertainty mostly relies on the experimental precision of the measurements, in the case of particle physics it is in great part a consequence of both facts that predictions rely on huge phase-spaces, making integration (numerical or analytic) hard, and the fact that the theory is quantum, making every prediction a probability density function.

In order to cope with those challenges, on the one hand new methods are developed to make integration more efficient (especially through algorithms such as Monte-Carlo integration). On the other hand, the search for processes with low probabilities of happening leads to the need of numerous experiments, and the treatment of such an amount of data can only be done properly through the use of statistics.

2.1.1 Basic definitions

In order to do so properly, it is necessary to define several tools to formulate precise results and draw rigorous conclusions. The first object, used to represent an unknown quantity such as a measurement whose outcome is unknown, is the random variable, followed closely by its probability density functions (pdf), representing the probability for the variable to take each possible value. Several of those, appearing recurrently, are labelled by specific names. The most useful in our case are:

- **Normal or Gaussian distribution:** The Gaussian Distribution is probably the most-used probability distribution, as it is very simply defined by two parameters (mean X_0 and variance σ^2), distributed along $P(X) \propto e^{-(X-X_0)^2/2\sigma^2}$. It particularly stands out among other distributions because of the Central Limit Theorem which says it is the limit towards

which tends the pdf of the mean of a large sample of independent identically-distributed random variables for any distribution that has a given mean and variance.

- **Poisson distribution:** This distribution represents the probable repartition around the expected value of outcomes of counting experiments. For a large number of expected events, the Poisson law gets asymptotically closer to a Gaussian distribution. In the case where we consider measurements of different collisions to be independent, this is the distribution followed by event-counting measurements in particle physics.
- χ^2 **distribution:** The χ^2 distribution with k degrees of freedom (d.o.f.) is the distribution of the sum of the squares of k independent normally-distributed random variables. Squares being used to calculate distances between points of a space, this distribution often appears in minimisation procedures.

Once these objects are defined, there are several ways to interpret their meaning, as well as the link between probabilities and statistics, and therefore to treat experimental results. Two among the most used are the bayesian approach (or inference) and frequentist approach.

Bayesian approach

The first one relies on the attempt of assessing the probability for an hypothesis to be true. It is named after Thomas Bayes, and more specifically after the rule he studied and worded at the end of the 16th century, so-called 'Bayes's rule', which gives a link between the probability of an hypothesis A before and after an experiment E . In terms of conditional probabilities, if $P(A|E)$ describes the conditional probability for A to be true knowing E is true, Bayes's law can be written as:

$$P(A|E) = \frac{P(E|A)}{P(E)}P(A)$$

$P(A|E)$ and $P(A)$ are respectively called the posterior and prior distributions. $P(E)$ represents the absolute probability for the outcome of the experiment to be E , and $P(E|A)$ is called the likelihood: it represents the probability that the experiment would give an outcome E if the hypothesis A were true. It might be calculated for a given hypothesis and is often written as a function of A , $\mathcal{L}(A|E) = P(E|A)$. The larger the likelihood, the more the experiment tends to favour the hypothesis. However, it is not a probability density function.

Frequentist approach

The other inference of statistics presented here is called the frequentist approach. It is based on the idea that an hypothesis is either true or false, or that a parameter only has one true value. The tests in this approach then come from the consideration that a set of measurement can be considered as one of an infinity of such sets, all statistically independent outcomes of the same experiment. In this approach, the validity of an hypothesis is assessed through its compatibility with the sample obtained experimentally. From the knowledge that this sample is

only one of the many possible outcomes, the probability of fluctuations is taken into account, and conclusions are drawn with a given Confidence Level (C.L.). C.L. might take any value from 0 to 1, but the usual ones correspond to the C.L. at which would be excluded a point outside of an interval of an integer number of standard deviations, $1\sigma, 2\sigma, 3\sigma, \dots$, around the mean for a 1-dimensional normal distribution. This corresponds to confidence levels approximately equal to 68.2%, 95.5%, 99.7%, \dots . Thus when tested in a frequentist way, an hypothesis is either rejected or not, and the result is given with a level of confidence that the right choice is being made.

2.1.2 Likelihood

Although these two approaches are often presented as opposed in the sense that one has a continuous value while the other either rejects or not the hypothesis, likelihood distributions are often used to conduct frequentist tests. However, to do so, it is convenient to use other forms of the likelihood. Indeed, when trying to use Bayes's law, we are confronted to two problems:

- $P(E)$, can be difficult or impossible to evaluate, even to define
- $P(A)$, the prior probability of model A, an input of the law is subjective, as there is no way to favour a given model with respect to another when no information is given as to its possible validity. The choice of a prior distribution is of great importance for decision theory.

Because of these two points, Bayes's law is also often used and expressed in terms of ratios of probabilities involving different assumptions: they can be linked through another ratio, the likelihood-ratio Λ , which compares $\mathcal{L}(A|E)$ and $\mathcal{L}(B|E)$, *i.e.* the probabilities of getting the measured sample E given hypothesis A or B . This has the advantage of eliminating of $P(E)$ in the expression of the law:

$$\frac{P(A|E)}{P(B|E)} = \Lambda \frac{P(A)}{P(B)} \quad \text{with} \quad \Lambda = \frac{P(E|A)}{P(E|B)}$$

When testing an hypothesis θ_0 against an alternative hypothesis θ_1 , the likelihood ratio can also be defined so that $\Lambda < 1$:

$$\Lambda = \frac{\mathcal{L}(\theta_0|x)}{\sup(\mathcal{L}(\theta|x) : \theta \in \theta_0, \theta_1)}$$

Furthermore, if either the tested or alternative hypotheses can be described by the sets of parameters Θ_0 and $\Theta \setminus \Theta_0$, the likelihood ratio test can also take the the form:

$$\Lambda = \frac{\sup(\mathcal{L}(\theta|x), \theta \in \Theta_0)}{\sup(\mathcal{L}(\theta|x), \theta \in \Theta)}, \quad \Theta_0 \subset \Theta$$

Finally, the function $\Delta\chi^2 = -2 \ln \Lambda$, often called log likelihood ratio, is sometimes used to replace the likelihood function, as it is additive when conducting independent experiments. Indeed, if x_1 and x_2 are results of independent experiments,

$$\Lambda(\theta|x_1, x_2) = P(x_1 \& x_2|\theta) = P(x_1|\theta) \times P(x_2|\theta) = \Lambda(\theta|x_1) \times \Lambda(\theta|x_2)$$

and therefore $\Delta\chi^2(\theta|x_1, x_2) = \Delta\chi^2(\theta|x_1) + \Delta\chi^2(\theta|x_2)$

The likelihood ratio and log likelihood ratio are often used in decision-making processes by conducting so-called tests labelled with their names: by defining a rejection region of the form $\theta|\Lambda(\theta) \leq c$, with $0 \leq c \leq 1$ chosen in order to match a given confidence level, we define a decision rule. However, the distribution of these likelihood functions can be very hard to predict, which makes it complicated to have a link between c and the desired confidence level. This issue can be coped with in some situations thanks to Wilks's theorem [9] which claims as follows:

“Theorem: If a population with a variate x is distributed according to the probability function $f(x, \theta_1, \dots, \theta_h)$ such that optimum estimates $\bar{\theta}_i$ of θ_i exist which are [normally] distributed [...], then when $\theta_i = \theta_{0,i}, i = m + 1, \dots, h$, $-2 \ln \Lambda$, where Λ is given by

$$\frac{\sup_{\theta \in \Theta_0} \left(\prod_{\alpha} f(x_{\alpha}, \theta_1, \dots, \theta_m, \theta_{0,m+1}, \dots, \theta_{0,h}) \right)}{\sup_{\theta \in \Theta} \left(\prod_{\alpha} f(x_{\alpha}, \theta_1, \dots, \theta_h) \right)},$$

is, except for terms of order $1/\sqrt{n}$, distributed like χ^2 with $h-m$ degrees of freedom.”

More simply stated, when testing hypotheses in $\Theta_0 \subset \Theta$ against the whole set Θ , if one can find normally spread estimates $\bar{\theta}_i$ of the parameters θ_i , the log likelihood ratio $-2 \ln \Lambda$ asymptotically follows a χ^2 distribution with $\dim(\Theta) - \dim(\Theta_0)$ d.o.f –hence the notation $\Delta\chi^2$

From the knowledge of the distribution of the likelihood, it is then possible to calculate values of c matching the desired confidence levels, to then use the values of the likelihood ratio in given models constrain them.

2.1.3 Best fit, maximum likelihood

The likelihood distribution can also be used to determine the most likely hypothesis, as the one with the greatest likelihood (the one in which the probability that the observed event would happen is the largest). Indeed, if we suppose the prior distribution is uniform to start with – meaning that we have no a priori knowledge of the validity of any of the hypotheses considered, which is a bold supposition– then the posterior probability distribution is simply proportional to the likelihood function. The most probable hypothesis is therefore the one maximising the likelihood function – or equivalently, minimising the log likelihood.

For a parameter θ , the value of the parameter giving a maximum likelihood is written $\hat{\theta}$: $\Lambda(\hat{\theta}) = \max(\Lambda(\theta))$.

2.1.4 CLs

The CLs [10] upper limit is a function of a random variable that can be used to constrain a parameter $\theta \geq 0$ of a pdf by testing it against the alternative hypothesis $\theta = 0$ using a sample.

Formally, if X is a random variable distributed along a pdf depending on a parameter $\theta \geq 0$, a CLs upper limit for θ , given a confidence level α , is a function $\theta_{up}(X)$ such that

$$\frac{P(\theta_{up}(X) < \theta | \theta)}{P(\theta_{up}(X) < \theta | 0)} \leq 1 - \alpha$$

A more convenient way to determine this limit is through the use of a test statistic $f_\theta(X)$, finding the value θ for which the ratio

$$\frac{P(f_\theta(X) \geq \bar{f}_\theta | \theta)}{P(f_\theta(X) \geq \bar{f}_\theta | 0)} = 1 - \alpha \quad (2.1)$$

where \bar{f}_θ is the value of the test statistic for the observed experiment.

Moreover, this upper limit can also be used before having access to the outcome of the experiment by the calculation of expected CLs, assessing the capacity of the experiment to discriminate values of θ . In order to do so, instead of the outcome of the experiment \bar{f}_θ , we use the median of the distribution of $f_0(X) = f_\theta(X)$ with $\theta = 0$. The limit obtained this way is called the expected limit: it represents the limit we can expect to put on θ if the experiment yields the median result, hypothesis $\theta = 0$ being true. By repeating the same procedure with values of \bar{f}_θ splitting the distribution of q_0 at $100 - 95 = 5\%$, $100 - 68 = 32\%$, 68% and 95% of its integrated value, we get expected values at $\pm 1\sigma$, $\pm 2\sigma$. These values define two zones where we can hope to be able to discriminate the hypothesis θ from $\theta = 0$. These zones should not to be mistaken with exclusion regions, since they were not based on any data.

2.1.5 p-value

The p-value can be considered as the basic tool used in the frequentist approach to test an hypothesis thanks to a set measurements on a sample. It is important to stress here that there is no alternative proposed to the hypothesis tested by the p-value: whether an hypothesis is rejected or not by this test yields no information about any other hypothesis. As illustrated on fig. 2.1, for a given quantity calculated from the experimental sample, the p-value represents the probability that, the hypothesis being true, the results of a similar experiment would have been more extreme than the observed ones. However, the signification of "more extreme" is up to the person conducting the test to determine. Moreover, the very definition of the p-value depends on the quantity calculated from the results of the experiment, and identical results might yield different p-values if the procedures leading to them were different. This causes some debate about the meaning and purpose of statistical testing.

In order to properly conduct a test based on the p-value, a significance level must be chosen beforehand, usually close to 0. The test then consists in comparing the p-value p to the significance level α in order to determine whether the hypothesis is rejected or not. For $p < \alpha$, the hypothesis is rejected by the test. In the alternative case however, $p \geq \alpha$, the hypothesis is not accepted as true, but the test cannot state whether the hypothesis is true or not. When the test is rejecting the hypothesis, the confidence level represents the chance that the hypothesis might actually be true and the test is giving a wrong conclusion. It is important that α is chosen before p is calculated, so that the test is not influenced by the knowledge of its value.

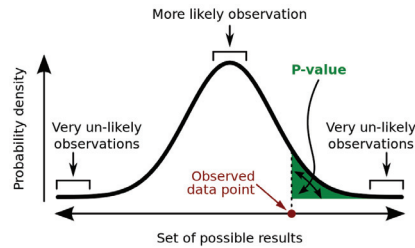


Figure 2.1: Illustration of the notion of p-value: probability of getting in an experiment a more extreme outcome than the one observed. Image courtesy of Wikimedia

2.1.6 Confidence intervals (C.I.) and exclusion regions

As results in statistics are never definite, presenting solely the best estimate of a parameter lacks some information about the uncertainty on the determination of this value. In this prospect, it is usual to define sets called confidence intervals. Their goal is to represent a subset of the parameter space wherein the true values of the parameters are likely to be.

As most of the concepts used in statistics, a confidence interval is defined with a confidence level, representing the probability that such an interval obtained from a given sample would contain the true value of the parameter. It also represents, for repeated experiments (or equivalently multiple samples), the expected proportion of such intervals that should contain the true value of the parameter. However this interval definition is ill suited for hypotheses based on several parameters, and this concept can be extended to confidence regions.

One way to define confidence regions is by determining its complementary set: exclusion regions at a given confidence level are regions of the parameter space in which hypotheses are likely not to be true, for instance excluded by a test, which brings us back to the concepts defined up until now. Whether the test is a p-value test or a likelihood-based test, exclusion regions are defined as the set of parameters individually not passing the test. Of course, the criterion on which the test is based has to match the confidence level required for the confidence region. For instance, for a likelihood ratio test based on a likelihood function complying with Wilks's theorem requirements, and difference of d.o.f. between tested and alternative hypothesis of 1, a confidence level of 95.4 corresponds to an exclusion region with $\Lambda < 0.1353$ or $\Delta\chi^2 > 4$, and with $\Lambda < 0.018$ or $\Delta\chi^2 > 8.02$ if difference in d.o.f is 3. However in the case of likelihoods, it is important to remember that the prior distribution is also of paramount importance in the process of making a decision.

2.2 Use in experiments

Measurements in particle physics are based on matching predictions of QFT with the observed distribution of events occurring in collisions. This brings a first source of uncertainty, as quantum theories are not deterministic about the outcome of a single experiment, but the experimental process itself brings in many more, through the complicated data-taking, sorting, extrapolating

and other algorithms. For instance, experiments at the LHC give results that vary with time because of the evolution of the detector itself with its exposure to radiation, variation that is taken into account by estimated correction factors. Another example comes from the fact that different particles with identical or close experimental signatures might be mistakenly identified as the other, leading to deformed distributions, which is taken into account by evaluating the rate of misidentification. Moreover, the cross sections calculated are not single numbers, but they are differential cross sections, distributions over the various dynamic variables characterising a collision. As the phase space explored by the many possible final states is continuous and huge, there is no way to gather enough events to cover and probe all of it precisely. Therefore, events are gathered in bins, and compared with integrated distributions on small parts of the phase space, the study of each bin representing a counting experiment. Those lead, as specified in the first part, to results following a Poisson distribution law, becoming for large numbers of expected events a Gaussian distribution centred on the theorised expected value ($= \text{probability} \times \text{number of draws/collisions}$), and a standard deviation of \sqrt{n} proving once again the importance of this distribution. These counts mix many interesting pieces of information, either from different processes mistakenly counted together, from different processes that are indistinguishable, or even from a same process. For instance $e^+e^- \rightarrow e^+e^-$ can be through annihilation of e^+e^- into H, Z, γ then decaying into e^+e^- , or e^+ and e^- can exchange a H, Z or γ . In that case, when considering the possible existence of the Higgs boson, it is interesting to compare SM predictions including the Higgs or without it. This is accomplished by separating the number of counted events into so-called “background” and “signal” events. The interesting quantity is the number of signal events s , but the measured one, n , includes the number of background events b , $n = b + s$, and we have to rely on statistics to assess the probability that within those n observed events, s were indeed signal events. In the rest of this chapter, unless mentioned otherwise, n , b and s might label total, background and signal numbers specific to a bin, production mode or selection channel, but in order not to use overcharged notations, we hope that the context will be sufficient to determine which one is being mentioned.

2.2.1 Selection channels

As the observation of collisions is indirect, the signals obtained in a colliding experiment can rarely be identified to a unique final state and for each process, the assessment of the possible backgrounds, through misidentification or indiscernibility of the final state, and the precise determination of their contribution is of utmost importance.

The experimental determination of what is being observed after a collision is a complicated process, involving expertise at every level, from the calibration of the response of each subdetector, to the characterisation of the experimental signature of a given particle through several variables. This point in particular, relies on a series of selections putting in correspondence information from every part of the detector, making a compromise between maximising the probability that a set of signals indeed correspond to a given particle, and minimising the rejection of these particles in the process.

When the particle content of an event is determined, associating to each particle in the final state its dynamical characteristics, it undergoes another selection procedure, sorting out events

Selection channel	$\hat{\sigma}_{gg}^i$	$\hat{\sigma}_{\text{VBF}}^i$	$\hat{\sigma}_{\text{WH}}^i$	$\hat{\sigma}_{\text{ZH}}^i$	$\hat{\mu}_i$	σ_i	$\hat{\sigma}_{gg}^i$	$\hat{\sigma}_{\text{VBF}}^i$	$\hat{\sigma}_{\text{WH}}^i$	$\hat{\sigma}_{\text{ZH}}^i$	$\hat{\mu}_i$	σ_i
	7 TeV						8 TeV					
Unconverted central low p_{Tt}	92.9	4.0	1.8	1	0.5	1.4	92.9	4.2	1.7	1.0	1.0	1.2
Unconverted central high p_{Tt}	66.5	15.7	9.9	5.7	0.2	1.9	72.5	14.1	6.9	4.2	0.8	1.7
Unconverted rest low p_{Tt}	92.8	3.9	2.0	1.1	2.4	1.6	92.5	4.1	2	1.1	0.9	1.4
Unconverted rest high p_{Tt}	65.4	16.1	10.8	6.1	10.3	3.8	72.1	13.8	7.8	4.6	1.8	1.8
Converted central low p_{Tt}	92.8	4.0	1.9	1.0	6.2	2.6	92.8	4.3	1.7	1.0	3.4	2.0
Converted central high p_{Tt}	66.6	15.3	10	5.7	-4.4	1.6	72.7	13.7	7.1	4.1	3.5	2.7
Converted rest low p_{Tt}	92.8	3.8	2.0	1.1	2.7	2.2	92.5	4.2	2	1.1	0.4	1.8
Converted rest high p_{Tt}	65.3	16.0	11.0	5.9	-1.7	3	70.8	14.4	8.3	4.7	0.3	2.1
Converted transition	89.4	5.2	3.3	1.7	0.3	3.7	88.8	6.0	3.1	1.8	5.5	3.3
2 jets	22.5	76.7	0.4	0.2	2.7	1.9	30.4	68.4	0.4	0.2	2.6	1.8

Table 2.1: ATLAS results for the various selection channels of the $H \rightarrow \gamma\gamma$ analysis [11].

with a common final state into different regions, called selection channels. The cuts used to define these channels are determined so that the event content of the channel is as specific as possible and the channels are mutually exclusive.

As those channels still mix different signals, an efficiency is defined for a given channel and signal, which represents the estimated proportion of events in selected in this channel corresponding to the considered signal. As an example, efficiencies from the CMS and ATLAS analyses looking for a Higgs boson decaying to $\gamma\gamma$ from the end of 2012([11] [12,13]) are given in tables 2.1 and 2.2. The details of the selection procedures can be found in the corresponding notes, from which the given efficiencies are evaluated. This estimation is performed using simulated events following the same (simulated) detection and selection procedures as the real data, giving us distributions for n , with the difference that the underlying processes are known, meaning that we can therefore differentiate b and s .

We can see for instance in the table that the ATLAS selection channel “2 jets” is efficiently selecting events including a Higgs produced through VBF, while events in “Unconverted central low p_{Tt} ” are more likely than others to be produced through the ggh mode. It is also interesting to note that as the two experiments were built on different concepts, with different credit or importance given to each subdetector, their selection procedures are different, without even the

Selection channel	$\hat{\sigma}_{\text{ggh}}^i$	$\hat{\sigma}_{\text{VBF}}^i$	$\hat{\sigma}_{\text{VH}}^i$	$\hat{\mu}_i$	σ_i	$\hat{\sigma}_{\text{ggh}}^i$	$\hat{\sigma}_{\text{VBF}}^i$	$\hat{\sigma}_{\text{VH}}^i$	$\hat{\mu}_i$	σ_i
	7 TeV					8 TeV				
Untagged 0	61	17	19	3.15	1.82	68	12	16	1.46	1.24
Untagged 1	88	6	6	0.66	0.95	88	6	6	1.51	1.03
Untagged 2	91	4	4	0.73	1.15	92	4	3	0.95	1.15
Untagged 3	91	4	4	1.53	1.61	92	4	3	3.78	1.77
Dijet Tag	27	73	1	4.21	2.04	-	-	-	-	-
Dijet tight	-	-	-	-	-	23	77	0	1.32	1.57
Dijet loose	-	-	-	-	-	53	45	2	-0.61	2.03

Table 2.2: CMS results for the various selection channels of the $H \rightarrow \gamma\gamma$ analysis [12, 13].

same number of channels, which might give the respective analyses different statistical sensitivities. Under the assumption that the events are correctly simulated, these numbers can be used as estimates of the composition of the signal when dealing with real data. However, these simulations and the optimisation of the selections have to be performed for each analysis, making the process very demanding in computer time.

2.2.2 Signal strengths

As we said previously, the interesting part in a set of observed events, the signal, cannot be distinguished experimentally from the background. The conducted statistical tests therefore aim at estimating from the data n_{obs} and the distributions $f(n_{\text{obs}} | n = b + s)$ determined in a given hypothesis, the probable values of s , by rejecting or not models according to their predictions for what s could be. Although s itself could be the object of the statistical test, as it changes from one bin to another it is hard to interpret intuitively. For this reason, a benchmark model is chosen in order to define the signal strength μ :

$$\mu = \frac{s}{s^{\text{ref}}}$$

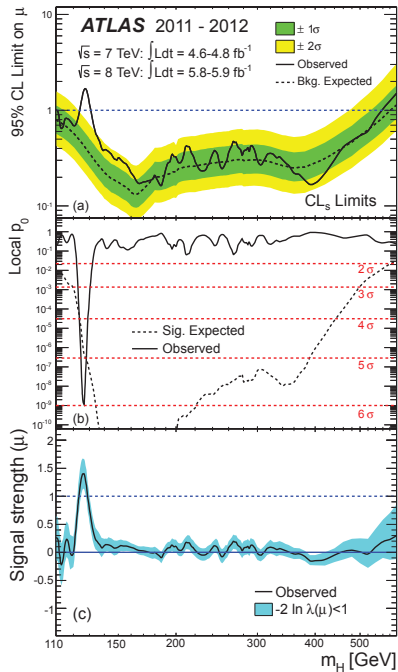
The usual benchmark model is of course the SM, and $s^{\text{ref}} = s^{\text{SM}}$. Concerning the background, it is supposed to be the same in the tested hypothesis and the benchmark model (otherwise the differences would be included in the signal), therefore $b = b^{\text{SM}}$. Moreover, even though this quantity can be defined for each bin, most models predict the same signal strength for many if not all bins, reducing significantly the number of parameters required to describe the hypothesis.

The hypothetical pdf used to estimate likelihoods or other statistics then becomes $f(n_{\text{obs}} | n = b + s) = f(n_{\text{obs}} | \mu)$, where μ might be a set of several values.

2.2.3 Tests in experiments

This section aims at making all the concepts introduced previously more explicit by interpreting the results displayed in plots published by experimentalists. The figure on the left represent 3

plots from an ATLAS analysis combining the different searches, published shortly after the claim of boson discovery [14], while the figure below on the right is taken from a CMS public note of the same period [12]. The first plot, as indicated, represents CLs upper limits (observed and expected)

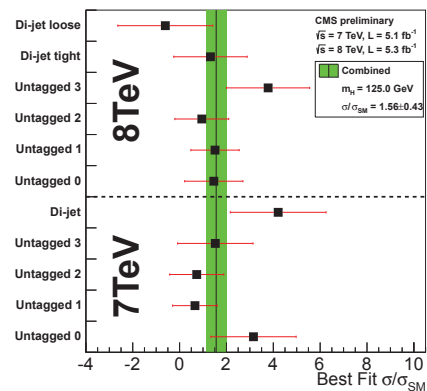


on $\mu \geq 0$ as a function of m_H , where μ here is an experimentally-motivated parameter multiplying all Higgs cross sections: the hypothesis $\sigma_H = \mu \sigma_H^{\text{SM}}$, whatever the production or decay mode, as unlikely as this hypothesis is. The hypothesis therefore has two parameters: μ and m_H , and μ is tested for different values of m_H independently, meaning that the test has to be performed for each value of m_H separately. The expected limits do not depend on the data, which explains the absence of the fluctuations we can see in the observed curve. From this curve we deduce that in the region between 115 and 460 GeV, with this amount of data, the ATLAS experiment could be expected to make the difference between the SM with ($\mu = 1$) and without ($\mu = 0$) the Higgs boson at 95% C.L., even with an unlikely fluctuation of the data. On the other hand, the observed CLs limits indicate, by following expected curve away from 125 GeV that nothing unusual is happening apart from fluctuations. Around 125 on the other hand, the observed CLs limit is outside of the expected 2σ band, which means that there is in the

signal a specificity that is more probably explained by the presence of a Higgs boson with μ than by a fluctuation of the Higgsless SM. The second diagram shows the local p-value for the SM without the Higgs. The test is local, meaning that only the data having an invariant mass around m_H is considered, and μ does not appear as the p-value test only relies on one hypothesis (the Higgsless SM here). The expected p-value is determined for a signal corresponding to the expected value of s for $\mu = 1$ i.e. the value of the p-value one could expect to get from an average sample of Higgs data for the tested m_H .

The fluctuations in the expected curve come from the different phenomenology of different values of m_H , giving varying sensitivities in each analysis. The observed curve, on the other hand, shows that for most masses, the data is well in agreement with the absence of a Higgs, but this hypothesis does not fare well around 125 GeV, where the Higgsless SM would have to experience a very unlikely fluctuation, with probability $p \approx 10^{-9}$, to be true and give the observed sample. This is more than the particle physicists consider as enough, which is

why the Higgsless SM is rejected (however, this does not prove the truth of the SM including



the Higgs, as the explanation could come from a different hypothesis). The last plot shows, once again for different fixed values of m_H , the value of μ maximising the likelihood evaluated from the observed sample, i.e. the value that predicts the observed sample with the highest probability. The blue band represents some uncertainty on this value: values of μ for which the log likelihood ratio is smaller than 1. If the likelihood as a function of μ is expected to be distributed as a Gaussian, which is the case for large expected event numbers, this band corresponds to a confidence interval at 68% C.L.. Once again, the message is clear that the absence of Higgses is favoured at most masses but for m_H around 125 GeV, where data hints at a scalar giving slightly higher signals than the SM Higgs. However, none of these results is a measurement of the mass of the observed boson, as m_H was not fitted to the data. The last figure represents another kind of hypothesis: one signal strength is defined per selection channel, and a best fit is determined for each based on the part of the sample going into this selection channel. A 1σ (68% C.L.) band is also determined. The green band is determined in the hypothesis that all of these signal strengths should have the same value, giving a result of the same kind as the last ATLAS diagram. However, this figure corresponds to a “slice” of the former, with only the $m_H = 125$ GeV hypothesis being considered.

2.2.4 Correlations

For independent random variables, all the tools presented until now are well behaved and it is easy to combine results from different samples. However, in the case where they are not independent, meaning for example that given results from a first experiment modify the idea of what the results of the next experiment could be, then the combination is harder to perform.

In our case, it is reasonable to consider that the various events are independent from one another and that a collision that occurred previously will have no influence on the physics of a later encounter. The variation caused by this indetermination is statistical uncertainty. But correlations start appearing with every step of the data processing, with systematic uncertainties. For instance if a bias is present in the estimation of the energy of photons produced in an event, this bias will be present in the determination of the invariant mass of every photon pair used to look for a Higgs boson, inducing a bias in its mass measurement through this channel. Correlations can also appear between the results of different experiments, as they rely on similar experimental procedures, and their interpretation are based on the same calculations within the SM. Those are theoretical uncertainties: if the calculations of cross sections for the production of the Higgs are off (and they are) because of approximations, the interpretation of the results will also be off. And getting a hint from an experiment that it might be so will let us think that the results in the experiment might also suffer from this problem. The only solution to treat these correlations correctly would be to keep track of every source of uncertainty and give this information along with the results. However this would represent an enormous amount of data, and results provided by experimentalists are often a lot simplified in order to be readable, which make further use by other parties impossible without loss of information. Fortunately, these correlations are sometimes small enough to be neglected. In the rest of this thesis, as there is no other choice for people outside experimental collaboration, we will consider that experimental results are independent, unless stated otherwise.

Chapter 3

Higgs couplings beyond the standard model

As seen in the first chapter, there are many reasons to think that the currently widely accepted model, the SM, as close to being complete as it is, is not the end of the story. In order to explain the observations the SM cannot cope with, the assumptions which it was built on can be (carefully) changed individually, each one leading to a new field of research. In some models, the symmetries of the Lagrangian, global or local, are modified or extended, in others the field content is modified. In almost all extensions though, both are modified in order to stay coherent, and each model create different predictions. However, lots of constraints come from the fact that the predictions have to be within experimental bounds, very close the the SM ones in the domains where it's successful. With the growing number of results from experiments focusing on various aspects of the SM predictions, models have to respect a large set of constraints, which are becoming more and more detailed.

In all BSM models, the EWSB has to happen, but it is sometimes achieved in a different way than in the SM. Along the years, many models were proposed, such as technicolor, strongly interacting light Higgs models (SILH), models built on space with more than 4 dimensions or supersymmetric models. Many of those were excluded by various experiments, and the Higgs-boson like scalar discovery at the LHC itself knocked its share out, either because they predicted something unobserved or because they did not predict the existence of such a scalar. In most models still, the couplings of the Higgs boson are modified. Therefore with their measurement, performed at the LHC, they provide an additional mean to constrain these models.

3.1 Parametrisations of the Higgs couplings

When studying properties of a model, it is possible to state them in an explicit way, without relying on properties of other models. Even though more precise and unavoidable in some cases, this might prove tedious, requiring lots of computations and results, sometimes redundant especially when considering modifications of an existing model. In this case, it is much more efficient to express the properties of the studied model relatively to those of a well-known benchmark model.

In our case, the obvious choice of benchmark model is the SM, in the same way as we defined the signal strengths, and its Higgs boson. However, the signal strengths are experimental quantities, not intuitive in terms of models, and in a more fundamental approach, it is possible to directly use the couplings of the interesting scalar. By making general simple assumptions under which many models fall, it is possible to build a generic and simple set of parameters to compare model predictions with the data. Recently, tools have even been developed to make the constraining procedures straightforward, including recast results and requiring as only input the values of the rescaled couplings in the model to be tested [15].

As we saw in the first part, in the SM the Higgs boson is coupled to the weak gauge bosons and fermions to which the Higgs mechanism effectively gives mass at low energies, and other couplings arise at loop level such as the ones to a pair of photons, a pair of gluons, or a photon and a Z . The channels involving those particles are therefore the main ones looked for at the LHC, and the couplings involved are the ones interesting to parametrise.

Several approaches to this parametrisation are used by different groups, among which the use of effective operators to represent new physics [16–18], or electroweak chiral Lagrangians [19, 20]. Those approaches have the advantage of using a well-oiled machinery of effective theories, including radiative corrections, but also face the drawbacks of displaying a large number of parameters, as well as not being able to describe models including new light particles not yet ruled out as we will see in the next chapter. The number of parameters is an important factor when it comes to choosing a parametrisation, as it should be balanced to the amount and quality of data available, since constraining a model allowing lots of different variations might prove very hard and very imprecise. An overview of effective Lagrangians for Higgs physics can be found in [21], including the treatment of radiative corrections.

We will however focus on the sets of parameters proposed in [22], recommended parametrisation for the study of Higgs couplings by the LHC Higgs Cross Section Working Group (LHCHSWG) and [23], two parametrisations which only focus on the couplings already existing in the SM.

3.1.1 Rescaled couplings

The first approach, better motivated from an experimental point of view and recommended in the first steps of Higgs studies at CERN by experimentalists and theorists in [22], consists in defining parameters rescaling experimental quantities, multiplying consistently SM cross sections by the right factors, separating production and decay in the narrow width approximation. In this approach, no difference is made between couplings arising at tree-level and couplings only existing through loops, and the factors are chosen in function of the couplings implied in the process. This leads us to the definition of 7 parameters: $\kappa_W, \kappa_Z, \kappa_\ell, \kappa_t, \kappa_b, \kappa_g$ and κ_γ , giving for example in terms of production cross sections:

$$\sigma_{Wh} = \kappa_W^2 \sigma_{Wh}^{\text{SM}}, \quad \sigma_{Zh} = \kappa_Z^2 \sigma_{Zh}^{\text{SM}}, \quad \sigma_{t\bar{t}h} = \kappa_t^2 \sigma_{t\bar{t}h}^{\text{SM}}.$$

and for the partial decay widths:

$$\Gamma_{WW} = \kappa_W^2 \Gamma_{WW}^{\text{SM}}, \quad \Gamma_{ZZ} = \kappa_Z^2 \Gamma_{ZZ}^{\text{SM}}, \quad \Gamma_{b\bar{b}} = \kappa_b^2 \Gamma_{b\bar{b}}^{\text{SM}}, \quad \Gamma_{\gamma\gamma} = \kappa_\gamma^2 \Gamma_{\gamma\gamma}^{\text{SM}}, \dots$$

The total cross section for a process with production mode p and decay mode i can, in the narrow width approximation, be written as

$$\sigma_{p \rightarrow H \rightarrow i} = \sigma_p \times BR_i = \sigma_p \times \frac{\Gamma_i}{\Gamma_H} = \kappa_p^2 \sigma_p^{\text{SM}} \times \kappa_i^2 BR_i^{\text{SM}} \times \frac{\Gamma_H^{\text{SM}}}{\Gamma_H(\kappa)} = \sigma_{p \rightarrow H \rightarrow i}^{\text{SM}} \times \kappa_p^2 \kappa_i^2 \frac{\Gamma_H^{\text{SM}}}{\Gamma_H(\kappa)}$$

where $\Gamma_H(\kappa) = \sum_i \Gamma_i = \sum_i \kappa_i^2 \Gamma_i^{\text{SM}}$ and therefore we can define

$$\mu_p^i = \kappa_p^2 \kappa_i^2 \frac{\Gamma_H^{\text{SM}}}{\Gamma_H(\kappa)} \quad (3.1)$$

When considering the couplings, this corresponds for fermions and weak bosons to the rescaling of the Higgs coupling $g_{H\bar{i}i}$ with respect its SM value:

$$\kappa_i = \frac{g_{H\bar{i}i}}{g_{H\bar{i}i}^{\text{SM}}}$$

In the case of particles coupling at loop level with the SM Higgs however (pairs of γ and g), those terms do not appear at tree level in the Lagrangian, and no such expression can be given.

In some cases, in order to reduce the number of parameters, we will restrain the study to BSM models with custodial symmetry, implying identical modification of the couplings with the W and Z, and in those cases we note $\kappa_W = \kappa_Z \stackrel{\text{not.}}{=} \kappa_V$.

3.1.2 Loop-inspired parametrisation

The difference between this second set of parameters, based on the ones presented in [24], and the one described previously only resides in the treatment of couplings appearing through loops, and $\kappa_W, \kappa_Z, \kappa_\ell, \kappa_t, \kappa_b$ keep the same definitions. However, unlike κ_g and κ_γ , the parameters κ_{gg} and $\kappa_{\gamma\gamma}$ are no longer defined as a function of observables, but at the level of the calculated amplitudes of the processes. Indeed, this parametrisation relies on the expressions given in equations 1.2 and 1.3, which in a BSM model take the form:

$$\Gamma(H \rightarrow gg) = \frac{G_F \alpha_s^2 m_H^3}{16\sqrt{2}\pi^3} \left| \frac{1}{2} \mathcal{A}_{1/2}^{\text{BSM}}(\tau_t) + \mathcal{A}_{\text{NP}}^g + \dots \right|^2 \quad (3.2)$$

$$\Gamma(H \rightarrow \gamma\gamma) = \frac{G_F \alpha^2 m_H^3}{128\sqrt{2}\pi^3} \left| 3 \left(\frac{2}{3} \right)^2 \mathcal{A}_{1/2}^{\text{BSM}}(\tau_t) + \mathcal{A}_1^{\text{BSM}}(\tau_W) + \mathcal{A}_{\text{NP}}^\gamma \right|^2 \quad (3.3)$$

where $\mathcal{A}_{\text{NP}}^{g/\gamma}$ represent the amplitudes of additional diagrams coming from New Physics (NP) contributing to decays to gluon and photon, \mathcal{A}^{BSM} represent amplitudes of diagrams existing in the SM but calculated within the BSM model, and \dots represent negligible contributions of light quarks. The next step in defining κ_{gg} and $\kappa_{\gamma\gamma}$ relies on the fact that, as the heaviest particle in the SM, the top quark plays a particular role in many BSM models, for instance with the introduction of top partners. Because of this, we choose to rescale the NP amplitudes to those

of the SM top quark (we could choose another without changing the generality of this approach), and define:

$$\begin{aligned}\kappa_{gg} &= \frac{\mathcal{A}_{\text{NP}}^g}{\frac{1}{2}C_t^g \mathcal{A}_{1/2}(\tau_t)} \\ \kappa_{\gamma\gamma} &= \frac{\mathcal{A}_{\text{NP}}^\gamma}{C_t^\gamma 3 \left(\frac{2}{3}\right)^2 \mathcal{A}_{1/2}(\tau_t)}\end{aligned}$$

where the coefficients C_t^γ and C_t^g contain the NLO QCD corrections to the SM top amplitudes, and equations 3.2 and 3.3 become

$$\begin{aligned}\Gamma_{\gamma\gamma} &= \frac{G_F \alpha^2 m_H^3}{128 \sqrt{2} \pi^3} \left| \kappa_W \mathcal{A}_1(\tau_W) + C_t^\gamma 3 \left(\frac{2}{3}\right)^2 \mathcal{A}_{1/2}(\tau_t) [\kappa_t + \kappa_{\gamma\gamma}] + \dots \right|^2 \\ \Gamma_{gg} &= \frac{G_F \alpha_s^2 m_H^3}{16 \sqrt{2} \pi^3} \left| C_t^g \frac{1}{2} \mathcal{A}_{1/2}(\tau_t) [\kappa_t + \kappa_{gg}] + \dots \right|^2\end{aligned}$$

In order to get more insight on the parameters it is interesting to note that $\mathcal{A}_{1/2}(\tau)$ and $\mathcal{A}_1(\tau)$ reach asymptotic values for small values of τ *i.e.* heavy particles in the loops. For instance, for a 125 GeV Higgs boson, we get

$$\mathcal{A}_1(\tau_W) = -8.32, \quad \mathcal{A}_{1/2}(\tau_t) = 1.37;$$

and the top amplitude is very close to its asymptotic value $\mathcal{A}_{1/2}(0) = 4/3$ while the amplitude for the W , lighter, significantly deviates from the asymptotic value $\mathcal{A}_1(0) = -7$.

As for the QCD corrections to the top loops $C_t^{g/\gamma}$, they can be computed in the asymptotic case where the top quark is very heavy which is a good approximation for a 125 GeV Higgs boson, and one gets ([25]):

$$C_t^\gamma = 1 - \frac{\alpha_s}{\pi}, \quad C_t^g = 1 + \frac{9}{2} \frac{\alpha_s}{\pi}.$$

It is useful to note that this treatment is different from the parametrisation proposed in [24], in which parameters κ_W , κ_t etc were not included.

Moreover, as we saw in the first chapter, at first order the Higgs production cross section through ggh is proportional to its partial width into two gluons. Therefore, the previous argument can also be used to express the ggh cross section as a function of κ_t and κ_{gg} .

With this set of parameters, the expression for μ_p^i is hardly more complicated than with the other parametrisation, as we will see in the next section that we only have to replace κ_g^2 and κ_γ^2 with the expressions 3.4 and 3.5.

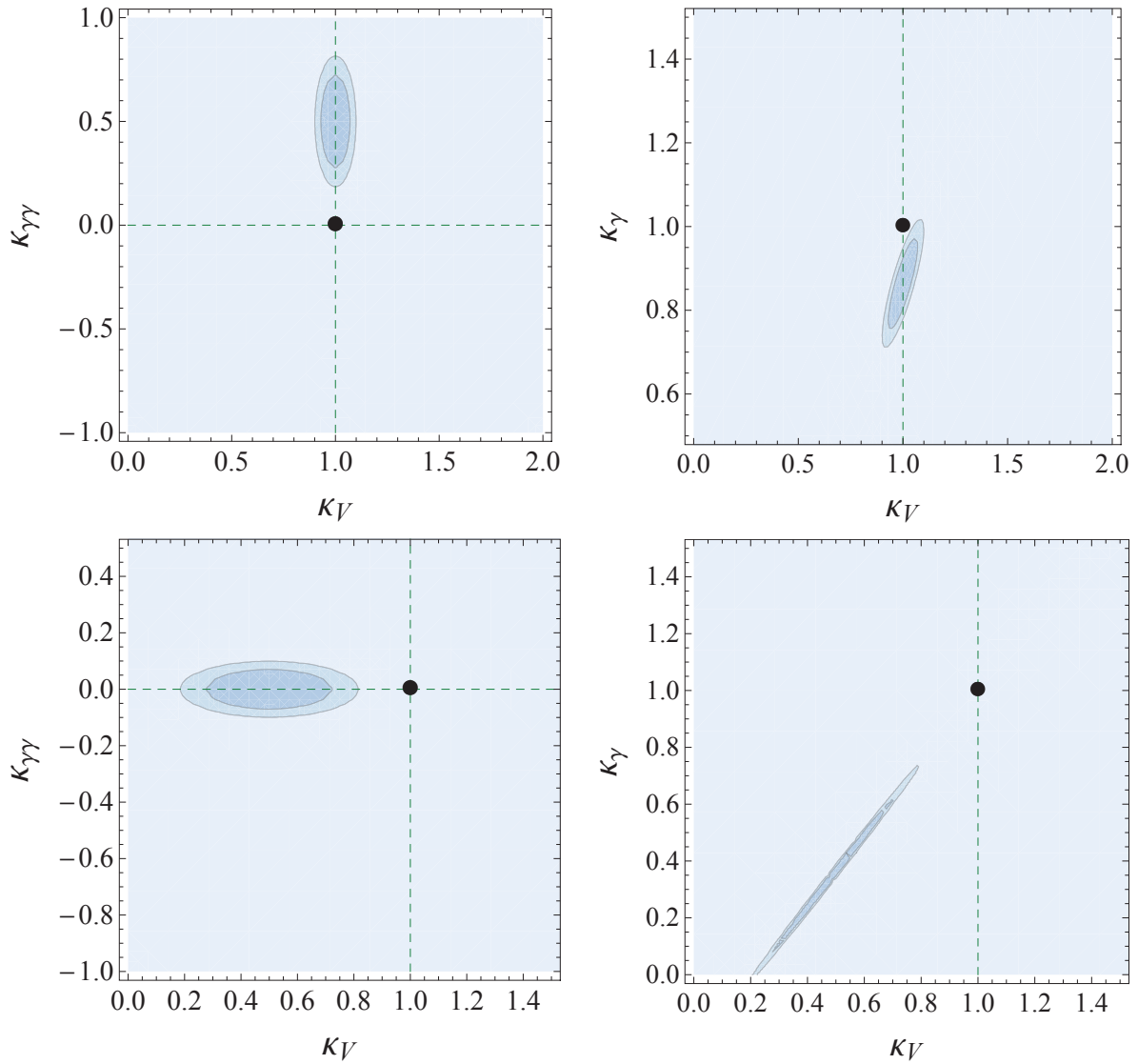


Figure 3.1: Comparison of the exclusion regions for a same artificial likelihood in both frameworks, in two models. *Top row:* $\kappa_V = 1$, $\kappa_{\gamma\gamma} \neq 0$. *Bottom row:* $\kappa_V \neq 1$, $\kappa_{\gamma\gamma} = 0$

3.1.3 Comparison of the two frameworks

These two parametrisation are built on the same number of parameters, and are mathematically equivalent. When neglecting the contribution of light fermions as we started doing in the last part, we can draw a relation between the different parameters:

$$\kappa_g^2(\kappa_t, \kappa_{gg}) = (\kappa_t + \kappa_{gg})^2, \quad (3.4)$$

$$\kappa_\gamma^2(\kappa_W, \kappa_t, \kappa_{\gamma\gamma}) = \frac{(\kappa_W A_W(\tau_W) + C_t^{\gamma\frac{4}{3}} \mathcal{A}_{1/2}(\tau_t) [\kappa_t + \kappa_{\gamma\gamma}])^2}{(\mathcal{A}_1(\tau_W) + C_t^{\gamma\frac{4}{3}} \mathcal{A}_{1/2}(\tau_t))^2}. \quad (3.5)$$

However, it appears clearly in these formulas that there is a correlation between the parameters of the first set, which is absent in the second one. This appears more clearly in figure 3.1, where are displayed exclusion contours at 95% C.L. in the two planes spanned by $\kappa_W = \kappa_V$ and $\kappa_{\gamma\gamma}$ on the left, and $\kappa_W = \kappa_V$ and κ_γ on the right. Those were obtained using likelihoods corresponding to imaginary experiment results corresponding to two models: one (top row) in which NP do not influence the coupling of weak gauge bosons to the scalar, $\kappa_V = 1$, but there are additional loops contributing to its decay to photons, $\kappa_{\gamma\gamma} \neq 0$ and the other (bottom row) where the coupling of the scalar to weak gauge bosons is modified, $\kappa_V \neq 1$ but no new physics loops appear, $\kappa_{\gamma\gamma} = 0$.

In the first case, the correlation is weak, as the ellipsis circling the exclusion region is slightly slanted in the diagram on the right, but it appears far more clearly on the bottom row, where the absence of new physics loops is much more clearly indicated by the figure on the left, which indicates that the experiment favours models without new loop contributions, while this feature is hidden by the dependence of κ_V of κ_γ in the figure on the right. Although points excluded on both figures correspond to the same underlying models, the physical implications can be read more easily when written in terms of $\kappa_{\gamma\gamma}$. Moreover, in some models such as minimal composite Higgs models with top partners, κ_t , $\kappa_{\gamma\gamma}$ and κ_{gg} take values correlated in such a way that κ_g and κ_γ are equal to 1, making these two parameters opaque to the BSM model.

3.2 Link with experimental constraints

As stated in part 2.2.2, experimentalists often use signal strengths as a single value to describe the signal observed in a selected set of events. Two sets of measurements described by different signal strengths will be presented here, as all experimental analyses do not present their results in the same way. However, in each case, the analyses are separated by final state in which the Higgs decays, and within an analysis, the various signal strengths will correspond to a discrimination between production modes. We will first see the method focusing on selection channels, only used to recast the experimental results at the end of 2012, while we will focus on the next subsection on the exclusion regions relying on the signal strength of the different production modes and directly given by the experiments. The second method will be applied to two sets of constraints: the one published at the end of 2012, and the legacy results of LHC Run I, released after further analysis at the end of the 2013-2014 break to upgrade the LHC to $\sqrt{\hat{s}} = 13 \text{ TeV}$.

3.2.1 Selection channels

The first way in which the experimentalists describe their results is by selection channels, as already described in section 2.2.1. This description, closer to experimental results as the results

are simply counts after cuts, is however not the most convenient for phenomenology purposes since different production modes are mixed in the various channels. As described in [26], in order to separate their contribution, it is necessary to use the efficiencies of the selections for each production mode. The signal strength likelihood in the channel i , extrapolated as a 1D normal distribution from the best fit $\hat{\mu}_i$ and standard deviation σ_i given by the experiments, must be compared to the reconstructed signal strength:

$$\mu_i = \frac{s^i}{s^{i,\text{SM}}} = \frac{\sum_p \sigma_p \epsilon_p^i}{\sum_p \sigma_p^{\text{SM}} \epsilon_p^i} \times \frac{BR_i}{BR_i^{\text{SM}}}, \quad (3.6)$$

where s^i is the predicted number of signal events in channel i in the studied model, and $s^{i,\text{SM}}$ that same number in the SM. For each production mode p (theoretical calculation at NLO) the efficiency of selection of a channel i (experimental observation) is given by ϵ_p^i , that we will consider stays the same with new physics. This assumption is in agreement with our parametrisation that only includes corrections that do not change the kinematics of the events. At last, BR_i and BR_i^{SM} are the branching ratios of the Higgs boson into the decay channel corresponding to the selection channel i , for both SM and studied model.

Tables 2.1 and 2.2 given in section 2.2.1 represent the results provided by the CMS and ATLAS collaboration concerning the selection channels of their $H \rightarrow \gamma\gamma$ analyses at the end of 2012 ([11–13]), in the following way:

- each line corresponds to a selection channel, *i.e.* a given set of cuts selecting events. The channels are mutually exclusive in order not to count an event twice.
- two different sets of results are given, separating the events from the 7 and 8 TeV datasets.
- the first columns give for each selection channel and production mode the value as a percentage of $\hat{\sigma}_p^i = (\sigma_p^{\text{SM}} \epsilon_p^i) / (\sum_{p'} \sigma_{p'}^{\text{SM}} \epsilon_{p'}^i)$ (table 2 in [12], table 6 in [11])
- the last two columns for each $\sqrt{\hat{s}}$ are the real experimental results: the best fit values $\hat{\mu}^i$ and standard deviations σ^i for a Higgs mass of $m_H = 125 \text{ GeV}$ (in the CMS case, they were obtained in a table on the analysis TWiki [13], while they had to be extracted from figures 14a and 14b for 7 TeV and 8 TeV respectively for the ATLAS analysis)

The definition of $\hat{\sigma}_p^i$ makes the expression of μ_i simpler, as it can then be written as

$$\mu_i = \sum_p \hat{\sigma}_p^i \mu_p \times \frac{BR_i}{BR_i^{\text{SM}}}, \quad \text{where } \mu_p = \frac{\sigma_p}{\sigma_p^{\text{SM}}}$$

The same kind of information is given in table 3.1 for the $H \rightarrow ZZ^* \rightarrow \ell^+ \ell^- \ell^+ \ell^-$ and $H \rightarrow b\bar{b}$ analyses: the best fit and standard deviations were taken from figure 19 in [27], and figure 16a in [28] for the ZZ^* analyses, and from the notes [29, 30] for $b\bar{b}$. However, as the signal in those analyses was not divided in selection channels at the end of 2012, the collaboration did not give the efficiency of their selections, and we had to resort to additional approximations. In the ZZ^* case, we supposed identical efficiency for each production mode, meaning that $\hat{\sigma}_p^{ZZ} = \sigma_p / \sigma_{\text{tot}}$,

and the values of σ_p , taken from [6], are given in table 3.1. In the case of the $b\bar{b}$ analyses, we had to resort to the same approximation, but as they focused on the VH production mode since other modes were expected to have the signal drowned into the QCD background, only the WH and ZH efficiencies were considered as non-zero.

Experiment	$\sigma_{\text{ggh}}[pb]$	$\sigma_{\text{VBF}}[pb]$	$\sigma_{\text{WH}}[pb]$	$\sigma_{\text{ZH}}[pb]$	$\sigma_{\text{tth}}[pb]$	$\hat{\mu}$	σ
CMS ZZ^*	15.32	1.222	0.5729	0.3158	0.08634	0.8	0.35
ATLAS ZZ^*						1.3	0.6
CMS $b\bar{b}$	0	0	0.5729	0.3158	0	1.3	0.7
ATLAS $b\bar{b}$						-0.4	1.1

Table 3.1: CMS and ATLAS results in the $H \rightarrow ZZ \rightarrow \ell^+ \ell^- \ell^+ \ell^-$ and $H \rightarrow b\bar{b}$ channels [27–30].

The results, when recast this way, therefore allows us to extrapolate a likelihood function for each single signal strength μ_i :

$$\mathcal{L}_i = \exp \left[-\frac{1}{2} \frac{(\mu_i - \hat{\mu}_i)^2}{\sigma_i^2} \right]$$

If we consider the measured signal strengths as independent random variables, it is possible to build a global likelihood \mathcal{L}_{exp} by taking their product, with $-2 \ln \mathcal{L}_{\text{exp}}$ being distributed as a χ^2 distribution with a number of d.o.f. equal to the number of selection channels. However by using this procedure, we are neglecting the correlations existing between the individual likelihoods. As long as uncertainties are dominated by statistical effects, this approach might hold, but as the samples grow, the approach will be more and more flawed.

In the case of the WW^* channel, the searches were actually at that time also performed in various selection channels, however the detailed efficiency of each signal region for the various production mechanisms were not publicly available. We therefore had to resort to the second way used by experiments to give their results to include the information from the WW^* and $\tau^+ \tau^-$ channels.

3.2.2 Exclusion contours

As mentioned previously, the likelihood \mathcal{L}_{exp} meets two serious obstacles: first, one needs the efficiency (or equivalently the signal sample composition) per production mode together with the best fit $\hat{\mu}_i$ in each sub-channel and, second, this procedure neglects the correlations between uncertainties of the different sub-channels. However, it is possible to go further by recasting the results of the couplings analyses made by the two collaborations. This method of extrapolating the experimental results was used in two contexts. At the end of 2012, it was used to include WW^* and $\tau^+ \tau^-$ constraints and at the same time compare results obtained through the two

likelihood reconstruction methods for the $\gamma\gamma$ channel. In a second step, it was also used alone in 2015 to extract the legacy constraints from the experimental collaborations, using all the data sample from Run I. This section will present both sets of data at the same time, while explaining the procedure. Further in the manuscript, the results used in each figure to apply constraints will be specified.

In their couplings analyses [31, 32], instead of providing the best fits and standard deviations of one-dimensional distributions (with $\hat{\mu}_i$ and σ_i), the experimental collaborations gave two-dimensional distributions ($(\hat{\mu}_{i,gg h/t\bar{t}h}, \hat{\mu}_{i,VBF/VH})$, with the one σ contour, or 68% C.L.). Examples of such contours are given in figure 3.2, at the end of 2012 for CMS and including all run I data from CMS and ATLAS. Under some acceptable assumptions, this information can be used to build the likelihood function of the corresponding decay channel, without explicit reference to sub-channels and efficiencies:

- VBF and VH production are rescaled in the same way. This is achieved by imposing $\kappa_Z = \kappa_W$, which is the case in any model respecting the custodial symmetry.
- For each decay channel i , there cannot be significant contributions from both the gluon fusion and the t quark associated production. At the time being, this is the case, since $t\bar{t}h$ is significant only in the $H \rightarrow b\bar{b}$ channel which is otherwise observable only through VH. However, searches for $t\bar{t}h \rightarrow t\bar{t}\gamma\gamma$ ([33, 34]), not yet competitive with $gg \rightarrow h \rightarrow \gamma\gamma$, might change this with more data.

As for the previous method, we must also assume that the Gaussian approximation is well motivated. We can then write the approximated log-likelihood of a given decay channel i as

$$-2 \ln \mathcal{L}_i = \begin{pmatrix} \mu_{i,gg h/t\bar{t}h} - \hat{\mu}_{i,gg h/t\bar{t}h} \\ \mu_{i,VBF/VH} - \hat{\mu}_{i,VBF/VH} \end{pmatrix}^T V_i^{-1} \begin{pmatrix} \mu_{i,gg h/t\bar{t}h} - \hat{\mu}_{i,gg h/t\bar{t}h} \\ \mu_{i,VBF/VH} - \hat{\mu}_{i,VBF/VH} \end{pmatrix}, \quad (3.7)$$

describing a two-dimensional paraboloid, defined by the symmetric matrix V_i and its centre $(\hat{\mu}_{i,gg h/t\bar{t}h}, \hat{\mu}_{i,VBF/VH})$. Those parameters are obtained by adjusting them to match the experimental exclusion contours to the ellipses described by the equation $-2 \ln \mathcal{L}_i = 2.3$, value corresponding to the 68% C.L. for a two-dimensional χ^2 distribution. Values inferred from the CMS figure at the end of 2012 can be seen in table 3.2. More precisely, those values were obtained by extracting from the vectorial images provided by the collaborations, in an automated way, the values of all the points of the exclusion contours. Those points were then fitted to ellipses with free center and correlation matrix.

For a more visual assessment of the validity of the Gaussian approximation, the two diagrams on the top row of figure 3.3 show for the ATLAS and CMS legacy results the superimposed exclusion contours and fitted ellipses. It is worth noting that the ATLAS diagram in figure 3.2 also includes a 95% C.L. exclusion contour, which enables us to perform a validity test for this reconstruction method: the third plot in figure 3.3 shows experimental 95% C.L. exclusion contour¹ superimposed with the 95% C.L. obtained with the fitted likelihood. Although the match is not

¹ In the absence of a common figure at the moment of work, the figures used here can be found in the following papers: $\gamma\gamma$, Fig. 20 in [36], $\tau^+\tau^-$ Fig. 12 in [37], WW^* Fig. 40 in [38] and $ZZ^* \rightarrow 4\ell$ Fig. 20 in [39]. However, ATLAS more recently provided such a plot, in figure 4 in [40]

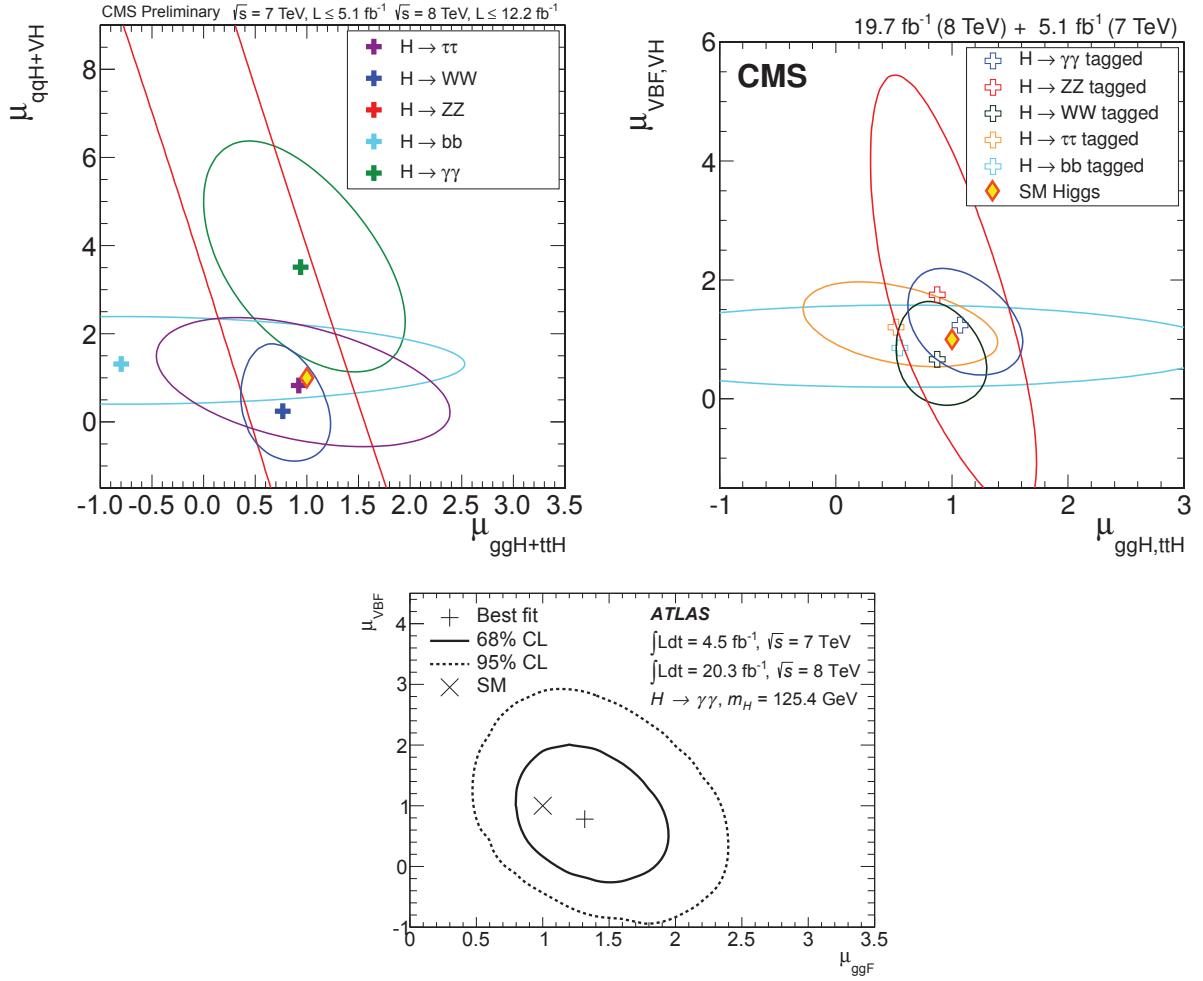


Figure 3.2: Examples of exclusion regions provided by the CMS and ATLAS collaborations in [31, 35, 36]. *Top row:* CMS exclusions at 68% C.L., at the end of 2012 (left) and with all data from run I (2011-2012) (right). *Bottom:* ATLAS exclusion regions at 68% and 95% C.L. in the $\gamma\gamma$ decay channel with all data from run I.

perfect, it is still satisfactory.

The main difference with the 1D version is that we do not get directly the $-2 \ln \mathcal{L}_i$ function, which *a priori* does not vanish anywhere, but its deviation to the best fit $\Delta\chi_i^2$ which vanishes at the best fit point. However we have checked that the resulting statistical test yields a conservative result as compared to the true χ^2 test, as long as each best value $-2 \ln \mathcal{L}_i(\hat{\mu})$ had a large p -value (*i.e.* not negligible as compared to one).

At the end of 2012 however, this procedure could only be used for CMS results, as the ATLAS collaboration had not yet given such exclusion contours, and only the ZZ^* , $\gamma\gamma$ and $b\bar{b}$ decay modes were included. Given that the uncertainties were at that point statistically dominated, they are

Canal	$(\hat{\mu}_{ggh/t\bar{t}h}, \hat{\mu}_{i,VBF/VH})$	V
$H \rightarrow \gamma\gamma$	(0.95, 3.77)	$\begin{pmatrix} 0.95 & -1.35 \\ -1.35 & 6.87 \end{pmatrix}$
$H \rightarrow WW^*$	(0.77, 0.39)	$\begin{pmatrix} 0.19 & 0.15 \\ 0.15 & 1.79 \end{pmatrix}$
$H \rightarrow \tau\tau$	(0.93, 0.89)	$\begin{pmatrix} 2.02 & -0.92 \\ -0.92 & 2.14 \end{pmatrix}$

Table 3.2: CMS results in the $H \rightarrow WW$, $H \rightarrow \tau\tau$ and $H \rightarrow \gamma\gamma$ channels. Results inferred from [31], using equation 3.7.

mostly uncorrelated hence we do not expect significant differences with the previous method in the CMS constraints, which we have checked by comparing the two methods on the same $H \rightarrow \gamma\gamma$ analysis from CMS. For the legacy constraints on the other hand, only the second reconstruction method was used.

In the following sections, we will use our reconstructed likelihood to derive confidence regions in the parameter space spanned by the κ s, using the expression for $\mu_p^i(\kappa)$ given in equation 3.1.

This requires the choice of a statistical test, and we have compared two different tests. The first is the profiled log-likelihood ratio, *i.e.* the quantity $\Delta\chi^2(\kappa) = \chi^2(\kappa) - \chi^2(\hat{\kappa})$ and the second is the full χ^2 test. They differ in the sense that the $\Delta\chi^2$ test is the assessment of a given hypothesis (κ) as compared to another hypothesis ($\hat{\kappa}$), whereas the χ^2 test assesses the κ hypothesis without reference to other hypotheses. Thanks to Wilks's theorem, we know that the $\Delta\chi^2$ distribution will have to be compared with a χ^2 distribution with d.o.f. equal to the number of parameters adjusted in the best fit, while the χ^2 test will follow a χ^2 distribution with a number of d.o.f. equal to the number of individual measurements included. Depending on the data, they will have a different power: in general the $\Delta\chi^2$ will be stronger, as long as the best fit $\hat{\kappa}$ is sufficiently likely; if this is not the case, then the χ^2 test should be used. This can be understood as the fact that the $\Delta\chi^2$ does not test whether a given choice of the parameters κ suitably describes the data, however it tests how a given point in the parameter space compares to the best fit point $\hat{\kappa}$. In the following sub-sections we present some sample constraints, where we have chosen the most appropriate test case by case. As a final remark, it is important to remember that the information we deal here are likelihoods and not probability density functions: the prior probability density function is absent, and we can only extract the information about which model is favoured by the studied experiment. However, we will consider in the following that the prior is uniform, in order to be able to draw conclusions from the distributions.

3.3 Constraints

The likelihood distributions obtained thanks to the methods described in the previous section can now be compared to the values of the parameters obtained for different models in order to constrain them. We will first display a short list of chosen models that can be described in our

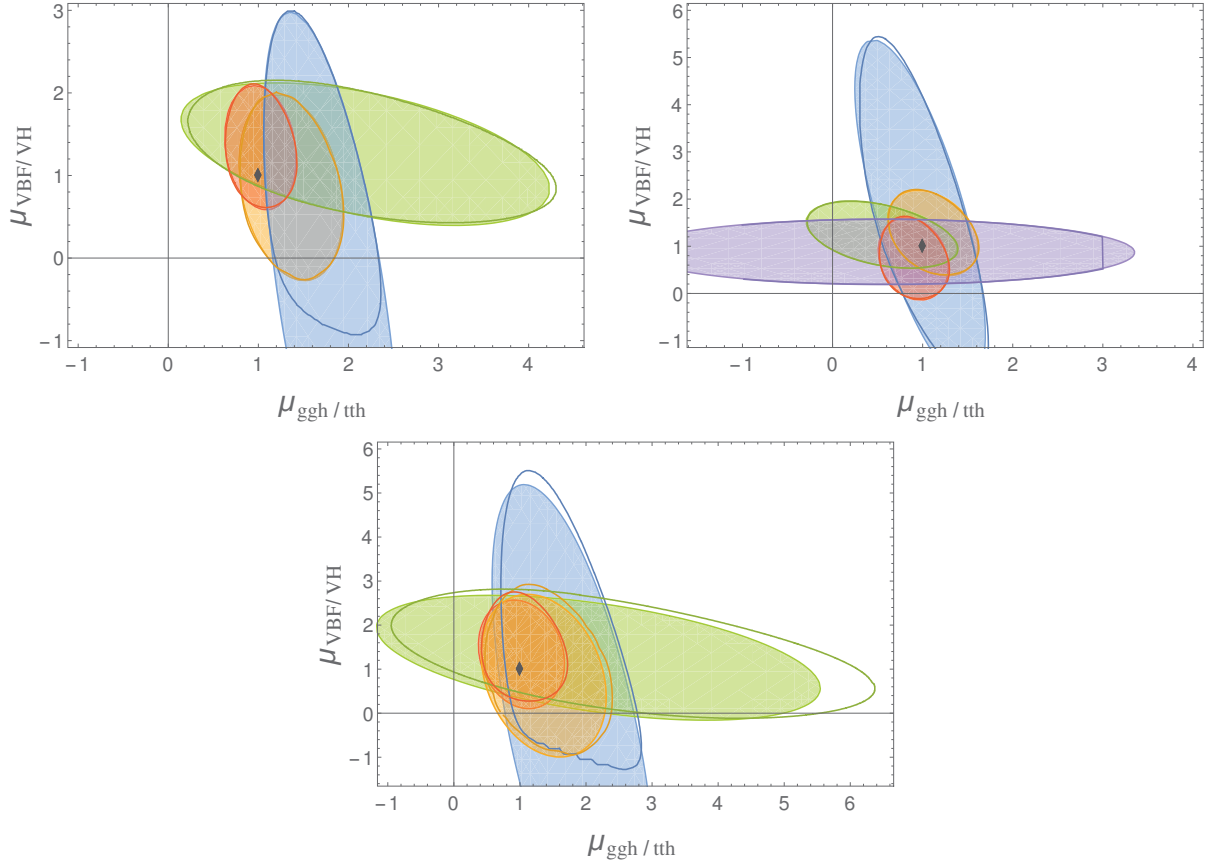


Figure 3.3: Illustration of the relevance of the hypothesis of Gaussian likelihood functions for the different decay channels, on the exclusion regions on legacy data from Run I. *Top row:* comparison of experimental 68% C.L. exclusion contours with the fitted contours (*right:* ATLAS data, *left:* CMS data). *Bottom figure:* comparison of experimental 95% C.L. exclusion contours with contours extrapolated from the 68% C.L. fit (ATLAS only). *Colour code per final state:* purple: $b\bar{b}$, yellow: $\gamma\gamma$, green: $\tau\tau$, red: WW , blue: ZZ . Gray rhombus: SM.

parametrisation, before moving on to the application of the constraints.

3.3.1 Models studied

The constraints on the parameters one would obtain by using this likelihood can be given in all generality without referring to specific models. However, to give a better idea of the discriminating power of these constraints, we give a list of sample models that can be described within this framework. To start with, it is in some cases possible to keep only the two parameters describing the loop couplings only. This can be justified when:

- new physics only enters via loops, while corrections to tree level couplings are small;

- the most sensitive measurements only involve loop induced couplings, while the effects on tree level processes are subleading.

In the second case, one can absorb the contribution of κ_t and κ_W into the loop parameters:

$$\begin{aligned}\kappa'_{gg} &= \kappa_{gg} + \kappa_t - 1, \\ \kappa'_{\gamma\gamma} &= \kappa_{\gamma\gamma} + \kappa_t - 1 + \frac{3\mathcal{A}_1(\tau_W)}{4\mathcal{A}_{1/2}(\tau_t)}(\kappa_W - 1).\end{aligned}$$

With the current lack of precision in the direct measurement of the $t\bar{t}h$ coupling, κ_t can always be absorbed in this way κ_{gg} and $\kappa_{\gamma\gamma}$, although this will no longer be the case when specific measurements become precise enough. Furthermore, a small contribution to $\kappa_W - 1$ can generate sizeable effects on $\kappa_{\gamma\gamma}$ due to the enhancement factor $\frac{3\mathcal{A}_1(\tau_W)}{4\mathcal{A}_{1/2}(\tau_t)} \sim -4.6$. We will therefore use this description for most models presented here.

- ◆ fourth generation, where the result is independent on the masses and Yukawa couplings. The point is given here for illustrative purposes; more complete constraints on this model exist, see for example [41, 42];
- ★ 6D UED model on the Real Projective Plane [43], with $m_{KK} = 600 \text{ GeV}$ is set to the LHC bound [44];
- the Minimal Composite Higgs [45, 46] (Gauge Higgs unification in warped space) with the IR brane at $1/R' = 1 \text{ TeV}$, where only W and top towers contribute significantly and the point only depends on the overall scale of the KK masses, as the other parameters are fixed by the W and top masses;
- ▼ a flat (W' at 2 TeV) and ♠ warped ($1/R'$ at 1 TeV) version of brane Higgs models, in both cases the hierarchy in the fermionic spectrum is explained by the localisation, and all light fermion towers contribute; notwithstanding the many parameters in the fermion sector, the result only depends on the overall scale of the KK masses.

The values for κ'_{gg} and $\kappa'_{\gamma\gamma}$ were computed using the results in [24], while the 6D UED model has been computed in [47]. For a few other models presented in the first paper though, the values of κ'_{gg} and $\kappa'_{\gamma\gamma}$ can be shown stand on a straight line going to the SM point with the variation of a single parameter.

As an example, we present here the case of the Simplest Little Higgs model (▲), described in section 3.3 in [24] and [48]. In this model, the electroweak $SU(2)$ gauge group is in a larger $SU(3)$ at higher energies, and spontaneously broken at low energies by triplets through a Higgs-like mechanism. It contains both a W partner W' and a top partner T . Moreover, mixing between the two states generates a modification of the couplings of the Higgs to the SM W and top. Therefore, there will be a contribution to κ_W and κ_t from the modified tree level couplings, and to κ_{gg} and $\kappa_{\gamma\gamma}$ from the W' and T loops. From the W sector, the contributions are:

$$\kappa_W = 1 - \frac{1}{3} \frac{m_W^2}{m_{W'}^2}, \quad \kappa_{\gamma\gamma}(W') = \frac{63}{16} \frac{m_W^2}{m_{W'}^2}, \quad \kappa_{gg}(W') = 0.$$

Here $m_{W'}$ is the mass of the W' new particle. From the top sector, we have:

$$\kappa_t = 1 + \frac{m_t^2}{m_T^2} - \frac{4}{3} \frac{m_W^2}{m_{W'}^2}, \quad \kappa_{gg}(T) = \kappa_{\gamma\gamma}(T) = -\frac{m_t^2}{m_T^2}.$$

When including the effects of κ_t and κ_W into $\kappa'_{\gamma\gamma}$ and κ'_{gg} , we get:

$$\kappa'_{\gamma\gamma} \simeq \left(\frac{47}{12} - \frac{3}{16} (7 + \mathcal{A}_1(\tau_W)) \right) \left(\frac{m_W}{m_{W'}} \right)^2 \quad \kappa'_{gg} \simeq -\frac{4}{3} \left(\frac{m_W}{m_{W'}} \right)^2$$

We can see that the corrections scale with the W' mass, and the point \blacktriangle corresponds to the value $m_{W'} = 500 \text{ GeV}$ within electroweak precision constraints for a model with T -parity.

Now is also a good time to note that in this model, the three non-zero parameters used in our constraint are actually correlated: $\kappa'_{gg} = -4(\kappa_W - 1) = -64/(125 - 9 \mathcal{A}_1(\tau_W))\kappa'_{\gamma\gamma}$. This raises the question of the number of d.o.f. of the χ^2 function the log-likelihood function the model follows. In the general case without underlying model, when exclusion regions are displayed in a plane, the likelihood from which they are extracted only depends on the two displayed variables, the others being either taken constant (in which case the number of d.o.f might be larger than 2) or minimised along (profiled likelihood) with a number of d.o.f. of 2. However we see that this does not match with the actual number of d.o.f of the considered model. Therefore, it is important when superimposing model points with exclusion regions that the result might only be for illustrative purposes, if the numbers of parameters do not match. In order to exclude a model, the value of the test function must be compared to the proper bound.

The other models lying on lines are:

- Colour octet model [49]: model where the scalar SM sector is extended with a weak doublet which is also a colour octet. Additional neutral and charged scalars therefore appear. The model point represented in all figure corresponds to $m_S = 750$, $\lambda_1 = 4$, $\lambda_2 = 1$, and $\lambda_3 = 2\lambda_2$, while the line corresponds to a varying value of m_S .

$$\kappa'_{\gamma\gamma} = \frac{3}{2} \frac{\lambda_1 v^2}{4m_{S^+}^2} \quad \kappa'_{gg} \simeq \frac{C(8)}{2} \frac{(2\lambda_1 + \lambda_2)v^2}{4m_S^2}$$

- ⊗ 5D UED [50]: a Universal Extra Dimension model with one extra dimension, where only the top and W Kaluza-Klein resonances contribute and the result scales with the size of the extra dimension. The model point here corresponds to $m_{KK} = 500 \text{ GeV}$, and the line corresponds to a varying m_{KK} .

$$\kappa'_{\gamma\gamma} = -\frac{63\pi^2}{16 \times 6} \left(\frac{m_W}{m_{KK}} \right)^2 + \frac{\pi^2}{6} \left(\frac{m_t}{m_{KK}} \right)^2 \quad \kappa'_{gg} = \frac{\pi^2}{6} \left(\frac{m_t}{m_{KK}} \right)^2$$

Model	parameter(s)	$\kappa_W - 1$	$\kappa'_{gg}(\kappa_t)$	$\kappa'_{\gamma\gamma}(\kappa_t)$	$\kappa'_{\gamma\gamma}(\kappa_t, \kappa_W)$
◆ 4 th generation	-	0	2	2	2
▲ Simplest Little Higgs	$m_{W'} = 500 \text{ GeV}$	-0.009	-0.034	0.067	0.11
* Littlest Higgs	$f = 700 \text{ GeV}$ $m_{W'} = 700 \text{ GeV}, x = 0$	-0.05	-0.11	-0.014	0.23
■ colour octet	$m_S = 750 \text{ GeV}$ $\lambda_1 = 4, \lambda_2 = 1$	0	0.37	0.17	0.17
⊗ 5D UED	$m_{KK} = 500 \text{ GeV}$	0	0.20	0.034	0.034
★ 6D UED (RP ²)	$m_{KK} = 600 \text{ GeV}$ ($R_5 = 1.5 R_4$)	0	1.00	0.84	0.84
● composite Higgs	$1/R' = 1 \text{ TeV}$	-0.04	-0.04	-0.03	0.14
▼ flat brane Higgs	$m_{W'} = 2 \text{ TeV}$	-0.005	-0.45	-0.47	-0.45
♠ warped brane Higgs	$1/R' = 1 \text{ TeV}$	-0.11	-0.65	-1.08	-0.57

Table 3.3: Higgs coupling parameters for various benchmark models: in parenthesis we indicate if κ_t and/or κ_W are included in the definition of the loop parameters. In the second column, the mass parameter the corrections are inversely proportional to (eventual other parameters are indicated in parenthesis). Here we only consider corrections to κ_W generated at tree level.

- * Littlest Higgs [51]: the Higgs in this model is one of a set of pseudo-Goldstone bosons in an $SU(5)/SO(5)$ non-linear sigma model. The result scales with the symmetry breaking scale f , which can also be set to low values for a model with T -parity [52], and taken to be $f = 700 \text{ GeV}$ for the sample point (there is also a very mild dependence on the mass of the extra gauge boson contributing to $\kappa_{\gamma\gamma}$, arbitrarily fixed to be equal to f and on the triplet VEV x , that we set to $x = 0$);

$$\kappa'_{\gamma\gamma} \simeq \frac{(195 + 64x - 73x^2)v^2}{128f^2} + \frac{9}{16}(7 + \mathcal{A}_1(\tau_W)) \left(\frac{m_W^2}{m_{W'}^2} - \frac{(5 - x^2)v^2}{8f^2} \right)$$

$$\kappa'_{gg} \simeq -\frac{(7 - 4x + x^2)v^2}{8f^2}$$

The values of the parameters κ_W , κ'_{gg} and $\kappa'_{\gamma\gamma}$, including either only the κ_t contribution or also the κ_W contribution, are given in table 3.3. We can note here that the values of κ_W are small for most of the models presented here, apart from the warped brane Higgs, which will need to be treated separately.

3.3.2 Generic model

We consider here the case presented in the previous subsection, where tree-level corrections can be included in the parameters describing the loop effects. In figure 3.4, the 68% and 95%

C.L. exclusion regions we get from the CMS and ATLAS results at the end of 2012 are displayed, using only selections channels or using the adjusted ellipses, along with the model points described previously. Once again, this plots cannot be used to as they stand to constrain models. However, it is qualitatively interesting to note that the model including a 4th generation of fermions stands far outside of the exclusion regions. As the phenomenology in the Higgs sector of this model does not depend on the masses of the new fermions (they appear in the loops, and give a constant asymptotic contribution as they should be heavy), we can say that the study of the Higgs couplings excludes this model.

By reducing to a two parameter fit on $\kappa'_{gg}, \kappa'_{\gamma\gamma}$, we made the assumption that κ_Z, κ_b and κ_τ are close to one, and that the changes in κ_t, κ_W are noticeable only in the loops, not in direct production or decays. As we said, all specific models fall into this category but the warped brane Higgs, for which κ_W deviates significantly from 1. To test this model, we will need to go beyond the 2-parameter description.

For simplicity, we assume that a custodial symmetry present in the BSM models imposes $\kappa_Z = \kappa_W = \kappa_V$, so that we can treat deviations from the SM couplings of both W and Z with a single parameter. This is usually the case in reasonable models of New Physics.

In the 3 parameter description of the models, the expression of the signal strengths in the $\gamma\gamma$ channel can be written as

$$\begin{aligned} \mu_{i, \gamma\gamma} &= \frac{(1 + \kappa'_{gg})^2 \sigma_{gg}^{SM} \epsilon_{gg}^i + \kappa_V^2 (\sigma_{VBF}^{SM} \epsilon_{VBF}^i + \sigma_{ZH}^{SM} \epsilon_{ZH}^i + \sigma_{WH}^{SM} \epsilon_{WH}^i)}{\sigma_{gg}^{SM} \epsilon_{gg}^i + \sigma_{VBF}^{SM} \epsilon_{VBF}^i + \sigma_{ZH}^{SM} \epsilon_{ZH}^i + \sigma_{WH}^{SM} \epsilon_{WH}^i} \times \frac{BR_{\gamma\gamma}}{BR_{\gamma\gamma}^{SM}} = \quad (3.8) \\ &= \frac{(1 + \kappa_{gg})^2 \hat{\sigma}_{gg}^i + \kappa_V^2 (1 - \hat{\sigma}_{gg}^i)}{1 + (\kappa_V^2 - 1)(BR_{WW+ZZ}^{SM}) + [(1 + \kappa_{gg})^2 - 1] BR_{gg}^{SM}} \left(1 + \frac{\kappa_{\gamma\gamma}}{\frac{9}{16} A_W(\tau_W) + 1} \right)^2. \end{aligned}$$

and for the ZZ channel:

$$\mu_{ZZ} = \frac{(1 + \kappa_{gg})^2 \sigma_{gg} + \kappa_V^2 \sum_{oth} \sigma_{oth}}{\sigma_{gg} + \sum_{oth} \sigma_{oth}} \frac{\kappa_V^2}{1 + (\kappa_V^2 - 1)(BR_{WW+ZZ}^{SM}) + [(1 + \kappa_{gg})^2 - 1] BR_{gg}^{SM}}. \quad (3.9)$$

In figure 3.5 the exclusion contours in the $(\kappa_{gg}, \kappa_{\gamma\gamma})$ plane obtained from the likelihood based on three parameters are shown by slicing the allowed region at the value $\kappa_V = 0.89$. This choice is motivated by the fact that this value corresponds to the brane Higgs model in table 3.3. Thus we are taking the precise slice where the model lies, but one should not forget that we are dealing with a three parameter space. In particular the interpretation is different from a profiling over κ_V . We see that the allowed region is very close to the one obtained in the 2 parameter case in figure 3.4.

With more recent data, it is possible to conduct the same procedure, as shown in figure 3.6 [53]. The experimental results used here come from the legacy analyses from the CMS and ATLAS collaborations cited before, in the exclusive form of exclusion contours in the $(\mu_{ggh/t\bar{t}h}, \mu_{VBF/VH})$ plane. The likelihoods from both experiments were combined by summing the log-likelihood functions, and the test used was based on the log-likelihood ratio with respect to the best fit, sticking with the hypothesis that there are no correlation between the different measurements, whether between channels or between experiments, as it is not possible for us to go beyond

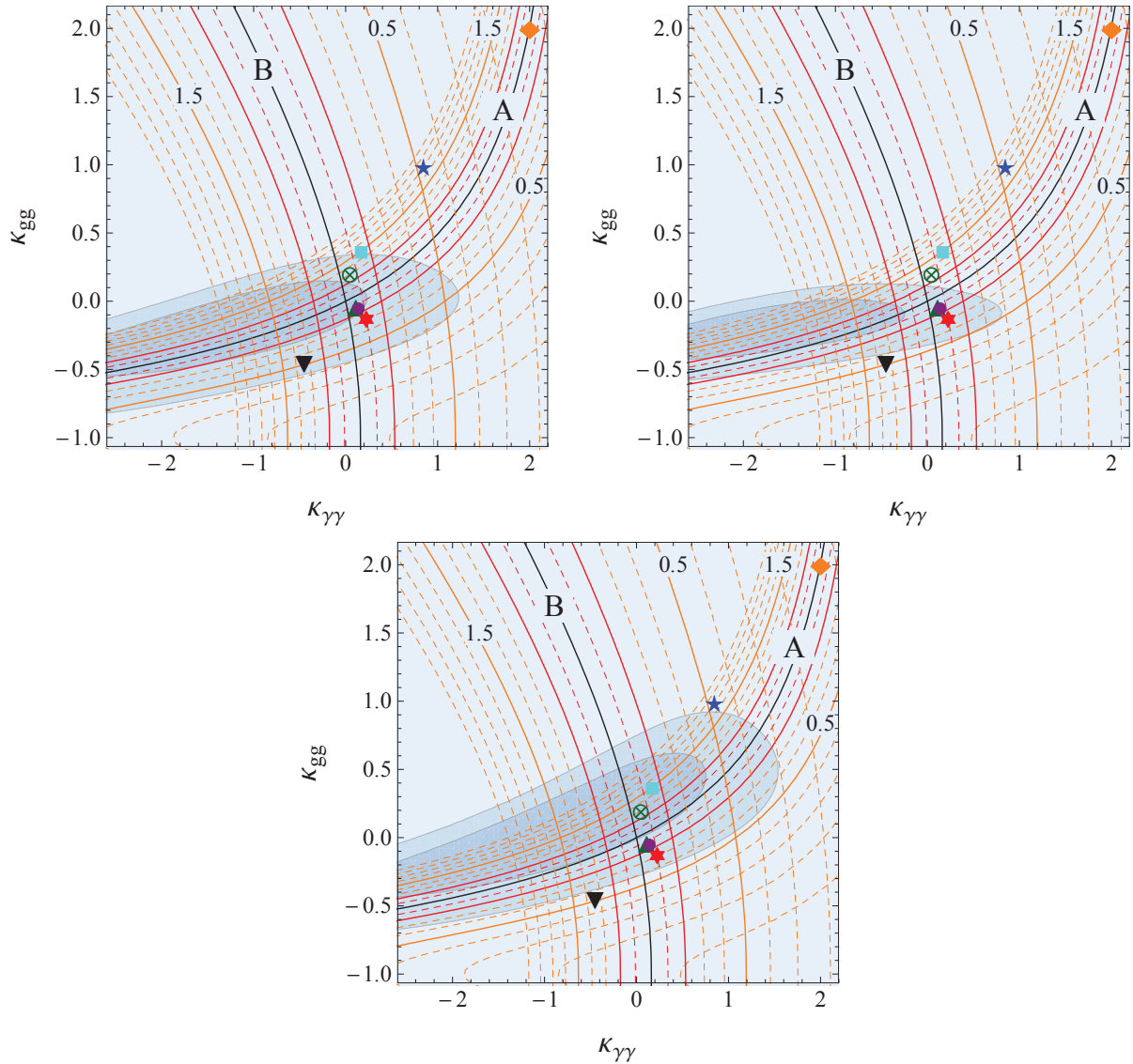


Figure 3.4: Exclusion contours in the plane of $\kappa'_{\gamma\gamma}$ and κ'_{gg} from LHC results at the end of 2012, for a Higgs boson with $m_H = 125$ GeV. The two solid lines correspond to parameters giving the SM values of the inclusive $\gamma\gamma$ channel (**A**), and of the VBF production cross section (**B**). Darker (lighter) blue are the 68% (95%) C.L. limits. *Top row, left*: Likelihood built from CMS individual selection channels for $\gamma\gamma$, ZZ and $\bar{b}b$ decay modes; *right*: likelihood built from all channels, including ellipses. *Bottom row*: Likelihood built from ATLAS selection channels measurements.

that hypothesis. Following the discussion about the number of d.o.f. that should have the χ^2 distribution the test statistic is compared to, two diagrams are shown, with a different convention. On the top left, the constraints are the same as previously, considering that only the parameters

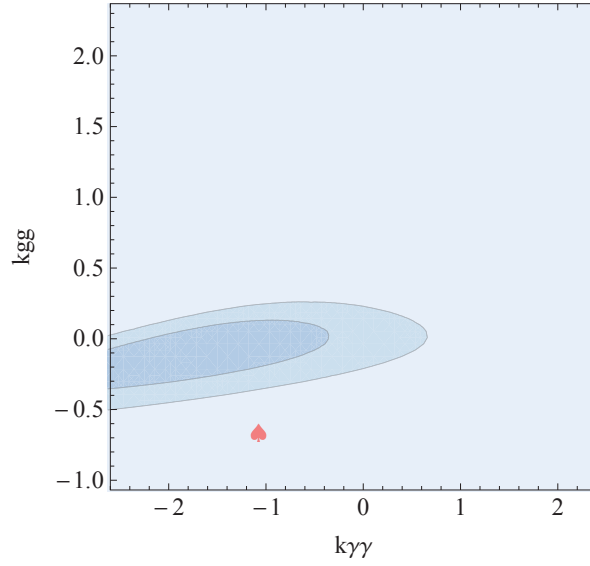


Figure 3.5: Exclusion regions for a three-parameter likelihood built from LHC data at the end of 2012, for a Higgs boson with $m_H = 125 \text{ GeV}$ using all channels from CMS. Here we present a slice of the allowed region for $\kappa_V = 0.89$. Darker (lighter) blue are the 68 and 95% C.L. limits.

κ'_{gg} and $\kappa'_{\gamma\gamma}$ vary, and all other parameters are fixed to 1, while the best fit, $\hat{\kappa}$ is restricted in that plane. On the top right however, we consider that the models do predict the given values of κ'_{gg} and $\kappa'_{\gamma\gamma}$, but that different values of the other parameters might also exist. In this case, we look for the best fit for the parameters $\hat{\kappa}$ in the whole 6-d parameter space, compare the likelihood function to the values of a χ^2 distribution with 6 d.o.f, and slice the resulting region in the plane where tree-level coupling modifiers take the value 1, where the studied models stand. The bottom plot, used as to see the evolution of the constraints, was drawn using the exclusion regions released by CMS ([54]) and ATLAS ([55]) for the 2013 Moriond conferences. On the figures, the 68%, 95% and 99.7% C.L. exclusion regions are given, along with a few model points described earlier and the straight lines they form when varying the parameter they depend on.

Moreover, from these constraints, we can compute values of the parameters for which the models are excluded, for instance along the lines found varying only one parameter. In table 3.4, four values are provided, corresponding to two different approaches of the way the model should match the observations, each one both for former constraints (results published for the Moriond 2013 conference) and the recent legacy ones.

The first and third lines of the table show the values of parameters excluded when comparing the model's log-likelihood ratio $\Delta\chi^2$ to a 6-d.o.f. χ^2 distribution. This means that we consider that the model in itself does not describe all new physics, and other modifications might have an influence on κ_b , κ_t , ..., but we slice the parameter space and constrain the models for which these parameters are indeed 1. By finding the value of the parameter for which the model reaches the border of the 95% C.L. exclusion region, we get a lower bound at 95% C.L. on this parameter.

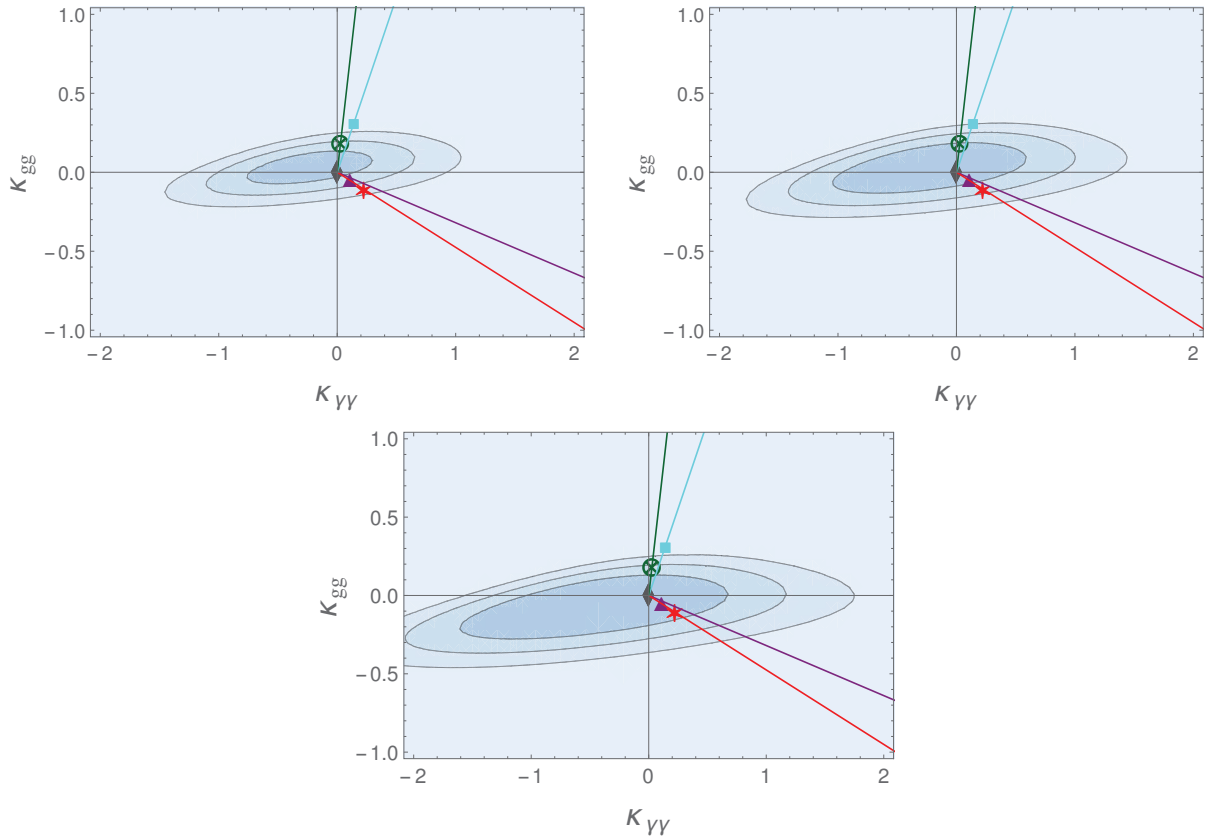


Figure 3.6: *Top*: Constraints from the legacy analyses on various models, in the plane spanned by $\kappa'_{\gamma\gamma}$ and κ'_{gg} , sliced for all other parameters equal to 1. *Left*: The $\Delta\chi^2$ distribution is used to draw exclusion regions at to 68%, 95% and 99.7% C.L. by comparing it to a 2 d.o.f χ^2 distribution and *right*: to a 6 d.o.f. one. *Bottom*: Same plot, compared to a 6 d.o.f χ^2 , from analyses released for the 2013 Moriond conferences ([54,55])

On the second and fourth lines, we instead consider that the only modifications to the Higgs couplings come from the model we are testing. The other κ s are then no longer free parameters, and Wilks's theorem asserts that the log-likelihood ratio function now follows a χ^2 distribution with n d.o.f., n being the number of parameters of the model (and the null hypothesis being of course the total χ^2 minimum, amongst points in κ space that can be described by model). The bounds are therefore tighter, and the values excluded higher. However the bounds on one of the parameters given in table 3.4 are the specific value of such a bound for fixed values of the other parameters.

From the values in this table, we can note that the most stringent bounds for given models are not necessarily the most recent ones. For instance, the colour octet and the UED models are

	χ^2	Colour Octet	5D UED	Simplest Little Higgs	Littlest Higgs
Previous analyses	6 d.o.f	$m_S = 1040 \text{ GeV}$	$m_{KK} = 480 \text{ GeV}$	$m_{W'} = 200 \text{ GeV}$	$m_{W'} = 475 \text{ GeV}$
	n d.o.f	$m_S = 1220 \text{ GeV}$	$m_{KK} = 660 \text{ GeV}$	$m_{W'} = 280 \text{ GeV}$	$m_{W'} = 540 \text{ GeV}$
Legacy analyses	6 d.o.f	$m_S = 835 \text{ GeV}$	$m_{KK} = 430 \text{ GeV}$	$m_{W'} = 250 \text{ GeV}$	$m_{W'} = 580 \text{ GeV}$
	n d.o.f	$m_S = 925 \text{ GeV}$	$m_{KK} = 530 \text{ GeV}$	$m_{W'} = 380 \text{ GeV}$	$m_{W'} = 690 \text{ GeV}$

Table 3.4: Values of the parameters excluded for different models under specific assumptions. The first two lines correspond to old data (2013) and the two last lines to legacy constraints. In each case, in the first lines model predictions are interpreted as following a 6-d.o.f χ^2 distribution and in the second line as a χ^2 distribution with number of parameters equal to the number of parameters of the model

less constrained by legacy results than by the former constraints. This can be easily understood by comparing the two diagrams representing constraints for a 6 d.o.f χ^2 in figure 3.6. The constraints on Little Higgs models, on the other hand, follow the expected variation, and are more constrained by more recent results.

3.3.3 Fermiophobic Higgs

In some cases, models are not represented by single points but still contain parameters that we can directly cast in our parametrisation. For instance, we consider here a class of models in which the Yukawa sector is absent and, therefore, all the Higgs phenomenology takes place via the couplings to vectors. As a consequence, the main decay channel $\bar{b}b$ disappears, as well as the main production mode, $gg \rightarrow h$ (occurring only through fermion loops). These two combined effects leave the inclusive cross-sections for bosonic channels not too different from the SM expectations. The overall effect of this new physics is included in the couplings of the Higgs boson to the W and Z bosons, through the coefficients κ_W and κ_Z . All fermionic κ_f are therefore set to zero, together with κ_{gg} and $\kappa_{\gamma\gamma}$. We do not assume custodial symmetry in order to probe all possible models in the two dimensional (κ_W, κ_Z) parameter space.

This might render impossible the use of the ellipse fit method for the extraction of likelihoods, since VBF and VH production modes are not rescaled in the same way. However it is possible to include the WW channel by noting that this channel was at the end of 2012 still quite insensitive to the VBF production mode (this is demonstrated in the CMS analysis [56]). Concerning the $\bar{\tau}\tau$ and $\bar{b}b$ channels, since this Higgs is fermiophobic, the signal is set to zero and therefore all production channels become irrelevant: in particular, we will have $\mu_{VBF} = \mu_{VH} = 0$ throughout the whole (κ_W, κ_Z) plane, thus this satisfies the requirement for the use of the ellipsis extraction method anyway, but for the $\gamma\gamma$ channel, where selection channels are available. In this case it turns out that the p-value of the best fit model point is low ($3.7 \cdot 10^{-3}$), hence the $\Delta\chi^2$ test tends to be weaker than what is usually expected. Thus we have used here an approximate χ^2 test instead, which explains why there are no 1 and 2 sigmas contours. The result is shown in figure 3.7: it shows a four-fold degeneracy of the χ^2 region with respect to the parameter space

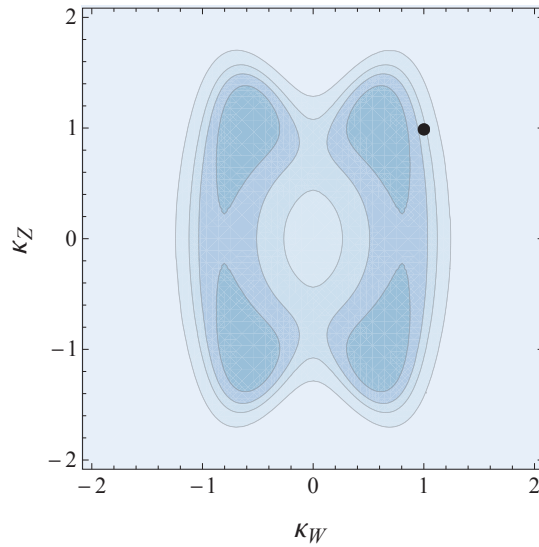


Figure 3.7: Fermiophobic Higgs model exclusion contours at the LHC with $m_H = 125 \text{ GeV}$ using all channels from CMS at the end of 2012, in the (κ_W, κ_Z) plane. Darker (lighter) blue are the 3, 3.5, 4 and 5 σ regions. The black dot labels the fermiophobic SM, $\kappa_W = \kappa_Z = 1$.

due to the obvious sign degeneracy of the two tree-level couplings. The black point corresponding to a fermiophobic SM is excluded by more than 3.5 sigmas *i.e.* at more than 99.9% *C.L.*.

3.3.4 Dilaton model

Another interesting class of models is represented by dilatons, which can play the role of an impostor of the Higgs. A dilaton can be thought of as a Pseudo-Nambu-Goldstone boson associated with an approximate scale invariance: it can give rise to phenomenology at colliders analogous to the one of a Higgs boson because it is expected to couple with the terms that break scale invariance, *i.e.* mass terms [57, 58]. Therefore, it can mimic a Higgs boson in Higgs-less models [59], or modify the couplings of a standard-like Higgs boson via mixing [60]. Dilatons are for example present in all extra-dimensional models, where they are associated with the compactification of the extra space dimensions, and in technicolour models, where they may appear as light scalar degrees of freedom of the confining theory [61, 62]. They have already been indicated as possible impostors of the Higgs.

In this section, we will study a simplified dilaton model, where the impersonator has couplings to all massive states in the SM equal to the SM Higgs boson up to a rescaling factor $\kappa_d = v/f$, where v is the SM Higgs vacuum expectation value, and f is the scale associated with the breaking of the scale invariance (typically one expects $f > v$). The model under consideration, therefore, has equal tree level couplings $\kappa_W = \kappa_Z = \kappa_f = \kappa_d$. Production cross sections and decay widths are accordingly modified, which allows us to get constraints on κ_d . We still study here in addition to this κ_d , the influence of new physics entering the loops, giving κ_{gg} and $\kappa_{\gamma\gamma}$

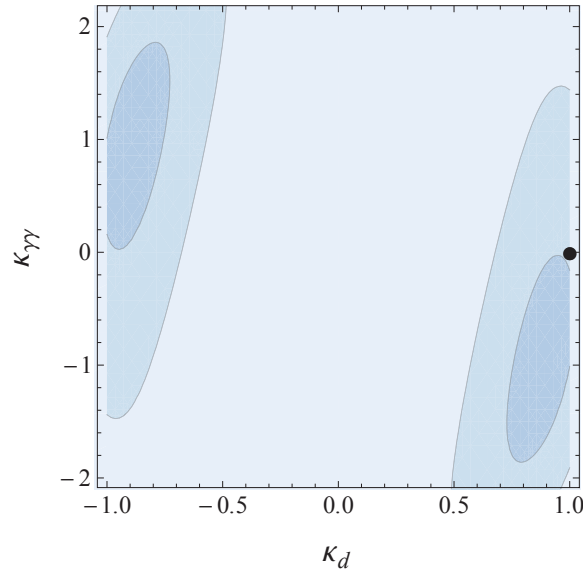


Figure 3.8: Exclusion contours for a dilatonic model at the LHC for a Higgs boson with $m_H = 125 \text{ GeV}$ using all channels from CMS. Here we present the allowed region in a slice $\kappa_{gg} = 0$, in the $(\kappa_d, \kappa_{\gamma\gamma})$ plane. Darker (lighter) blue are the 68% and 95% C.L. exclusion regions.

coefficients, and thus perform a 3 parameter fit. We use here again the χ^2 statistical test rather than the $\Delta\chi^2$, since we expect this kind of model to be strongly constrained. In figure 3.8 we show a slice of the parameter space for $\kappa_{gg} = 0$, which includes the SM Higgs point ($\kappa_d = 1$, $\kappa_{\gamma\gamma} = 0$). The standard model like case is consistent with the previous constraints from the CMS data within a bit more than 1 sigma, as expected. The best fit corresponds to a slightly smaller value of $|\kappa_d| < 1$, however with new physics in the Higgs to $\gamma\gamma$ loop (when assuming $\kappa_{gg} = 0$). In any case there is neither strong exclusion nor strong indication for such a dilation scenario in the data at the end of 2012: the only information we can extract is that small values of $\kappa_d \ll 1$ are disfavoured, even by allowing for arbitrary NP contributions in the $\gamma\gamma$ loop. If this conclusion were to hold a stronger statistical significance, any model of dilatons described by our simplified parametrisation might be excluded.

Chapter 4

Search for possible light additional scalars

As we have seen in the previous chapter, BSM models might modify the scalar sector by modifying the couplings of the observed scalar with respect to the SM. But many models modify it further and contain an extended scalar sector, as there are several theoretical reasons to enlarge it. No theory should be put aside without being tested, and the addition of scalar particles to the SM spectrum is no exception. Moreover, some BSM models predicting the presence of the Higgs boson can only do so if it appears alongside a larger set of scalars. This is the case for instance in supersymmetry, or in some models where the Higgs boson is a composite object.

Of course, searches for scalars have already been conducted in other colliders (especially looking for the Higgs boson), and new scalars would have to abide by those constraints. But as we just said, those mostly focused on looking for a boson similar to the Higgs boson. So what if the particle spectrum contained another scalar, but with different couplings? These experiments, designed to maximize sensibility to a Higgs boson, left a loophole through which it could have avoided discovery. In this chapter we'll propose to extend the parametrisation presented in the previous chapter to additional scalars lighter than the observed one, and then try to constrain such particles, first in a general parametrisation, and then in the framework of two well studied sample models: the two-Higgs-doublet model (2HDM) and the next-to-minimal supersymmetric standard model (NMSSM).

4.1 Description of the parametrisation

The framework for the search of another scalar has no particular reason to be different from the framework used for the first one. The only difference is that we no longer expect to find a Higgs-boson-like particle. However, once again in order to make the constraints easy to apply to a wide variety of models, we will choose a benchmark model: our reference will be the couplings of a would-be SM Higgs boson of the same mass as the studied scalar. This reference might not be the best suited, since we know from the observation of the 125 GeV boson that a new scalar will be different from an additional Higgs scalar, but we will stick to it for the lack of a better

consensus.

For direct searches for light scalars, we define parameters in the very same way as the ones defined for the deviation of the observed scalar from the SM Higgs: a difference is made between couplings existing at tree level and those only appearing with loops. As the previous set of parameters will still be used to impose constraints, indices are used to differentiate the two scalars, and h_1 is used to designate the new light scalar, while h_2 labels the 125 GeV, heavier boson. We therefore get twice as many parameters:

$$\begin{aligned} g_{h_i bb} &= \kappa_{b,i} g_{hbb}^{\text{SM}} & g_{h_i tt} &= \kappa_{t,i} g_{htt}^{\text{SM}} \\ g_{h_i \tau^+ \tau^-} &= \kappa_{\tau,i} g_{h\tau^+ \tau^-}^{\text{SM}} & g_{h_i ZZ, WW} &= \kappa_{V,i} g_{hZZ, WW}^{\text{SM}} \end{aligned} \quad (4.1)$$

As we did for some models for the first scalar, we assume custodial symmetry in this scalar's sector, meaning that W and Z boson couplings are rescaled by a common factor $\kappa_{V,i}$, and that the rescaling factors for the different generations of each kind of fermion are the same labelled after the heavy generation.

Constraints

In order to have realistic points for our two specific models (2HDM and NMSSM), we have applied constraints of two kinds: model-dependent ones and model-independent ones. The latter are purely related to the neutral Higgs phenomenology and can be dealt with at the level of the parametrisation, while the former stem from other sectors and will thus be different in each model. The reader should keep in mind that the goal of these constraints is not to come up with a competitive bound on the parameters of the presented models, but rather to show with realistic model points that such a situation is well motivated to be investigated at LHC.

Concerning the model-independent ones on the neutral Higgs sector, our main interest will be in the LEP limits and the LHC measurements. It turns out that the relevant observables can be completely determined by the value of the $\kappa_{X,i}$ parameters, plus the mass of the light scalar h_1 , which has the important consequence that the test can be carried out at the level of the parametrization, without reference to the actual model. Concerning the LEP limits, we used the program HiggsBounds [63]¹, which takes as input the effective couplings. Those are either directly related to $\kappa_{X,1}$ parameters for tree-level couplings, or through the adapted version of the formulae in equations 3.3 and 3.2 for loop-level couplings. For the couplings of h_2 measured at the LHC, we used the $\Delta\chi^2(\kappa_{X,2})$ test procedure detailed in chapter 3, based on the 2D contours in the (μ_{ggh}, μ_{VBF}) plane. We define allowed points by this test as points in the 95% confidence region.

On the whole, the set of constraints we will have, with the model-specific constraints, includes one likelihood function assessing the compatibility of h_2 with LHC measurements, giving us a 95% confidence level zone, along with additional bounds : LEP, EWPT, flavour. Only points passing each constraint at 95% C.L. are kept in the sample. For the sake of simplicity, we did not build a global likelihood with all the constraints, as this study is more a proof of concept for

¹Note that the version of HiggsBounds available at the moment of this work (4.1.0) did not include the most sensitive limit on $h \rightarrow \text{hadrons}$, hence we included ourselves the results from [64]

the use of the parametrization rather than a full analysis, which can anyway only be performed properly by experimentalists, taking correlations into account between individual likelihoods.

4.2 Two-Higgs Doublet Model

The Two Higgs Doublet Model (2HDM) is a common extension of the SM that relies on the fact that in order to include the Higgs mechanism in the SM, a new type of particle is included, a fundamental scalar. And in the SM, it is the only particle of its kind to exist. Some BSM models aim at removing this specificity by using a non fundamental scalar in its place, but others argue otherwise, that if such a fundamental scalar exists, others might also be present. Some studies have been carried out [49], showing that in order not to have too large deviations from the SM predictions (especially when precisely measured electroweak quantities and flavour physics are concerned), an extended scalar sector has to respect a few constraints, mainly leaving room for particles sharing their quantum numbers with the Higgs, or to a strong octet and weak doublet with hypercharge 1/2. The 2HDM is therefore the model built using two Higgs doublets, whence the name.

As it is a very simple extension, it has been widely studied theoretically [65] as well as concerning its phenomenology in various colliders. In particular at the LHC after the Higgs boson discovery, both cases where a scalar lighter than the 125 GeV one appears ([66–68]), or a heavier one does ([69–79]) have been examined. We will however in this section focus on the use of the proposed parametrisation to constrain this kind of model.

4.2.1 Description

The 2HDM field content is therefore simply the one of the SM extended by a field with the same quantum numbers as the Higgs.

Type	Notation	$SU(3)_C$	$SU(2)_W$	$U(1)_Y$	$U(1)_{em}$
Scalar (boson, s=0)	$\Phi_1 = \begin{pmatrix} \phi_1^+ \\ \phi_1^0 \end{pmatrix}$	1	2	1/2	$\begin{pmatrix} 1 \\ 0 \end{pmatrix}$
	$\Phi_2 = \begin{pmatrix} \phi_2^+ \\ \phi_2^0 \end{pmatrix}$	1	2	1/2	$\begin{pmatrix} 1 \\ 0 \end{pmatrix}$

In the same way as the Standard Model, the EWSB comes from the fact that a field acquires a vev, making the solution to a set of gauge-symmetric equations non-gauge-symmetric, and as was seen as we went through the SM, one of the determining parts added to the SM Lagrangian for the Higgs mechanism to occur was the self-interaction potential of the Higgs doublet. It is still the case in the 2HDM, but the vev is now acquired by a linear combination of the two doublets, as the potential becomes more complex, with 6 real and 4 complex parameters instead

of 2 real ones in the SM. The most general renormalisable potential based on the two doublets Φ_1, Φ_2 can be written in the form:

$$\begin{aligned} \mathcal{V} = & m_{11}^2 \Phi_1^\dagger \Phi_1 + m_{22}^2 \Phi_2^\dagger \Phi_2 - \left[m_{12}^2 \Phi_1^\dagger \Phi_2 + h.c. \right] \\ & + \frac{1}{2} \lambda_1 \left(\Phi_1^\dagger \Phi_1 \right)^2 + \frac{1}{2} \lambda_2 \left(\Phi_2^\dagger \Phi_2 \right)^2 + \lambda_3 \left(\Phi_1^\dagger \Phi_1 \right) \left(\Phi_2^\dagger \Phi_2 \right) + \lambda_4 \left(\Phi_1^\dagger \Phi_2 \right) \left(\Phi_2^\dagger \Phi_1 \right) \\ & + \left\{ \frac{1}{2} \lambda_5 \left(\Phi_1^\dagger \Phi_2 \right)^2 + \left[\lambda_6 \left(\Phi_1^\dagger \Phi_1 \right) + \lambda_7 \left(\Phi_2^\dagger \Phi_2 \right) \right] \left(\Phi_1^\dagger \Phi_2 \right) + h.c. \right\}. \end{aligned} \quad (4.2)$$

where the parameters λ_{1-4} , m_{11}^2 and m_{22}^2 are real and λ_{5-7} and m_{12}^2 are complex, and all others are real.

As in the SM, this potential reaches its minimal values on a space stable under $SU(2)_W \times U(1)_Y$ gauge transformations, but the vacuum state, picking one specific equilibrium state, spontaneously breaks the symmetry. In this vacuum, both doublets acquire *vevs*, which can be written

$$\langle \Phi_1 \rangle = \frac{1}{\sqrt{2}} \begin{pmatrix} 0 \\ v_1 \end{pmatrix} \quad \text{and} \quad \langle \Phi_2 \rangle = \frac{1}{\sqrt{2}} \begin{pmatrix} 0 \\ v_2 \end{pmatrix}$$

where $\sqrt{v_1^2 + v_2^2} = v$, and we define the angle β by $\tan \beta = v_2/v_1$, so that the actual only field acquiring the vev is the field obtained by the rotation of Φ_1 by an angle β in the (Φ_1, Φ_2) space. Moreover, after symmetry breaking, three degrees of freedom no longer appear in the effective Lagrangian, Goldstone bosons serving as longitudinal polarisations of the massive weak gauge bosons, but as four real fields were included with the additional doublet, instead of the one Higgs boson in the SM, there are five leftover fields. The \mathcal{CP} -odd and charged scalars are the components of the doublet orthogonal to the one obtaining a vev, obtained by rotating Φ_2 by an angle β . Being the only bosons with those quantum numbers, they cannot mix with others, which makes them mass eigenstates. The neutral \mathcal{CP} -even parts of the two doublets, on the other hand, do mix through the potential, and the mass eigenstates are found by rotating Φ_1 and Φ_2 by another angle, α . These five states are then labelled $h_{1,2}$ for the two \mathcal{CP} -even neutral states (with $m_{h1} < m_{h2}$), A^0 for the \mathcal{CP} -odd neutral state and H^\pm for the two charged ones, which also are charge-conjugates. It is also convenient to define the angle of the combined rotation: $\tilde{\alpha} = \beta - \alpha$.

The set of parameters describing the potential can then be modified without losing its generality:

$$\begin{aligned} & \lambda_1, \lambda_2, \lambda_3, \lambda_4, \lambda_5, \lambda_6, \lambda_7, m_{11}^2, m_{22}^2, m_{12}^2 \\ & \quad \quad \quad \Updownarrow \\ & m_{h1}, m_{h2}, m_{A^0}, m_{H^+} = m_{H^-}, \tan \beta, \sin(\beta - \alpha) = s_{\tilde{\alpha}}, v, \lambda_6, \lambda_7, m_{12}^2. \end{aligned} \quad (4.3)$$

With this convention, the expression for the masses of the gauge bosons remain unchanged, but their couplings to each of the \mathcal{CP} -even neutral scalars are different from the SM ones, as we will see a bit further.

The other sector linked to the Higgs, the Yukawa couplings, is also modified in the 2HDM by the presence of the second doublet, as each term is doubled, the fermions having the possibility to couple to each doublet. This leads to phenomenological difficulties because of the apparition of flavour changing neutral currents (FCNC) in a too-chaotic Yukawa sector, strongly constrained experimentally. However, it is easy to build a model avoiding them by complying with the hypotheses of the Glashow-Weinberg theorem: there are no tree-level FCNCs in a 2HDM where all fermions with the same quantum numbers couple to the same Higgs doublet. Without loss of generality in the definition of the doublets, one can label as Φ_1 the doublet to which up-type quarks are coupled, and 4 different types of 2HDM therefore arise with the 4 possible combinations of doublets coupling to down-type quarks and charged leptons.

	Type			
	I	II	III	IV
Up Quarks	1	1	1	1
Down Quarks	1	2	2	1
Leptons	1	2	1	2

Couplings of the \mathcal{CP} -even scalars to fermions are therefore also modified, and depend on the Yukawa type of the model considered. In particular, we have in all types for up-type quarks (and any particle coupling to the doublet Φ_1 and weak gauge bosons the following couplings to the two \mathcal{CP} -even Higgses:

$$\begin{aligned}
\kappa_{V,1} &= s_{\tilde{\alpha}} & \kappa_{V,2} &= c_{\tilde{\alpha}} \\
\kappa_{t,1} &= s_{\tilde{\alpha}} + \frac{c_{\tilde{\alpha}}}{\tan\beta} = \kappa_{V,1} + \frac{\kappa_{V,2}}{\tan\beta} & \kappa_{t,2} &= c_{\tilde{\alpha}} - \frac{s_{\tilde{\alpha}}}{\tan\beta} = \kappa_{V,2} - \frac{\kappa_{V,1}}{\tan\beta},
\end{aligned} \tag{4.4}$$

where we also show the relation in terms of κ parameters. Modifiers of the couplings to the doublet Φ_2 (for b quarks in type II and III and leptons in II and IV) can easily be obtained from equation 4.4 by exchanging $\tan\beta \leftrightarrow -1/\tan\beta$. Another coupling is also modified: the charged Higgs contributes to the decay of each \mathcal{CP} -even to two photons:

$$\kappa_{\gamma\gamma} = \frac{\frac{g_{h_i H^+ H^-} v}{m_{H^+}^2} \mathcal{A}_0(\tau_{H^+})}{\frac{4}{3} \mathcal{A}_1(\tau_t)}$$

where $g_{h_i H^+ H^-}$ has the dimension of an energy and $\mathcal{A}_0(\tau) = -\tau^{-2}(\tau - f(\tau))$ is the form factor for a scalar loop, equivalent to those of fermions and vectors given for equation 1.2. Finally, a useful relationship to understand correlations between parameters in this model is that we have for any fermion family, which comes from the unitarity of the $VV \rightarrow ff$ process:

$$\kappa_{f,1}\kappa_{V,1} + \kappa_{f,2}\kappa_{V,2} = 1. \tag{4.5}$$

In the following we will study the type I and type II phenomenologies of this model by probing a part of their parameter space of the model by a numerical scan over the parameters, in the following ranges:

$m_{h_1} (GeV)$	$m_{h_2} (GeV)$	$m_{A^0} (GeV)$	$m_{H^+} (GeV)$	$s_{\tilde{\alpha}}$	$\tan \beta$	$v (GeV)$
[70, 120]	125	[300, 1000]	[300, 1000]	[-1, 1]	[0.35, 50]	246

while λ_6 , λ_7 and m_{12}^2 are zero as we stick to a pure \mathbb{Z}_2 -symmetric model.

4.2.2 Model specific constraints

In the 2HDM case, we will check on the theoretical side the perturbativity of the couplings (granting the validity of the diagrammatic approach), and unitarity and stability of the potential. The stability of the potential, characterises whether the vev v is a stable vacuum for the doublets or whether it is meta-stable/unstable. These tests appear as a 0/1 selection, as model points either pass those test or not, without need for a confidence level. On the experimental side we will look at the electroweak precision test (S, T and U parameters described further), the muon anomalous magnetic moment (Δa_μ) and observables from flavor physics: $B \rightarrow X_s \gamma$, $B_s \rightarrow \bar{\mu} \mu$, ΔM_d . Although $B \rightarrow \tau \nu$ is known to be useful to constrain the 2HDM, we did not include it as it is useful only for models with large $\tan \beta$, but our parameter space does not contain such points, previous constraints implying in our exact \mathbb{Z}_2 -symmetric case that $\tan \beta < 8$. Those quantities have been evaluated using 2HDMC [80] and SuperIso [81], and the experimental bounds are given in table 4.1.

Oblique parameters

The oblique parameters were introduced [82] in order to describe the deviation of precise measurements from predictions in the SM electroweak sector. The amplitudes of electroweak charged and neutral current interactions are affected by the vacuum polarizations (*i.e.* polarizations of vectors such as gauge bosons in the vacuum) through their modification of the gauge bosons propagators present in the matrix elements expressions. Thus, these corrections are called “oblique”, as opposed to “direct” corrections affecting vertices. They are generally called S , T and U , and are given by:

$$\begin{aligned} \alpha S &= 4e^2 [\Pi'_{33}(0) - \Pi'_{3Q}(0)] \\ \alpha T &= \frac{e^2}{s_W^2 c_W^2 m_Z^2} [\Pi_{11}(0) - \Pi_{33}(0)] \\ \alpha U &= 4e^2 [\Pi'_{11}(0) - \Pi'_{33}(0)] \end{aligned}$$

Furthermore, these parameters can be used to describe observables in electroweak processes.

For instance (see definitions in [82]),

$$\begin{aligned}\rho_*(0) - 1 &= \frac{m_W^2}{m_Z^2} \propto T, \\ Z_{Z^*}(q^2) - 1 &\propto S, \\ Z_{W^*}(q^2) - 1 &\propto S + U.\end{aligned}$$

As stated before, being described by a weakly coupled theory, observables involving the electroweak interaction are calculable and measurable with high precision in a perturbative approximation. As a consequence, those precise measurements, sensitive to BSM physics, can be used to constrain models.

The S, T, U oblique parameters should be handled with care in models where new particles couple to the light fermions involved in the measurement of electroweak observables, which might be the case here ([83]). However non-oblique modifications to these observables only occur in the 2HDM for low values of $\tan\beta$, which are excluded from our parameter space by the $B \rightarrow X_s\gamma$ flavour constraint.

Observable	Exp. bound
{S,T,U}	{[-0.10, 0.11],[-0.10, 0.13],[-0.03, 0.19]} [84]
Δa_μ	$\Delta a_\mu < 4.5 \times 10^{-9}$ [85]
$B \rightarrow X_s\gamma$	$\text{Br } B \rightarrow X_s\gamma = 3.43 \pm 0.9 \times 10^{-4}$ [86] ²
$B_s \rightarrow \bar{\mu}\mu$	$1.5 \times 10^{-9} < \text{Br } B_s \rightarrow \bar{\mu}\mu < 3.3 \times 10^{-9}$ [87]
ΔM_d	$\Delta M_d = 0.53 \pm 0.16 \text{ ps}^{-1}$ [86] ²

Table 4.1: *Experimental constraints to be applied on the two sample models.*

4.3 NMSSM

The NMSSM is the simplest extension of the MSSM (Minimal Supersymmetric Standard Model, which is itself the minimal extension of the Standard Model that allows for Supersymmetry), obtained by adding a singlet chiral superfield to the matter spectrum. There are several reasons to prefer the NMSSM as compared to the MSSM: some theoretical (the NMSSM solves what is known as the μ problem), and some phenomenological since its phenomenology is more flexible. In particular, our study deals with the case where the second \mathcal{CP} -even Higgs is the SM-like Higgs, and this possibility is now extremely constrained if not excluded in the MSSM by experimental data (see e.g. [90]). The implication of Higgs measurements has been discussed in many publications (see [91–95], among others), in particular with a light scalar in [96–101]. We choose here to

²We have incorporated the theoretical uncertainty obtained in [88, 89] to the experimental measurement, treating it as a nuisance parameter.

deal with a NMSSM with a \mathbb{Z}_3 -symmetric superpotential. We will not detail its construction, the interested reader can find it in one of the many reviews on the subject (for instance [102]). We used `NMSSMTools-4.0` [103] to compute the relevant observables. Note that we do not take the provided Higgs signal strengths, but in compliance with our parametrisation we use the reduced couplings, and recompute signal strengths ourselves.

4.3.1 Description

The scalar sector of the NMSSM is derived from the one in the MSSM where it is a type II 2HDM by adding another scalar, singlet of $SU(2)$, which gives rise to two additional residual scalars, one \mathcal{CP} -even and one \mathcal{CP} -odd. The three \mathcal{CP} -even scalars are labeled $h_{1,2,3}$, and the two \mathcal{CP} -odd $a_{1,2}$.

We will use the following parameter space: we choose common masses for sfermions, $M_{\tilde{f}} = 500 \text{ GeV}$ for sleptons and $M_{\tilde{q}} = 2 \text{ TeV}$ for squarks, together with vanishing trilinear couplings, except for A_t . This ensures that we are above LHC limits and at the same time decouple them from Higgs physics (apart from the corrections to the Higgs masses). We choose the gaugino masses to be $M_1 = 100 \text{ GeV}$, $M_2 = 500 \text{ GeV}$ and $M_3 = 1 \text{ TeV}$: since we are not interested in Dark Matter observables, we can leave those fixed. The reason why we free ourselves from this constraint is that a correct value of the relic density can often be achieved without changing the Higgs Physics, for instance simply by adjusting $m_{\tilde{\chi}_1^0}$ (which can be done by playing on M_1) so that we sit on a resonance (Z , h_1 or h_2). In particular we have checked that even with $M_1 = 100 \text{ GeV}$, many of our points exhibit a mostly bino (i.e. with a bino fraction larger than 80%) and partly singlino and Higgsino neutralino – which can hence benefit from such a resonance – and that selecting those points does not affect our conclusions on the Higgs sector. We leave thus a refined analysis to a future study. The remaining parameters will be varied in the following range:

$\tan \beta$	μ_{eff}	λ	κ	A_λ	A_κ	A_t
[1, 50]	[100, 600] (GeV)	[0, 0.75]	[0, 0.3]	[-1, 1] (TeV)	[-1, 1] (TeV)	[-4, 4] (TeV)

We keep A_t as a free parameter as it drives most of the radiative corrections to the Higgs masses. We will impose the constraint $m_{h_2} = 125.5 \pm 3 \text{ GeV}$, where the uncertainty is purely theoretical. A flat scan of such a parameter space would give very few points abiding by this constraint (as most of the time h_2 would be heavier), so we used a genetic algorithm based scan: the basic idea is to start from a random population of points in the parameter space that we subsequently evolve by mutations and crossovers and finally select on their ability to pass the constraints that we impose on the phenomenology (in particular $m_{h_2} = 125.5 \pm 3$), and repeating this operation until we find enough correct points.

As an aside, note that we do not impose constraints on the \mathcal{CP} -odd scalars a_1 , a_2 and on the heaviest \mathcal{CP} -even h_3 from direct searches, choice that we justify by the fact that a_2 and h_3 are heavy (above 1 TeV) and that they take most of the $\tan \beta$ enhancement effect, so that prospects

for discovering a_1 (which is lighter) are rather dim. We also stick to the case $m_{a_1} > 125 \text{ GeV}$, to prevent decays of h_1, h_2 to a_1 .

4.3.2 Model specific constraints

In the case of the NMSSM, few model-specific constraints were used, and those which were used were already defined in the 2HDM case: we also used the bound on the muon anomalous magnetic moment and flavour constraints from $B \rightarrow X_s \gamma$, $B_s \rightarrow \bar{\mu} \mu$. Note that in both cases we do not include direct search for charged Higgs since it is too heavy to be constrained ($m_{H^\pm} > 300 \text{ GeV}$).

4.4 Results

We will now use our parametrisation to try and answer the following question: given what we know from LHC measurements about the SM-like Higgs and the null result of the searches for scalars at LEP, are there still non-excluded regions predicting such a scalar observable at the LHC?

4.4.1 Generic model

Without specifying any underlying model, the answer cannot be detailed as much as we would want to: indeed if h_1 and h_2 are uncorrelated, what we know on h_2 couplings has no influence on those of h_1 . The only constraints we have on h_1 therefore come from LEP data, and since LEP and LHC use different production mechanisms (relying on the coupling to electroweak boson for LEP and gluons for LHC³) the null searches at LEP impact very mildly LHC prospects. In terms of parameters, these statements translate as follows: in order to have avoided detection at LEP, this scalar needs either to decay to non-detected states or to be less produced than expected for a Higgs boson of this mass. Our two models having no important invisible decay modes, we will focus on the non-production case. At LEP, production was dominated by EW gauge vectors mediated processes, which vanish quickly if $\kappa_{V,1}$ is taken to be small. Also, at small masses the $H \rightarrow b\bar{b}$ decay mode is by far dominant and often the most constraining at LEP, meaning that reducing it by having $\kappa_{b,1}$ close to 0 will boost the branching ratios of all other decay modes. Combining those two effects, one gets a boosted signal at LHC in modes other than $H \rightarrow b\bar{b}$ that would have gone unobserved at LEP. Another parameter that is not constrained by LEP searches is $\kappa_{gg,1}$, which can enhance a lot production at LHC through the gluon fusion process. We can see this effect in figure 4.1, where we studied the case where all couplings of the light scalar to fermions and loop-induced parameters are taken to be free, but we assume that $\kappa_{V,1}$ and $\kappa_{V,2}$ respect the constraint $\kappa_{V,1}^2 + \kappa_{V,2}^2 = 1$. This induces a constraint from LHC data on the parameters related to the light scalar. In this figure, we show model points passing the combined constraints from LEP and LHC, the point colour depends on the mass of the light scalar, according to the colour scale standing to the right of each plot. The left plot

³LHC is also sensitive to VH or VBF production, but one usually expect gluon fusion to be dominant.

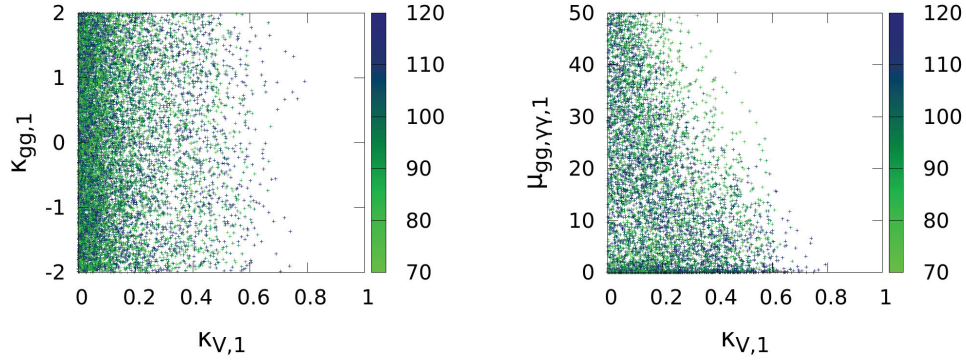


Figure 4.1: *Left*: Model points for various effects of loops ($\kappa_{gg,1}$) as a function of the effective coupling $\kappa_{V,1}$ for models allowed by LHC and LEP constraints, colour according to the mass of the light scalar given as a legend. *Right*: Signal strength of the $gg \rightarrow h_1 \rightarrow \gamma\gamma$ signal for the same model points.

represents the effect of loops as a function of the effective coupling $\kappa_{V,1}$ of the light scalar to SU(2) gauge bosons, while the right one represents the signal strength of the $\gamma\gamma$ decay signal of the scalar, the scalar being produced solely through gluon fusion, as a function again of $\kappa_{V,1}$. We can make two interesting observations here. First, we can see on the left plot that although the maximal allowed value for $\kappa_{V,1}$ depends on the mass of the scalar, at a given mass there doesn't seem to be a constraint on $\kappa_{gg,1}$ from this analysis. This has an influence on the right picture, where we can see that some model points that escaped exclusion by LEP might have a sizeable signature at the LHC in the $h_1 \rightarrow \gamma\gamma$ decay channel, and this quite independently of the mass of the light scalar.

4.4.2 2HDM and NMSSM

If we want to have further information and correlation between h_1 and h_2 , the answer depends on the hypothesized model, and thus we will compare our two sample models as examples, the 2HDM and the NMSSM.

On the experimental side, it is important to note that most of the LHC analyses start at $m_H > 110 \text{ GeV}$, while our approach allows to handle a more general situation, and indeed the LHC collaborations are now studying also the scenario of a lighter Higgs boson. While starting at $m_H > 110 \text{ GeV}$ is a valid approach when looking for the SM Higgs since LEP already ruled it out for lower masses, it has no support when looking for a non-SM Higgs such as the one that we are dealing with. While such a search certainly presents new challenges from the experimental point of view (not all final states may be exploitable), we do think that it is worth studying, since many models still allow for light additional scalars. We will not dwell more on the subject of experimental sensitivity, and, for the sake of concreteness, we shall focus on the search channel $h_1 \rightarrow \gamma\gamma$.

We show in figure 4.2 the reach of the signal strength μ in the channel $gg \rightarrow h_1 \rightarrow \gamma\gamma$ for both models. This is an important piece of information, since it already tells us that the LHC has the power to discriminate some of the scenarios: indeed, corresponding to the model-independent case discussed previously, some allowed points of the NMSSM and, to a lesser extent, of type-I 2HDM can reach high values ($\mu_{gg \rightarrow h_1 \rightarrow \gamma\gamma}$ can reach 3 in the NMSSM and 0.5 in 2HDM-I), whereas 2HDM-II shows much more modest values. We remind that the 95% excluded signal strength reported by ATLAS and CMS lies around 1 at $m_H = 110 \text{ GeV}$, so points with $m_{h_1} > 100$ and $\mu_{gg \rightarrow h_1 \rightarrow \gamma\gamma} > 1$ are probably probed by the current data-set. The color code is the following: green points pass all “non-Higgs” constraints (in particular, flavour observables), blue points also pass the LEP constraints and finally red points are, in addition to that, compatible at 95% with the SM-like Higgs couplings measured at the LHC. It is also worthwhile to compare the production cross-section through gluon fusion and through Vector Boson Fusion (VBF) or associated vector boson production⁴ (VH), as shown in the plots on the second row of figure 4.2: as the two have different kinematics properties, the sensitivity towards a VBF dominated sample may differ from the one of a gluon-fusion dominated one. We see that in the 2HDM case, we can have a very different composition whereas in the NMSSM the composition will be the one of the SM. Coming back to the model independent case, we can see here that within the two sampled models no big effect appear in $\mu_{gg \rightarrow h_1}$ from $\kappa_{gg,1}$, as there are no new coloured particles in the 2HDM, and the NMSSM has identical rescaling for VBF and gluon fusion. However, other sample models might provide with a sizeable $\kappa_{gg,1}$, unconstrained and give the same kind of increment in event rates.

The various features that appear at the level of signal strengths are better understood at the level of the $\kappa_{X,i}$ parameters. Thus, we show on the top row plots of figure 4.3 the relation between m_{h_1} and $\kappa_{V,1}$, making the LEP exclusion explicit. Since LEP is sensitive to all possible final states of h_1 , its exclusion directly scales with the rate of production along with a vector boson (VH). It turns out that the NMSSM can weaken the bounds at low m_{h_1} : this stems from the fact that we can have a suppressed coupling to down-type quarks without a suppressed coupling to up-type quarks (a situation that cannot be reproduced in 2HDM-I and that is forbidden by flavour tests in 2HDM-II), leading thus to an enhancement of the branching fraction to jets where the limit is weaker than for $\bar{b}b$ final state. We note that the LHC constraint also impacts this plot: this is due to the relation $\kappa_{V,1}^2 + \kappa_{V,2}^2 = 1$ which is exact in 2HDM, and turns out to hold to a very good approximation in the NMSSM⁵. As a short parenthesis, let us notice that in the case of 2HDM-II, some values of $\kappa_{V,1}$ are forbidden: this is due to an interplay between flavour and LHC constraints. First, let us point out that the main contribution to the flavour observables in the 2HDM comes from the charged Higgs: it turns out that in our set-up, where both h_1 and h_2 are light, the charged Higgs cannot decouple if the perturbativity of the Higgs potential is to be preserved. Moreover, it occurs that since the coupling of the charged Higgs to up-type quarks, which is independent of the Yukawa pattern, has a dominant impact on flavour observables, all types end up with a similar constraint on $\tan \beta$, namely $\tan \beta \in [2, 8]$. Then, we deduce from equation 4.4, that in order to have $|\kappa_{b,2}| \approx 1$ ⁶ in type II, we need $\kappa_{V,2} \approx 2/\tan \beta$.

⁴Since our parametrization respects custodial symmetry, we have $\mu_{\text{VBF}} = \mu_{\text{VH}}$.

⁵For all our points, h_3 turned out to be very heavy and to play no role in EWSB.

⁶The approximation is rather loose, *i.e.* $|\kappa_{b,2}| = 1 \pm 0.5$ is compatible with LHC Higgs couplings

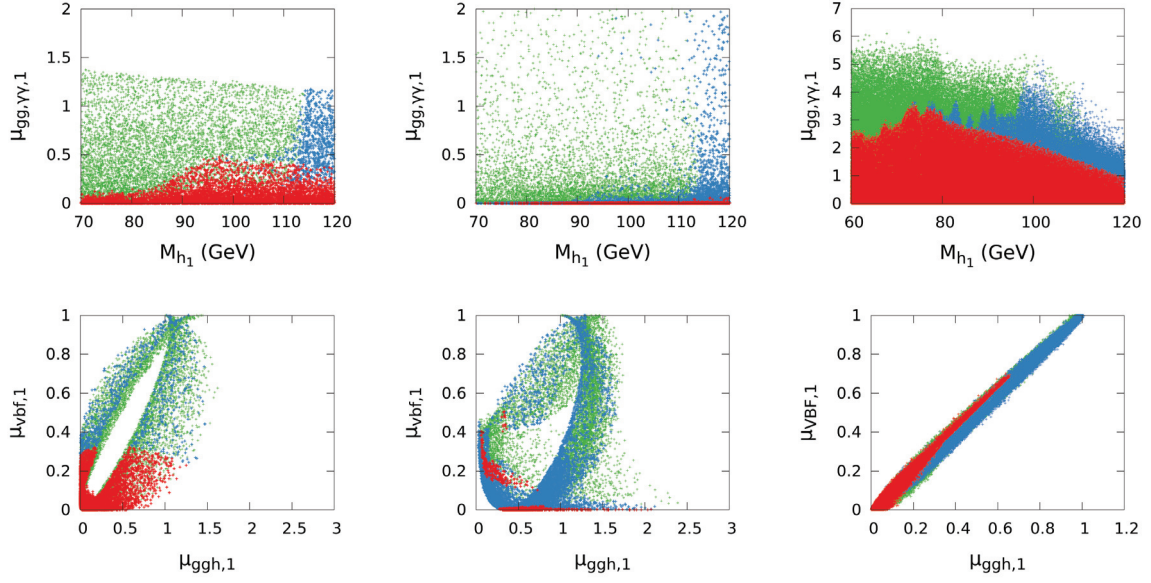


Figure 4.2: Models from left to right : 2HDM(I), 2HDM(II), NMSSM. Top: signal strength in the $gg \rightarrow h_1 \rightarrow \gamma\gamma$ channel. Bottom: ggh production mode versus VBF, both normalized to the SM. The colour code is the following: Green points are all points passing flavour and theoretical constraints, blue points are a subset of those which also pass LEP constraints on h_1 and red points pass in addition the LHC couplings constraint on h_2 .

Thus the constraint on $\tan\beta$ from flavour physics translates to a constraint on $\kappa_{V,1}$ due to the Higgs coupling data. Incidentally, note that the NMSSM avoids this constraint thanks to its third scalar: the latter, heavy, will take most of the $\tan\beta$ enhancements, making thus the relation between $\tan\beta$ and $\kappa_{b,1}$ not as strict as in the 2HDM-II.

We also learn from figure 4.3 that the correlations between $\kappa_{V,1}$ and $\kappa_{t,1}$ differ significantly between the two models: in the NMSSM they have the same behaviour (which explains thus why μ_{VBF} behaves the same way as μ_{ggh}) while in the 2HDM, $\kappa_{t,1}$ can reach high values even for $\kappa_{V,1} \approx 0$.

A crucial point in disentangling the phenomenology of different models is through the coupling to b quarks, which is parametrized by $\kappa_{b,1}$: we show the $(\kappa_{V,1}, \kappa_{b,1})$ plane in the bottom row of figure 4.3. One notices that in the 2HDM-II case, there is no possibility for $\kappa_{b,1}$ to vanish if $\kappa_{V,1}$ does not, situation that differs significantly from 2HDM-I or the NMSSM. Such a feature would not come unnoticed at the LHC: indeed, since the width of a SM light Higgs is dominated by the $\bar{b}b$ decay, having $\kappa_{b,1} \approx 0$ will enhance all other decay modes, in particular the $\gamma\gamma$ one. In fact all points with a signal strength in the $gg \rightarrow h_1 \rightarrow \gamma\gamma$ channel higher than 1 in figure 4.2 benefits from this mechanism. The largest enhancements also benefit from a non-vanishing $\kappa_{\gamma\gamma,1}$

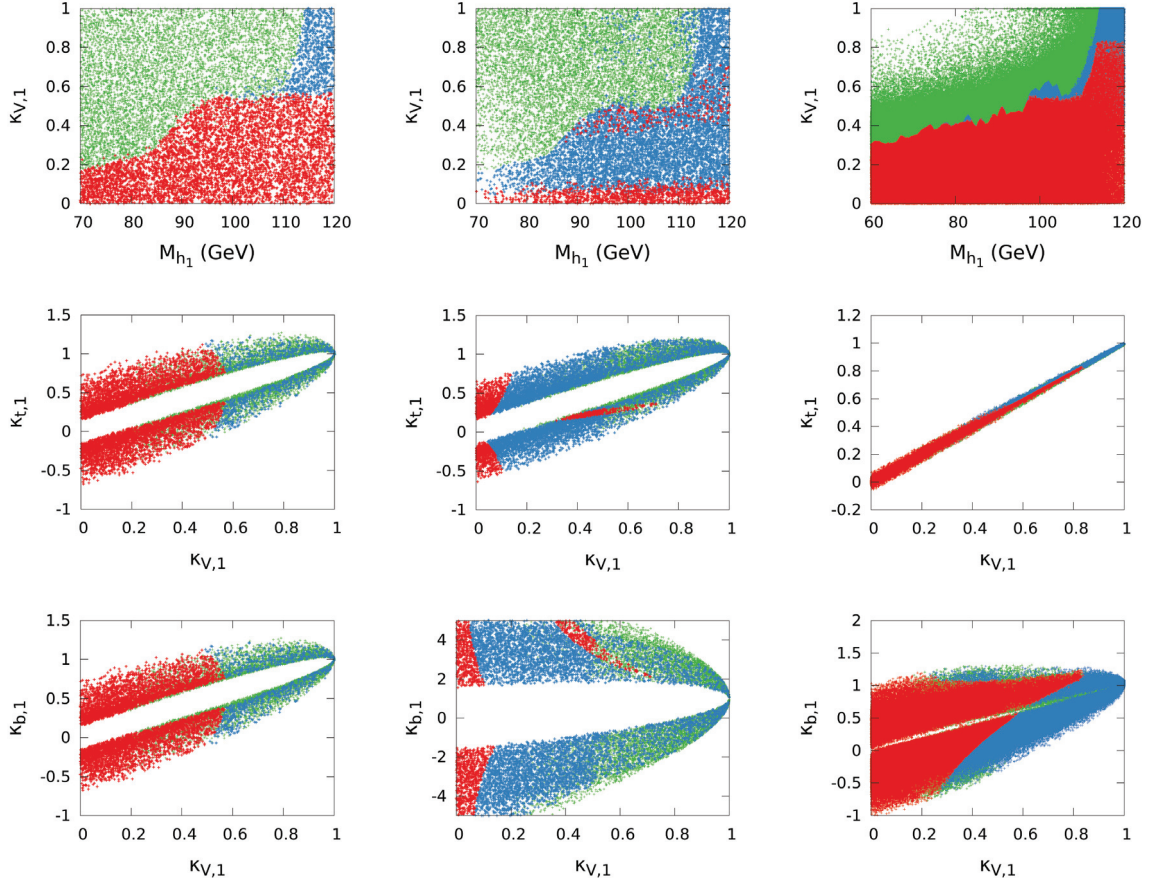


Figure 4.3: Correlations between $\kappa_{V,1}$, $\kappa_{t,1}$, $\kappa_{b,1}$ and m_{h_1} : left column corresponds to 2HDM(I), middle one to 2HDM(II) and right one to the NMSSM. Colour code identical to figure 4.2

parameter: in particular some of the NMSSM points are noticeably enhanced by the chargino contribution. Thus in this case the significant difference of signal strengths from various theories can be explained in a universal way through the correlations of the κ parameters, without need of the underlying theory.

Another feature of 2HDM-II shows up in the $(\kappa_{V,1}, \kappa_{b,1})$ and $(\kappa_{V,1}, \kappa_{t,1})$ planes of figure 4.3: we see that the points allowed by LHC constraints for which $\kappa_{V,1}$ does not vanish form lines which are either $\kappa_{t,1} = \kappa_{V,1}/2$ or $\kappa_{b,1} = 2/\kappa_{V,1}$. This can be understood from eq.4.5: approximating $|\kappa_{V,2}| \approx 1 - \kappa_{V,1}^2/2$ and $|\kappa_{f,2}| \approx 1$ (which is the limit of h_2 being completely SM-like with respect to fermions), one obtain the two solutions $\kappa_{f,1} = \kappa_{V,1}/2$ or $\kappa_{f,1} = 2/\kappa_{V,1}$, depending on the sign of $\kappa_{V,2}\kappa_{f,2}$. For the time being, LHC constraints on $\kappa_{b,2}$ or $\kappa_{t,2}$ are not strong enough to justify the approximation $|\kappa_{f,2}| \approx 1$, which is why there are no such lines in type I. However in type II, the Yukawa structure is such that, for $\tan\beta > 1$, small variations of $\kappa_{t,2}$ will correspond to

large variations of $\kappa_{b,2}$. The latter being not too loosely constrained⁷, the former will stay in a narrow band. This narrow band will thus translate to a line $\kappa_{t,1} = \kappa_{V,1}/2$, as foreseen by our earlier argument. Note that type III exhibits a very similar behavior as of type II, while type IV is in-between type I and type II: in this case $\kappa_{t,2}$ and $\kappa_{b,2}$ vary the same way, but now $\kappa_{\tau,2}$ exhibits large variations, and will thus constrain them. The LHC constraint on $\kappa_{\tau,2}$ being looser than $\kappa_{b,2}$, the allowed bands will be broader.

These observations tend to show that the possibility of an extra scalar, lighter than 125 GeV , is still compatible with current experimental data in different models of New Physics, suggesting that dedicated analyses in this mass range at the LHC are an interesting possibility for the experimental collaborations. Such a study was carried out by the ATLAS collaboration [104], mainly constraining the signal strength $\mu_{gg \rightarrow \gamma\gamma}$ represented in figure 4.2, but giving constraints on fiducial cross sections. However, presenting the results using a generic parametrisation similar to ours comes with the advantage of being easily related to purely experimental quantities (such as cross-sections) and at the same time allowing a clear disentangling of some specific models in terms of correlations of the different κ parameters. In addition to that, some effects at the experimental level, such as an enhancement in the channel $gg \rightarrow h_1 \rightarrow \gamma\gamma$, could be shown directly in terms of the allowed values for the κ s, without considering the underlying model: such a feature would greatly simplify the study of the phenomenology of an additional light scalar.

⁷The main constraint on $\kappa_{b,2}$ does not come from the $VH \rightarrow V\bar{b}b$ analysis, but rather from the total width of the Higgs, which affect all signal strengths.

Chapter 5

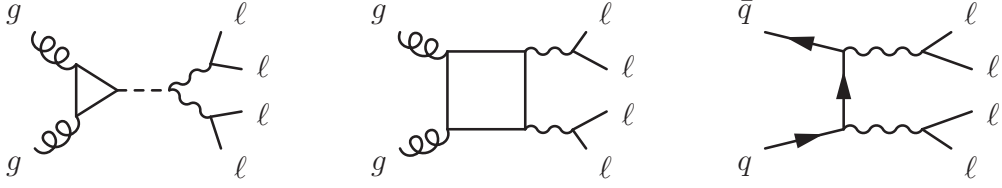
Further developments

The process of building models and constraining them is a never ending process, as they both depend on the development of new techniques, on the precision of calculations, on the results, expected or not, of ongoing and future experiments, which themselves are progressively made better with technological improvements. The parametrisation and techniques presented in this thesis are therefore not the final word of this story. In this chapter, we will present a few concepts that might be used to improve the constraining procedure presented until now.

5.1 Off-shell implications

At first approximation, a particle can be said to be on-shell if its invariant mass, p^2 is close to its mass squared m^2 . This comes from the propagation factor in amplitude calculations, of the form $1/(p^2 - m^2 - i\Gamma)$, making a process involving this particle in this region of phase space more likely. It is therefore obvious that the name off-shell describes situations in which this relation no longer holds, but the particle can still appear on even shorter time scales, and is called virtual.

In previous chapters of this thesis, most of the information about the observed boson was gathered from measurements where the Higgs boson was on shell. But during the LHC upgrade pause in 2013-2014, more innovative methods were thought of, among which the measurement of the contribution of the Higgs boson to processes in regions of phase space where it is off-shell [105–108]. Soon after that, analyses were implemented and results were published by the CMS and ATLAS collaboration about searches for $H \rightarrow ZZ \rightarrow 4\ell$ in [109–111]. However in these analyses, this measurement was used as a way to constrain the total Higgs width. In the case where new particles form loops to take part in the coupling of the Higgs boson to gluons, this approach is no longer valid as it relies on using a common rescaling factor μ_{ggH} between on-shell and off-shell measurements, making this constraint model-dependent [108, 112]. We will see in this section in which way the parametrisation described previously can be used to get information from these measurements, disentangling the top and NP contributions to the gluon-fusion production signal strength μ_{ggH} when new coloured states are heavy enough, which was not possible using only on-shell measurements.



In order to make our analysis comparable with the experimental results, we computed cross sections using the selection procedure of the CMS analysis [109], which selected a region of phase space in order to enhance the rate of events coming from the $gg \rightarrow ZZ$ process, which consists of a box diagram plus the s-channel Higgs, over the $q\bar{q} \rightarrow ZZ$ background. The Higgs contribution, indiscernible from the box diagram, consists mainly of a gluon fusion production followed by the decay to two Z bosons, which interferes with the box diagram (see diagrams above). In [109], on-shell and off-shell cross sections are given, and can be translated in terms of the parameters introduced in this thesis as:

$$\sigma_{gg \rightarrow H \rightarrow ZZ^*}^{\text{on-shell}} = \frac{\kappa_g^2 \kappa_Z^2}{m_H \Gamma_H} \quad \text{and} \quad \sigma_{gg \rightarrow H^* \rightarrow ZZ}^{\text{off-shell}} = \frac{\kappa_g^2 \kappa_Z^2}{4m_Z^2}$$

and we can see that the width Γ_H is not the only parameter entering these cross sections. Indeed, one can compensate a non-standard value of the width in the on-peak measurement by a modification of the effective couplings to g and Z to get a standard rate, while this rescaling of the couplings might influence the off-shell cross-section. Taking this into account, the analysis constraint on the width relies on two assumptions: that the increase of the width is not related to the modification of those SM couplings and therefore comes from BSM decay channels (meaning that if the couplings to SM particles are larger than expected, the observed rates of on-shell decays to SM particles stay the same from the existence of additional BSM invisible decays), and that κ_g does not contain a contribution from new loops. Indeed, it was pointed out in [112] that for partonic centre-of-mass energies above the $2m_t$ threshold, the top loop which is the main contributor to the ggh coupling in the SM becomes resolved, while it is not for $\sqrt{\hat{s}} = 125 \text{ GeV}$. This implies that the form factors in the two cases will be quite different. If additional loops appear however, in which heavier particles run, the difference between the form factors for $\sqrt{\hat{s}} = 125 \text{ GeV}$ and in the off-shell region would not be the same, giving different values for the effective coupling κ_g for the two cross-sections. Such new coloured states appear in many BSM models alongside modification of the top tree-level couplings to the Higgs, causing mixed effects in the cross sections which might cancel each other, as could happen for example in the case of a heavy vector-like quark mixing to the top via Yukawa-like interactions, as in models of Composite Higgs with top partners. Moreover, because of direct searches at colliders and in particular at the LHC, such states are experimentally bound to be rather heavy, making our heavy-loop approximation well-motivated. For the study of such cases, we will see that the definitions of parameters κ_t and κ_{gg} are particularly well suited to disentangle these measurements for different values of $\sqrt{\hat{s}}$.

On-shell, neglecting light quark loops, the parameters in the two sets presented in chapter 3 are simply related: $\kappa_g = \kappa_t + \kappa_{gg}$, and an experimental degeneracy appears between κ_t and κ_{gg} which can at this level only be dealt with by the direct measurement of κ_t , for instance through the selection of the $t\bar{t}h$ production mode. However, because of the effects discussed previously,

we will see that this degeneracy is removed when including off-shell measurements. It is important to remember here that the parameter κ_{gg} is defined from the on-shell amplitudes. On the other hand, it is also important to remember that the form factors appearing in the amplitudes of the loop diagrams reach asymptotic values for large masses of the particles running in the loops. This remains true when the Higgs boson is off-shell, but the “heavy” character of the particle is estimated with respect to $\sqrt{\hat{s}}$. It is that the top quark can no longer be considered as heavy in this prospect in the off-shell region, but if the new particle can, its contribution will properly be described by κ_{gg} , and the two parameters will appear in a different combination in the two measurements, making it possible to separate the two effects.

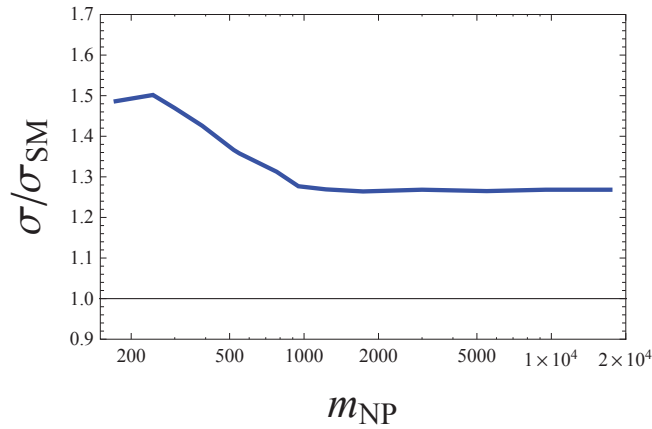


Figure 5.1: Dependence on the new-physics mass of the cross section of the $gg \rightarrow VV$ process in the off-shell region, normalized to the SM cross section for the same process.

To see to what extent this statement holds in the experimentally-defined off-shell region, we considered the process $gg \rightarrow ZZ \rightarrow l^+l^-l'^+l'^-$ with an additional state contributing to the Higgs production, and the dependence of its off-shell cross section on the mass of the NP particle running in the loop. By the term off-shell cross section, we designate the cross section integrated over a range $\sqrt{\hat{s}} > 330 \text{ GeV}$ after the basic experimental cuts, following definitions in [109]. It might be worth noting however that our definition does not correspond however either to the “off-shell” ($m_{4\ell} > 220 \text{ GeV}$) or “signal-enriched” ($m_{4\ell} > 330 \text{ GeV}$ plus a cut on a matrix element MELA discriminant) regions defined in that experimental analysis, since we did not impose the MELA cut.

In order to estimate the cross sections, we used the partially-analytical and partially-numerical code `gg2VV` [113], itself based on the codes `FeynArts`, `LoopTools` and `FormCalc`, which we modified to include an additional heavy particle loop to the Higgs production. More specifically, at amplitude level, a term similar to the one corresponding to the top loop was added, but with a modified mass m_{NP} . This corresponds to a case where a heavy top-like fermion runs in the loop. Moreover, we added two coefficients in front of the terms corresponding to the top loop amplitude and in front of the newly added one, respectively corresponding to κ_t and κ_{gg} . That the first corresponds to κ_t is obvious, however the second one is less immediate. It is once again

necessary to remember that form factors reach an asymptote for heavy particles in the loop, and that the two amplitudes present in the definition are calculated for $\sqrt{\hat{s}} = 125 \text{ GeV}$ where the top can also be considered as heavy, and $\mathcal{A}_{1/2}(\tau_t) \approx 1.37$ while $\mathcal{A}_{1/2}(\tau_{\text{NP}})$ is closer to $4/3$ since $m_{\text{NP}} > m_t$. The coefficient in front of the newly added amplitude is therefore $\kappa_{gg} \times \frac{\mathcal{A}_{1/2}(\tau_t)}{\mathcal{A}_{1/2}(\tau_{\text{NP}})} \approx \kappa_{gg}$ with a roughly 3% approximation.

Figure 5.1 shows the evolution of the off-shell cross section in this model normalised to the SM off-shell cross section as a function of the mass m_{NP} of the additional state, varying from m_t to $100 m_t$, while κ_t and κ_{gg} are fixed at 1. We can see that when m_{NP} reaches values between 500 GeV and 1 TeV , the values of the cross section become fairly constant, proving that above these masses, the approximation of infinite mass, and therefore the possibility to use a common κ_{gg} for the treatment of on-shell and off-shell measurements, is reasonable.

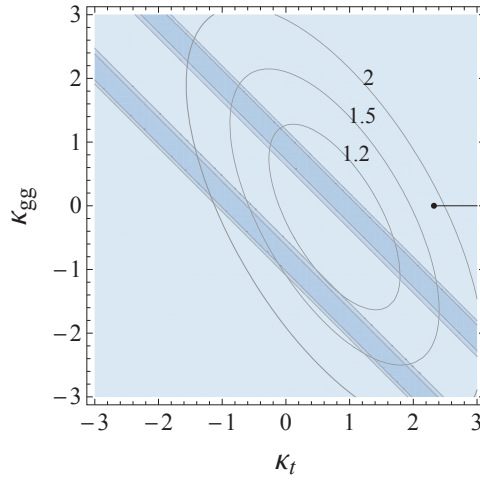


Figure 5.2: Regions allowed at 68 and 95.5% C.L. by the on-peak coupling constraints (diagonal bands), compared to the off-shell iso-cross section lines for the $gg \rightarrow VV$ process at 1.2, 1.50 and 2 times the SM cross section. The dot and black line correspond to the $\kappa_{gg} = 0$ case where the CMS bound can be recast to the constraint $\kappa_t < 2.3$.

On figure 5.2, information concerning both peak and off-shell measurements are shown as a function of κ_t and κ_{gg} , and m_{NP} is fixed at a large value. The on-shell constraints are obtained by profiling the likelihood on $\kappa_{\gamma\gamma}$, as additional non-coloured charged particles could take part in that coupling. As we did not include constraints on the $t\bar{t}h$ production mode that come from specific searches (which are anyway quite loose), there is no way to distinguish κ_t from κ_{gg} and the on-shell constraints are degenerate in the direction where $\kappa_t + \kappa_{gg}$ is constant, forming bands. The bands appearing in figure 5.2 correspond to exclusion regions at 68 and 95% C.L.

On the other hand, the off-shell cross section is represented as ellipses giving iso-off-shell cross sections. Those were obtained by fitting a paraboloid to values of the off-shell cross-sections computed on an array of values of κ_t and κ_{gg} , and taking constant slices of this paraboloid. The curves shown on figure 5.2 correspond to 1.2, 1.5 and 2 times the SM off-shell cross section. We

can see that this curve indeed allows to discriminate values in the $\kappa_t + \kappa_{gg} \sim \pm 1$ region favoured by the on-shell measurements.

To see to what extent a doubled off-shell cross section is interesting, one can look at table 1 of [109], where the off-shell signal-enriched region after MELA discrimination is shown to contain 11 events against the expected 11.4 ± 0.8 : these numbers, when compared to the 1.8 expected $gg \rightarrow VV \rightarrow 4\ell$ events, show that at 95% C.L. the study is indeed sensitive to an approximate doubling of the $gg \rightarrow VV$ cross section.

The last feature appearing on figure 5.2 are the black dot and line appearing on the right. These correspond to the recasting of the CMS analysis in our framework. However, as this analysis does not include additional loops, the constraint on the Higgs width can only be used with the additional hypothesis that $\kappa_{gg} = 0$. In that case, an effective rescaling factor ξ of the width, $\Gamma_H = \xi \Gamma_H^{\text{SM}}$, can be compensated on-peak by having $\kappa_t = \sqrt{\xi}$. Therefore, the published bound $\Gamma_H < 5.4 \Gamma_H^{\text{SM}}$ at 95% C.L. translates as an upper bound on $\kappa_t < \sqrt{5.4} = 2.3$ (dot in figure 5.2, with the excluded line for larger values of κ_t). We can see that this dot is close to the iso-cross section contour giving a doubled cross section, which is consistent with the previous argument relying on numbers of events. This bound, however, only applies to positive values of κ_t and does not cover the possibility of negative couplings, for which the interference term has different sign, and we can see on figure 5.2 that $\kappa_t = -2.3$ would give a much larger off-shell cross section.

It is finally interesting to have a look at the direct bound on κ_t coming from the measurement of the $t\bar{t}h$ associated production at the time of the analysis, with the Higgs decaying to a $b\bar{b}$ pair. Assuming that the Higgs decay rate to $b\bar{b}$ is SM like, the cross section is simply proportional to κ_t^2 : from the CMS published bound [114] based on an integrated luminosity of 19.5 fb^{-1} at 8 TeV , we can extract $|\kappa_t| < \sqrt{4.2} = 2.05$, while the ATLAS measurement with full 8 TeV dataset leads to $|\kappa_t| < \sqrt{4.1} = 2.02$ at 95% C.L. [115]. Those two constraints are therefore of the same order as what one could hope to get from an analysis on off-shell measurements by the experiments similar to the one presented in this section. Moreover, the use of the complete parametrisation presented in chapter 3 would allow to use all those measurements within a common framework.

To put this part in perspective, it is useful to recall that the new physics loop can also be probed by measuring the transverse momentum distribution of the Higgs against a radiated jet [116, 117]. However this measurement, like any other measurement on the Higgs mass peak, suffers from the degeneracy between ad-hoc rescaling of couplings and width while only off-shell measurements are directly sensitive to the couplings strength. It is also worth noting that some new physics models might also get a contribution to the $gg \rightarrow ZZ$ process from a box diagram similar to the SM one, in which case the proposed parametrisation would no longer be a valid approach and should be extended. Finally, another approach to consider is that the κ_t - κ_{gg} degeneracy might also disappear from future observations of the $gg \rightarrow hh$ process.

5.2 Likelihood functions

Several of the assumptions made in this thesis that made the recasting of the constraints less precise might be avoided. Among these, the shape of the likelihood and the correlation of uncertainties are two aspects on which the methods presented here could be improved. On the first hand, when adjusting the exclusion contours to ellipses in part 3.2.2, we assumed that the likelihood function for the μ_S was spread as a Gaussian. However, these distributions are based on the combination of many measurements and techniques, and nothing guarantees they should be as well behaved as we would like. Although this approximation is still expected to be good, the information of the exclusion regions is not enough, and the proper way to make information public was discussed at several meetings, which resulted in the publication of a note [118] advocating for the publication by the experiments of a more complete description of the likelihood functions. This was attempted in different ways, by the two experiments. The CMS collaboration published some of the exclusion regions superimposed with a colour-coded map of the likelihood function they were based on, as for instance in figure 23 in [119], reproduced here in figure 5.3. However, data is hard to extract in an automated way from this kind of figure. On the other hand, the ATLAS collaboration opted for the publication of likelihood grids along with their analysis [120]. The files, in root format, are stored on an online platform and publicly available [121]. With these grids, mapping the values of the likelihood on the discretised parameter plane, one has direct access to the likelihood of a particular (approximate) parameter point. However, the publication of such likelihoods is not yet common and most analyses still stick to the publication of exclusion regions.

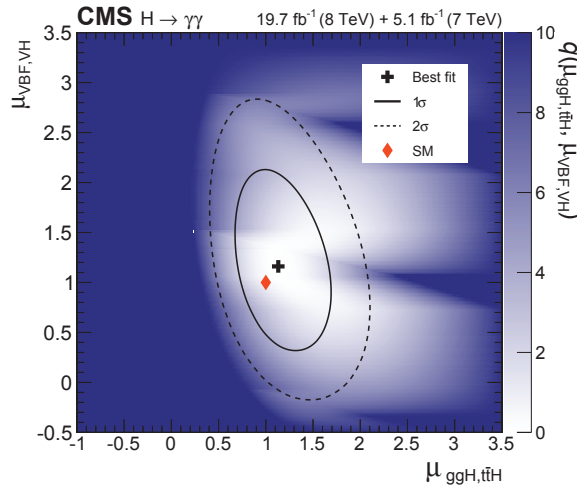


Figure 5.3: Map of the log-likelihood ratio $\Delta\chi^2(\mu_{ggH/t\bar{t}H}, \mu_{VBF/VH})$ from the CMS $\gamma\gamma$ analysis [119]

Another effort in the prospect of making data more easily and correctly usable by people outside the experiments was made jointly by the CMS and ATLAS collaborations in [122]. As we

said, theoretical uncertainties are a source correlations in measurements of different experiments. By performing this common analysis, where μ and m_H are studied together, the experimentalists got rid of the misinterpretation that would be done by interpreting the two measurements as independent. However, no other study has yet been published, in particular with other decay modes than $\gamma\gamma$ and 4ℓ , and for other parametrisation of the results than a global μ .

However, seeing these developments, there is good hope that future analyses will make constraining procedures by non-experimentalists more precise.

5.3 Pseudo-observables

One of the weaknesses of the approach studied up until now, sometimes called the “ κ framework”, is also one of its qualities: it is simple. For this reason, it fails to describe some possible New Physics effects, for instance modifying the angular distributions of events. This can be seen as a consequence of the fact that it is inspired by experimental studies looking for a standard Higgs boson. Although the modification we advocated for is a bit more inspired by the study of BSM models, the other extreme, purely theory inspired, relies on effective field theories (EFT). This definition, relying on including every possible operator, not necessarily renormalisable, that could arise from new physics above a given scale, compatible with the symmetries required by the model builder. This approach, and the techniques developed alongside it through years, has the advantages of being exhaustive and of permitting to estimate the importance of various terms through power counting. However it also suffers from its generality, and requires the introduction of a lot of parameters, as many as operators exist. One solution lies in-between, in the form of pseudo-observables, which were already used at LEP. Their use at LHC is the topic of recent workshops [123]. Like the κ -framework, it is experimentally motivated, but also includes some of the extensivity of EFT. The idea is to model the observables through the amplitudes of the processes involved, while describing more than the SM terms. The example of $H \rightarrow 4\ell$ is particularly interesting, and in this short description we will focus on $H \rightarrow e^+e^-\mu^+\mu^-$ ([124, 125]). The amplitude of this process, supposing chirality- and flavour-conserving interactions, can be written as:

$$\mathcal{A}(H \rightarrow ee\mu\mu) = i \frac{2m_Z^2}{v} \sum_{\text{chiralities}} (\bar{e}\gamma_\alpha e)(\bar{\mu}\gamma_\beta \mu) \times \mathcal{T}^{\alpha\beta}(p_e, p_\mu)$$

where p_e and p_μ are the momenta of the electron and muon pairs, and $\mathcal{T}^{\alpha\beta}(p_e, p_\mu)$ represents the structure of the couplings within the process. By requiring Lorentz symmetry, the only possible form for \mathcal{T} is:

$$\mathcal{T}^{\alpha\beta}(p_e, p_\mu) = F_1^{e\mu}(p_e^2, p_\mu^2)g^{\alpha\beta} + F_3^{e\mu}(p_e^2, p_\mu^2) \frac{q_e \cdot q_\mu g^{\alpha\beta} - q_\mu^\alpha q_e^\beta}{m_Z^2} + F_4^{e\mu}(p_e^2, p_\mu^2) \frac{\epsilon^{\alpha\beta\rho\sigma} q_\mu^\rho q_e^\sigma}{m_Z^2}$$

and we get three form factors depending on the momenta of the lepton pairs. Their fit would be possible with lots of data, but with a limited amount, it is simpler to parametrize them. By

counting the number of Z poles, which is a model dependent choice believing partly in the SM (no other light particles), and noting P_Z the propagator of the Z boson, we can decompose for instance $F_1^{e\mu}$ into:

$$F_1^{e\mu}(p_e^2, p_\mu^2) = \kappa_Z \frac{g_Z^e g_Z^\mu}{P_Z(q_e^2) P_Z(q_\mu^2)} + \epsilon_{Z\mu} \frac{g_Z^e}{P_Z(q_e^2)} + \epsilon_{Ze} \frac{g_Z^\mu}{P_Z(q_\mu^2)}$$

5 parameters, pseudo-observables, have been introduced here: $\kappa_Z, \epsilon_{Ze}, \epsilon_{Z\mu}, g_Z^e$ and g_Z^μ . The last two ones are not directly related to Higgs physics, but are deviation of the Z vector coupling to a pair of leptons, and can be constrained through LEP pseudo-observables. As for the other three, κ_Z is the same as the one introduced in the κ framework, while $\epsilon_{Ze/\mu}$ are 0 in the SM. Those new terms, introducing new dependencies, allow to describe distributions different from the SM ones, in particular on the angular side, with the possibility of describing the results of experiments in more detail.

Conclusion

Throughout this thesis, we have been able to grasp the importance of the way results are communicated in a scientific community. Because of statistical implications, constraining a model is not always a matter of comparing a value to a bound, but might get much more complicated, and the constraints are sometimes only valid under stringent hypotheses. The choice of a proper way of describing results therefore lies in a compromise between the generality of the hypotheses, as we may want to cover as many models as possible, and the number of quantities necessary to describe them, which we want to be as small as possible to have meaningful constraints. From this point of view, there is not one correct way of describing the results, but there might be several, covering different hypotheses, and they change as the precision of the experiments increase.

The measurement of the Higgs couplings is no exception to this fact, and even though with time the use of pseudo-observables might become preferable to the use of the κ framework, we have seen that the latter is quite efficient in constraining models, with reasonable assumptions. Moreover, with the particular treatment of loop-induced couplings presented here, the underlying models appear more obviously. However, as this parametrisation contains more than two parameters, the communication of results through figures is incomplete, and likelihood functions would allow an easier use of the publicly available results. We were still able to effectively put constraints on a set of chosen models in which these loops are important, such as models with extra dimensions, fermiophobic Higgs models, or models with a 4th generation of fermions.

In a second step, we saw that this parametrisation is also versatile in the sense that it might easily be generalised and used to constrain other scalars than the Higgs boson. In particular, we saw that LEP exclusions of a light standard Higgs boson actually leave room for a light scalar detectable at the LHC. Furthermore, by studying the 2HDM and the NMSSM on a large portion of parameter space in which such a scalar exists, we proved that this case can arise from reasonable and yet unconstrained models, advocating for searches for light scalars at the LHC. Moreover, by using the presented parametrisation, results from measurements concerning the two scalars would be easier to use together.

Finally, this parametrisation also proved its power by its use in the off-shell region. Although two signal strengths are needed to describe the on-shell and off-shell Higgs production via gluon fusion, we showed using a toy model that the framework we advocated for does not need to be extended to describe the contribution of heavy loops to this process coherently in both regions.

As a side note, the work presented in this thesis led to the writing of several papers:

- Higgs couplings beyond the Standard Model [23]
- Searching for a lighter Higgs boson: Parametrization and sample tests [126]
- Higgs couplings: disentangling New Physics with off-shell measurements [127]
- Higgs Couplings and BSM Physics: Run I Legacy Constraints [53]

Bibliography

- [1] S. Glashow, "Partial Symmetries of Weak Interactions," *Nucl.Phys.* **22** (1961) 579–588.
- [2] S. Weinberg, "A model of leptons," *Phys. Rev. Lett.* **19** (Nov, 1967) 1264–1266.
<http://link.aps.org/doi/10.1103/PhysRevLett.19.1264>.
- [3] A. Salam, "Weak and Electromagnetic Interactions," *Conf.Proc.* **C680519** (1968) 367–377.
- [4] P. W. Anderson, "Random-phase approximation in the theory of superconductivity," *Phys. Rev.* **112** (Dec, 1958) 1900–1916.
<http://link.aps.org/doi/10.1103/PhysRev.112.1900>.
- [5] A. Djouadi, "The anatomy of electroweak symmetry breaking: Tome i: The higgs boson in the standard model," *Physics Reports* **457** no. 14, (2008) 1 – 216.
<http://www.sciencedirect.com/science/article/pii/S0370157307004334>.
- [6] L. H. C. S. W. Group, "Higgs cross sections at 7, 8 and 14 tev."
<https://twiki.cern.ch/twiki/bin/view/LHCPhysics/CrossSections>.
- [7] R. D. Peccei and H. R. Quinn, "CP conservation in the presence of pseudoparticles," *Phys. Rev. Lett.* **38** (Jun, 1977) 1440–1443.
<http://link.aps.org/doi/10.1103/PhysRevLett.38.1440>.
- [8] M. C. Gonzalez-Garcia, M. Maltoni, and T. Schwetz, "Updated fit to three neutrino mixing: status of leptonic CP violation," *JHEP* **11** (2014) 052, arXiv:1409.5439 [hep-ph].
- [9] S. S. Wilks, "The large-sample distribution of the likelihood ratio for testing composite hypotheses," *Ann. Math. Statist.* **9** no. 1, (03, 1938) 60–62.
<http://dx.doi.org/10.1214/aoms/1177732360>.
- [10] A. L. Read, "Presentation of search results: The CL(s) technique," *J. Phys.* **G28** (2002) 2693–2704. [,11(2002)].
- [11] A. Collaboration, "Observation of an excess of events in the search for the Standard Model Higgs boson in the gamma-gamma channel with the ATLAS detector," Tech. Rep.

- ATLAS-CONF-2012-091, CERN, Geneva, Jul, 2012.
<https://cds.cern.ch/record/1460410>.
- [12] C. Collaboration, "Evidence for a new state decaying into two photons in the search for the standard model Higgs boson in pp collisions," Tech. Rep. CMS-PAS-HIG-12-015, CERN, Geneva, 2012. <http://cds.cern.ch/record/1460419>.
- [13] C. Collaboration.
<https://twiki.cern.ch/twiki/bin/view/CMSPublic/PhysicsResultsHIG>.
- [14] **ATLAS** Collaboration, G. Aad *et al.*, "Observation of a new particle in the search for the Standard Model Higgs boson with the ATLAS detector at the LHC," *Phys. Lett.* **B716** (2012) 1–29, arXiv:1207.7214 [hep-ex].
- [15] J. Bernon and B. Dumont, "Lilith: a tool for constraining new physics from Higgs measurements," arXiv:1502.04138 [hep-ph].
- [16] F. Bonnet, M. B. Gavela, T. Ota, and W. Winter, "Anomalous Higgs couplings at the LHC, and their theoretical interpretation," *Phys. Rev.* **D85** (2012) 035016, arXiv:1105.5140 [hep-ph].
- [17] F. Bonnet, T. Ota, M. Rauch, and W. Winter, "Interpretation of precision tests in the Higgs sector in terms of physics beyond the Standard Model," *Phys. Rev.* **D86** (2012) 093014, arXiv:1207.4599 [hep-ph].
- [18] T. Corbett, O. J. P. Eboli, J. Gonzalez-Fraile, and M. C. Gonzalez-Garcia, "Constraining anomalous Higgs interactions," *Phys. Rev.* **D86** (2012) 075013, arXiv:1207.1344 [hep-ph].
- [19] J. R. Espinosa, C. Grojean, M. Muhlleitner, and M. Trott, "Fingerprinting Higgs Suspects at the LHC," *JHEP* **05** (2012) 097, arXiv:1202.3697 [hep-ph].
- [20] J. R. Espinosa, C. Grojean, M. Muhlleitner, and M. Trott, "First Glimpses at Higgs' face," *JHEP* **12** (2012) 045, arXiv:1207.1717 [hep-ph].
- [21] G. Passarino, "NLO Inspired Effective Lagrangians for Higgs Physics," *Nucl. Phys.* **B868** (2013) 416–458, arXiv:1209.5538 [hep-ph].
- [22] **LHC Higgs Cross Section Working Group** Collaboration, A. David *et al.*, "LHC HXSWG interim recommendations to explore the coupling structure of a Higgs-like particle," arXiv:1209.0040 [hep-ph].
- [23] G. Cacciapaglia, A. Deandrea, G. D. La Rochelle, and J.-B. Flament, "Higgs couplings beyond the Standard Model," *JHEP* **1303** (2013) 029, arXiv:1210.8120 [hep-ph].
- [24] G. Cacciapaglia, A. Deandrea, and J. Llodra-Perez, " $H \rightarrow \gamma\gamma$ beyond the Standard Model," *JHEP* **0906** (2009) 054, arXiv:0901.0927 [hep-ph].

- [25] M. Spira, A. Djouadi, D. Graudenz, and P. M. Zerwas, "Higgs boson production at the LHC," *Nucl. Phys.* **B453** (1995) 17–82, arXiv:hep-ph/9504378 [hep-ph].
- [26] A. Azatov, R. Contino, and J. Galloway, "Model-Independent Bounds on a Light Higgs," *JHEP* **04** (2012) 127, arXiv:1202.3415 [hep-ph]. [Erratum: JHEP04,140(2013)].
- [27] C. Collaboration, "Evidence for a new state in the search for the standard model Higgs boson in the H to ZZ to 4 leptons channel in pp collisions at $\sqrt{s} = 7$ and 8 TeV," Tech. Rep. CMS-PAS-HIG-12-016, CERN, Geneva, 2012. <https://cds.cern.ch/record/1460664>.
- [28] A. Collaboration, "Observation of an excess of events in the search for the Standard Model Higgs boson in the $H \rightarrow ZZ^{(*)} \rightarrow 4\ell$ channel with the ATLAS detector.," Tech. Rep. ATLAS-CONF-2012-092, CERN, Geneva, Jul, 2012. <https://cds.cern.ch/record/1460411>.
- [29] C. Collaboration, "Search for the standard model Higgs boson produced in association with W or Z bosons, and decaying to bottom quarks for HCP 2012," Tech. Rep. CMS-PAS-HIG-12-044, CERN, Geneva, 2012. <https://cds.cern.ch/record/1493618>.
- [30] A. Collaboration, "Search for the Standard Model Higgs boson produced in association with a vector boson and decaying to bottom quarks with the ATLAS detector," Tech. Rep. ATLAS-CONF-2012-161, CERN, Geneva, Nov, 2012. <https://cds.cern.ch/record/1493625>.
- [31] C. Collaboration, "Combination of standard model Higgs boson searches and measurement of the properties of the new boson with a mass near 125 GeV," Tech. Rep. CMS-PAS-HIG-12-045, CERN, Geneva, 2012. <http://cds.cern.ch/record/1494149>.
- [32] A. Collaboration, "Coupling properties of the new Higgs-like boson observed with the ATLAS detector at the LHC," Tech. Rep. ATLAS-CONF-2012-127, CERN, Geneva, Sep, 2012. <https://cds.cern.ch/record/1476765>.
- [33] **ATLAS** Collaboration, T. A. collaboration, "Search for ttH production in the $H \rightarrow \gamma\gamma$ channel at $\sqrt{s} = 8$ TeV with the ATLAS detector,".
- [34] **CMS** Collaboration, V. Khachatryan *et al.*, "Search for the associated production of the Higgs boson with a top-quark pair," *JHEP* **09** (2014) 087, arXiv:1408.1682 [hep-ex]. [Erratum: JHEP10,106(2014)].
- [35] **CMS** Collaboration, V. Khachatryan *et al.*, "Precise determination of the mass of the Higgs boson and tests of compatibility of its couplings with the standard model predictions using proton collisions at 7 and 8 TeV," *Eur. Phys. J.* **C75** no. 5, (2015) 212, arXiv:1412.8662 [hep-ex].

- [36] **(ATLAS Collaboration)** Collaboration, G. Aad *et al.*, “Measurement of Higgs boson production in the diphoton decay channel in pp collisions at center-of-mass energies of 7 and 8 TeV with the ATLAS detector,” *Phys. Rev. D* **90** (Dec, 2014) 112015.
<http://link.aps.org/doi/10.1103/PhysRevD.90.112015>.
- [37] **ATLAS Collaboration** Collaboration, G. Aad *et al.*, “Evidence for the Higgs-boson Yukawa coupling to tau leptons with the ATLAS detector,” Tech. Rep. arXiv:1501.04943. CERN-PH-EP-2014-262, CERN, Jan, 2015.
- [38] **ATLAS Collaboration** Collaboration, G. Aad *et al.*, “Observation and measurement of Higgs boson decays to WW^* with the ATLAS detector,” Tech. Rep. arXiv:1412.2641. CERN-PH-EP-2014-270, CERN, Dec, 2014.
- [39] **(ATLAS Collaboration)** Collaboration, G. Aad *et al.*, “Measurements of Higgs boson production and couplings in the four-lepton channel in pp collisions at center-of-mass energies of 7 and 8 TeV with the ATLAS detector,” *Phys. Rev. D* **91** (Jan, 2015) 012006.
<http://link.aps.org/doi/10.1103/PhysRevD.91.012006>.
- [40] **ATLAS** Collaboration, G. Aad *et al.*, “Measurements of the Higgs boson production and decay rates and coupling strengths using pp collision data at $\sqrt{s} = 7$ and 8 TeV in the ATLAS experiment,” arXiv:1507.04548 [hep-ex].
- [41] A. Djouadi and A. Lenz, “Sealing the fate of a fourth generation of fermions,” *Phys. Lett.* **B715** (2012) 310–314, arXiv:1204.1252 [hep-ph].
- [42] O. Eberhardt, G. Herbert, H. Lacker, A. Lenz, A. Menzel, U. Nierste, and M. Wiebusch, “Impact of a Higgs boson at a mass of 126 GeV on the standard model with three and four fermion generations,” *Phys. Rev. Lett.* **109** (2012) 241802, arXiv:1209.1101 [hep-ph].
- [43] G. Cacciapaglia, A. Deandrea, and J. Llodra-Perez, “A Dark Matter candidate from Lorentz Invariance in 6D,” *JHEP* **03** (2010) 083, arXiv:0907.4993 [hep-ph].
- [44] G. Cacciapaglia and B. Kubik, “Even tiers and resonances on the Real Projective Plane,” *JHEP* **02** (2013) 052, arXiv:1209.6556 [hep-ph].
- [45] K. Agashe, R. Contino, and A. Pomarol, “The Minimal composite Higgs model,” *Nucl. Phys.* **B719** (2005) 165–187, arXiv:hep-ph/0412089 [hep-ph].
- [46] K. Agashe and R. Contino, “The Minimal composite Higgs model and electroweak precision tests,” *Nucl. Phys.* **B742** (2006) 59–85, arXiv:hep-ph/0510164 [hep-ph].
- [47] K. Nishiwaki, K.-y. Oda, N. Okuda, and R. Watanabe, “A Bound on Universal Extra Dimension Models from up to 2fb^{-1} of LHC Data at 7TeV,” *Phys. Lett.* **B707** (2012) 506–511, arXiv:1108.1764 [hep-ph].

- [48] M. Schmaltz, “The Simplest little Higgs,” *JHEP* **08** (2004) 056, arXiv:hep-ph/0407143 [hep-ph].
- [49] A. V. Manohar and M. B. Wise, “Flavor changing neutral currents, an extended scalar sector, and the Higgs production rate at the CERN Large Hadron Collider,” *Phys. Rev. D* **74** (Aug, 2006) 035009. <http://link.aps.org/doi/10.1103/PhysRevD.74.035009>.
- [50] T. Appelquist, H.-C. Cheng, and B. A. Dobrescu, “Bounds on universal extra dimensions,” *Phys. Rev. D* **64** (Jun, 2001) 035002. <http://link.aps.org/doi/10.1103/PhysRevD.64.035002>.
- [51] N. Arkani-Hamed, A. Cohen, E. Katz, and A. Nelson, “The Littlest Higgs,” *JHEP* **0207** (2002) 034, arXiv:hep-ph/0206021 [hep-ph].
- [52] I. Low, “T parity and the littlest Higgs,” *JHEP* **0410** (2004) 067, arXiv:hep-ph/0409025 [hep-ph].
- [53] J.-B. Flament, “Higgs Couplings and BSM Physics: Run I Legacy Constraints,” arXiv:1504.07919 [hep-ph].
- [54] **CMS** Collaboration, “Combination of standard model Higgs boson searches and measurements of the properties of the new boson with a mass near 125 GeV,”.
- [55] **ATLAS** Collaboration, “Combined coupling measurements of the Higgs-like boson with the ATLAS detector using up to 25 fb⁻¹ of proton-proton collision data,”.
- [56] **CMS** Collaboration, “Evidence for a particle decaying to W^+W^- in the fully leptonic final state in a standard model Higgs boson search in pp collisions at the LHC,”.
- [57] J. Fan, W. D. Goldberger, A. Ross, and W. Skiba, “Standard Model couplings and collider signatures of a light scalar,” *Phys. Rev.* **D79** (2009) 035017, arXiv:0803.2040 [hep-ph].
- [58] W. D. Goldberger, B. Grinstein, and W. Skiba, “Distinguishing the Higgs boson from the dilaton at the Large Hadron Collider,” *Phys. Rev. Lett.* **100** (2008) 111802, arXiv:0708.1463 [hep-ph].
- [59] C. Csaki, J. Hubisz, and S. J. Lee, “Radion phenomenology in realistic warped space models,” *Phys. Rev.* **D76** (2007) 125015, arXiv:0705.3844 [hep-ph].
- [60] M. Battaglia, S. De Curtis, A. De Roeck, D. Dominici, and J. F. Gunion, “On the complementarity of Higgs and radion searches at LHC,” *Phys. Lett.* **B568** (2003) 92–102, arXiv:hep-ph/0304245 [hep-ph].
- [61] T. Appelquist and Y. Bai, “A Light Dilaton in Walking Gauge Theories,” *Phys. Rev.* **D82** (2010) 071701, arXiv:1006.4375 [hep-ph].

- [62] D. Elander, C. Nunez, and M. Piai, "A Light scalar from walking solutions in gauge-string duality," *Phys. Lett.* **B686** (2010) 64–67, arXiv:0908.2808 [hep-th].
- [63] P. Bechtle, O. Brein, S. Heinemeyer, O. Stål, T. Stefaniak, *et al.*, "HiggsBounds-4: Improved Tests of Extended Higgs Sectors against Exclusion Bounds from LEP, the Tevatron and the LHC," arXiv:1311.0055 [hep-ph].
- [64] **LEP Higgs Working Group for Higgs boson searches** Collaboration, "Flavor independent search for hadronically decaying neutral Higgs bosons at LEP," arXiv:hep-ex/0107034 [hep-ex].
- [65] G. Branco, P. Ferreira, L. Lavoura, M. Rebelo, M. Sher, *et al.*, "Theory and phenomenology of two-Higgs-doublet models," *Phys.Rept.* **516** (2012) 1–102, arXiv:1106.0034 [hep-ph].
- [66] A. Celis, V. Ilisie, and A. Pich, "LHC constraints on two-Higgs doublet models," *JHEP* **1307** (2013) 053, arXiv:1302.4022 [hep-ph].
- [67] B. Coleppa, F. Kling, and S. Su, "Constraining Type II 2HDM in Light of LHC Higgs Searches," arXiv:1305.0002 [hep-ph].
- [68] S. Chang, S. K. Kang, J.-P. Lee, K. Y. Lee, S. C. Park, *et al.*, "Two Higgs doublet models for the LHC Higgs boson data at $\sqrt{s} = 7$ and 8 TeV," arXiv:1310.3374 [hep-ph].
- [69] C.-W. Chiang and K. Yagyu, "Implications of Higgs boson search data on the two-Higgs doublet models with a softly broken Z_2 symmetry," *JHEP* **1307** (2013) 160, arXiv:1303.0168 [hep-ph].
- [70] A. Barroso, P. Ferreira, R. Santos, M. Sher, and J. P. Silva, "2HDM at the LHC - the story so far," arXiv:1304.5225 [hep-ph].
- [71] B. Grinstein and P. Uttayarat, "Carving Out Parameter Space in Type-II Two Higgs Doublets Model," *JHEP* **1306** (2013) 094, arXiv:1304.0028 [hep-ph].
- [72] C.-Y. Chen, S. Dawson, and M. Sher, "Heavy Higgs Searches and Constraints on Two Higgs Doublet Models," *Phys.Rev.* **D88** (2013) 015018, arXiv:1305.1624 [hep-ph].
- [73] N. Craig, J. Galloway, and S. Thomas, "Searching for Signs of the Second Higgs Doublet," arXiv:1305.2424 [hep-ph].
- [74] O. Eberhardt, U. Nierste, and M. Wiebusch, "Status of the two-Higgs-doublet model of type II," arXiv:1305.1649 [hep-ph].
- [75] G. Belanger, B. Dumont, U. Ellwanger, J. Gunion, and S. Kraml, "Global fit to Higgs signal strengths and couplings and implications for extended Higgs sectors," *Phys.Rev.* **D88** (2013) 075008, arXiv:1306.2941 [hep-ph].

- [76] V. Barger, L. L. Everett, H. E. Logan, and G. Shaughnessy, “Scrutinizing $h(125)$ in Two Higgs Doublet Models at the LHC, ILC, and Muon Collider,” arXiv:1308.0052 [hep-ph].
- [77] P. Ko, Y. Omura, and C. Yu, “Higgs phenomenology in Type-I 2HDM with $U(1)_H$ Higgs gauge symmetry,” arXiv:1309.7156 [hep-ph].
- [78] A. Celis, V. Ilisie, and A. Pich, “Towards a general analysis of LHC data within two-Higgs-doublet models,” arXiv:1310.7941 [hep-ph].
- [79] K. Cheung, J. S. Lee, and P.-Y. Tseng, “Higgcision in the Two-Higgs Doublet Models,” arXiv:1310.3937 [hep-ph].
- [80] D. Eriksson, J. Rathsman, and O. Stal, “2HDMC: Two-Higgs-doublet model calculator,” *Comput.Phys.Commun.* **181** (2010) 833–834.
- [81] F. Mahmoudi, “SuperIso v2.3: A Program for calculating flavor physics observables in Supersymmetry,” *Comput.Phys.Commun.* **180** (2009) 1579–1613, arXiv:0808.3144 [hep-ph].
- [82] M. E. Peskin and T. Takeuchi, “Estimation of oblique electroweak corrections,” *Phys. Rev. D* **46** (Jul, 1992) 381–409.
<http://link.aps.org/doi/10.1103/PhysRevD.46.381>.
- [83] W. Grimus, L. Lavoura, O. Ogreid, and P. Osland, “The Oblique parameters in multi-Higgs-doublet models,” *Nucl.Phys.* **B801** (2008) 81–96, arXiv:0802.4353 [hep-ph].
- [84] **Particle Data Group** Collaboration, J. Beringer *et al.*, “Review of Particle Physics (RPP), section 10.7.,” *Phys.Rev.* **D86** (2012) 010001.
- [85] **Muon G-2 Collaboration** Collaboration, G. Bennett *et al.*, “Final Report of the Muon E821 Anomalous Magnetic Moment Measurement at BNL,” *Phys.Rev.* **D73** (2006) 072003, arXiv:hep-ex/0602035 [hep-ex].
- [86] **Heavy Flavor Averaging Group** Collaboration,
“<http://www.slac.stanford.edu/xorg/hfag>,”.
- [87] **CMS and LHCb** Collaboration, “Combination of results on the rare decays $B_{(s)}^0 \rightarrow \mu^+ \mu^-$ from the CMS and LHCb experiments,” CMS-PAS-BPH-13-007, LHCb-CONF-2013-012.
- [88] F. Mahmoudi and O. Stal, “Flavor constraints on the two-Higgs-doublet model with general Yukawa couplings,” *Phys.Rev.* **D81** (2010) 035016, arXiv:0907.1791 [hep-ph].
- [89] M. Misiak, H. Asatrian, K. Bieri, M. Czakon, A. Czarnecki, *et al.*, “Estimate of $\text{BR}(B \rightarrow X_s \gamma)$ at $\mathcal{O}(\alpha_s^2)$,” *Phys.Rev.Lett.* **98** (2007) 022002, arXiv:hep-ph/0609232 [hep-ph].

- [90] A. Arbey, M. Battaglia, A. Djouadi, and F. Mahmoudi, “An update on the constraints on the phenomenological MSSM from the new LHC Higgs results,” *Phys.Lett.* **B720** (2013) 153–160, arXiv:1211.4004 [hep-ph].
- [91] S. King, M. Muhlleitner, R. Nevzorov, and K. Walz, “Natural NMSSM Higgs Bosons,” *Nucl.Phys.* **B870** (2013) 323–352, arXiv:1211.5074 [hep-ph].
- [92] T. Cheng, J. Li, T. Li, and Q.-S. Yan, “Natural NMSSM confronting with the LHC7-8,” arXiv:1304.3182 [hep-ph].
- [93] R. Barbieri, D. Buttazzo, K. Kannike, F. Sala, and A. Tesi, “Exploring the Higgs sector of a most natural NMSSM,” *Phys.Rev.* **D87** (2013) 115018, arXiv:1304.3670 [hep-ph].
- [94] C. Beskidt, W. de Boer, and D. Kazakov, “A comparison of the Higgs sectors of the MSSM and NMSSM for a 126 GeV Higgs boson,” arXiv:1308.1333 [hep-ph].
- [95] K. Choi, S. H. Im, K. S. Jeong, and M.-S. Seo, “Higgs phenomenology in Peccei-Quinn invariant NMSSM,” arXiv:1308.4447 [hep-ph].
- [96] G. Belanger, U. Ellwanger, J. F. Gunion, Y. Jiang, S. Kraml, *et al.*, “Higgs Bosons at 98 and 125 GeV at LEP and the LHC,” *JHEP* **1301** (2013) 069, arXiv:1210.1976 [hep-ph].
- [97] D. G. Cerdeno, P. Ghosh, and C. B. Park, “Probing the two light Higgs scenario in the NMSSM with a low-mass pseudoscalar,” *JHEP* **1306** (2013) 031, arXiv:1301.1325 [hep-ph].
- [98] N. D. Christensen, T. Han, Z. Liu, and S. Su, “Low-Mass Higgs Bosons in the NMSSM and Their LHC Implications,” *JHEP* **1308** (2013) 019, arXiv:1303.2113 [hep-ph].
- [99] R. Barbieri, D. Buttazzo, K. Kannike, F. Sala, and A. Tesi, “One or more Higgs bosons?,” *Phys.Rev.* **D88** (2013) 055011, arXiv:1307.4937 [hep-ph].
- [100] J. Cao, F. Ding, C. Han, J. M. Yang, and J. Zhu, “A light Higgs scalar in the NMSSM confronted with the latest LHC Higgs data,” arXiv:1309.4939 [hep-ph].
- [101] M. Badziak, M. Olechowski, and S. Pokorski, “125 GeV Higgs and enhanced diphoton signal of a light singlet-like scalar in NMSSM,” arXiv:1310.4518 [hep-ph].
- [102] U. Ellwanger, C. Hugonie, and A. M. Teixeira, “The Next-to-Minimal Supersymmetric Standard Model,” *Phys.Rept.* **496** (2010) 1–77, arXiv:0910.1785 [hep-ph].
- [103] U. Ellwanger, J. F. Gunion, and C. Hugonie, “NMHDECAY: A Fortran code for the Higgs masses, couplings and decay widths in the NMSSM,” *JHEP* **0502** (2005) 066, arXiv:hep-ph/0406215 [hep-ph].

- [104] **ATLAS Collaboration** Collaboration, G. Aad *et al.*, “Search for Scalar Diphoton Resonances in the Mass Range 65 – 600 GeV with the ATLAS Detector in pp Collision Data at $\sqrt{s} = 8$ TeV,” arXiv:1407.6583 [hep-ex].
- [105] N. Kauer and G. Passarino, “Inadequacy of zero-width approximation for a light Higgs boson signal,” *JHEP* **1208** (2012) 116, arXiv:1206.4803 [hep-ph].
- [106] F. Caola and K. Melnikov, “Constraining the Higgs boson width with ZZ production at the LHC,” *Phys.Rev.* **D88** (2013) 054024, arXiv:1307.4935 [hep-ph].
- [107] J. M. Campbell, R. K. Ellis, and C. Williams, “Bounding the Higgs width at the LHC using full analytic results for $gg \rightarrow e^-e^+\mu^-\mu^+$,” *JHEP* **1404** (2014) 060, arXiv:1311.3589 [hep-ph].
- [108] J. S. Gainer, J. Lykken, K. T. Matchev, S. Mrenna, and M. Park, “Beyond Geolocating: Constraining Higher Dimensional Operators in $H \rightarrow 4\ell$ with Off-Shell Production and More,” arXiv:1403.4951 [hep-ph].
- [109] **CMS Collaboration** Collaboration, V. Khachatryan *et al.*, “Constraints on the Higgs boson width from off-shell production and decay to Z-boson pairs,” arXiv:1405.3455 [hep-ex].
- [110] “Determination of the off-shell Higgs boson signal strength in the high-mass ZZ final state with the ATLAS detector,” Tech. Rep. ATLAS-CONF-2014-042, CERN, Geneva, Jul, 2014. <http://cds.cern.ch/record/1740973>.
- [111] **ATLAS** Collaboration, G. Aad *et al.*, “Constraints on the off-shell Higgs boson signal strength in the high-mass ZZ and WW final states with the ATLAS detector,” *Eur. Phys. J.* **C75** no. 7, (2015) 335, arXiv:1503.01060 [hep-ex].
- [112] C. Englert and M. Spannowsky, “Limitations and Opportunities of Off-Shell Coupling Measurements,” arXiv:1405.0285 [hep-ph].
- [113] N. Kauer, “Interference effects for $H \rightarrow WW/ZZ \rightarrow \ell\bar{\nu}_\ell\bar{\ell}\nu_\ell$ searches in gluon fusion at the LHC,” *JHEP* **1312** (2013) 082, arXiv:1310.7011 [hep-ph].
- [114] **CMS** Collaboration, V. Khachatryan *et al.*, “Search for a standard model Higgs boson produced in association with a top-quark pair and decaying to bottom quarks using a matrix element method,” *Eur. Phys. J.* **C75** no. 6, (2015) 251, arXiv:1502.02485 [hep-ex].
- [115] “Search for the Standard Model Higgs boson produced in association with top quarks and decaying to $b\bar{b}$ in pp collisions at $\sqrt{s} = 8$ TeV with the ATLAS detector at the LHC,” Tech. Rep. ATLAS-CONF-2014-011, CERN, Geneva, Mar, 2014.
- [116] A. Azatov and A. Paul, “Probing Higgs couplings with high p_T Higgs production,” *JHEP* **1401** (2014) 014, arXiv:1309.5273 [hep-ph].

- [117] C. Grojean, E. Salvioni, M. Schlaffer, and A. Weiler, "Very boosted Higgs in gluon fusion," *JHEP* **1405** (2014) 022, arXiv:1312.3317 [hep-ph].
- [118] F. Boudjema *et al.*, "On the presentation of the LHC Higgs Results," 2013. arXiv:1307.5865 [hep-ph].
<http://inspirehep.net/record/1244142/files/arXiv:1307.5865.pdf>.
- [119] **CMS** Collaboration, V. Khachatryan *et al.*, "Observation of the diphoton decay of the Higgs boson and measurement of its properties," *Eur. Phys. J.* **C74** no. 10, (2014) 3076, arXiv:1407.0558 [hep-ex].
- [120] **ATLAS** Collaboration, G. Aad *et al.*, "Measurements of Higgs boson production and couplings in diboson final states with the ATLAS detector at the LHC," *Phys. Lett.* **B726** (2013) 88–119, arXiv:1307.1427 [hep-ex]. [Erratum: *Phys. Lett.*B734,406(2014)].
- [121] **ATLAS** Collaboration, "Data from Figure 7 from: Measurements of Higgs boson production and couplings in diboson final states with the ATLAS detector at the LHC,".
- [122] **ATLAS, CMS** Collaboration, G. Aad *et al.*, "Combined Measurement of the Higgs Boson Mass in pp Collisions at $\sqrt{s} = 7$ and 8 TeV with the ATLAS and CMS Experiments," *Phys. Rev. Lett.* **114** (2015) 191803, arXiv:1503.07589 [hep-ex].
- [123] *Pseudo-observables: from LEP to LHC*. 2015.
<https://cds.cern.ch/record/2005323>.
- [124] M. Bordone, A. Greljo, G. Isidori, D. Marzocca, and A. Pattori, "Higgs Pseudo Observables and Radiative Corrections," arXiv:1507.02555 [hep-ph].
- [125] M. Gonzalez-Alonso, A. Greljo, G. Isidori, and D. Marzocca, "Pseudo-observables in Higgs decays," *Eur. Phys. J.* **C75** no. 3, (2015) 128, arXiv:1412.6038 [hep-ph].
- [126] G. Cacciapaglia, A. Deandrea, G. D. La Rochelle, and J.-B. Flament, "Searching for a lighter Higgs boson: Parametrization and sample tests," *Phys. Rev.* **D91** no. 1, (2015) 015012, arXiv:1311.5132 [hep-ph].
- [127] G. Cacciapaglia, A. Deandrea, G. Drieu La Rochelle, and J.-B. Flament, "Higgs couplings: disentangling New Physics with off-shell measurements," *Phys. Rev. Lett.* **113** no. 20, (2014) 201802, arXiv:1406.1757 [hep-ph].